

M. Sc. Eda Jagst

**Surface Functional Group Characterization
Using Chemical Derivatization X-ray
Photoelectron Spectroscopy (CD-XPS)**

Die vorliegende Arbeit entstand an der BAM Bundesanstalt für Materialforschung und -prüfung.

Impressum

**Surface Functional Group Characterization
Using Chemical Derivatization X-ray
Photoelectron Spectroscopy (CD-XPS)**

2011

Herausgeber:

BAM Bundesanstalt für Materialforschung und -prüfung

Unter den Eichen 87

12205 Berlin

Telefon: +49 30 8104-0

Telefax: +49 30 8112029

E-Mail: info@bam.de

Internet: www.bam.de

Copyright © 2011 by

BAM Bundesanstalt für Materialforschung und -prüfung

Layout: BAM-Arbeitsgruppe Z.64

ISSN 1613-4249

ISBN 978-3-9813853-4-2

Surface Functional Group Characterization
Using
Chemical Derivatization X-ray Photoelectron Spectroscopy
(CD-XPS)

im Fachbereich
Biologie, Chemie, Pharmazie
der Freien Universität Berlin
eingereichte Dissertation

vorgelegt von
Eda Jagst
Berlin, Januar 2010

1. Gutachter: Prof. Dr. M. Hennecke

2. Gutachter: Prof. Dr. R. Haag

Disputation am: 07. Juni 2010

Acknowledgements

I would like to thank my supervisor Dr. W.E.S. Unger (Federal Institute of Material Research and Testing (BAM), VI.43 Surface and Thin Film Analysis) for providing me the opportunity to work on this project, for his excellent guidance and help throughout this work and for his generosity of time and ideas during the compilation of this thesis.

I would like to thank Prof. Dr. M. Hennecke (President of the BAM) for his supervision and Prof. Dr. R. Haag (Free University Berlin, Institute of Chemistry) for being the second examiner of this work.

Sincere thanks to Dr. T. Gross, Mr. A. Lippitz for their valuable technical supervision and support during the entire course of this work. Thanks are also due to the entire BESSY II staff for their support during experiments. I am also grateful to all the members of Division VI.43 in BAM for a friendly work atmosphere.

I am grateful to Dr. Graf, Dr. Dietrich, Manuela Büttner, Marion Männ and Matthias Weise for their support and for the nice time.

Many thanks to Dr. Swaraj for sharing his valuable knowledge of plasma polymerization and enlightning discussions. I would also thank to my practical student U. Zimmermann for his contributions to the plasma equipment.

I kindly acknowledge the financial support of the BAM presidency by the "BAM Doktoranden-Programm".

I would also like to thank my parents and friends for their moral support during this work.

And my very special thanks go to "meine Männer" Alex and Arda. Without you, everything would be meaningless. I love you both. Thank you very very much for your patience, help and faith in me.

Table of contents

1. Introduction	1
2. Chemical derivatization X-ray photoelectron spectroscopy (CD-XPS)	4
2.1. Introduction.....	4
2.2. Chemical derivatization methods and reagents used for amino and hydroxyl group derivatizations.....	7
2.3. Characterization of derivatized surfaces by other analytical methods.....	11
3. Experimental	15
3.1. Surface characterization techniques.....	15
3.1.1. X-Ray Photoelectron Spectroscopy (XPS).....	15
3.1.1.1. Surface analysis by XPS.....	16
3.1.1.2. Qualitative analysis.....	16
3.1.1.3. Quantitative analysis.....	17
3.1.1.4. Instrumentation of XPS.....	17
3.1.2. Near-edge X-ray absorption fine structure (NEXAFS).....	18
3.1.2.1. Instrumentation of NEXAFS.....	19
3.1.3. Error estimations.....	19
3.1.4. ¹ H - Nuclear magnetic resonance spectroscopy (¹ H-NMR).....	19
3.1.4.1. Instrumentation of NMR.....	20
3.2. Preparation of test samples.....	21
3.2.1. Liquid phase derivatization reactions of PFB and TFBA.....	21
3.2.1.1. Chemicals used.....	21
3.2.1.2. Reaction of 4,4'-methylenebis(2,6-dimethylaniline) with PFB.....	21
3.2.1.3. Reaction of 4,4'-methylenebis(2,6-dimethylaniline) with TFBA.....	22
3.2.1.4. Reaction of 4,4'-methylenebis(2,6-diethylaniline) with PFB.....	22
3.2.1.5. Reaction of 4,4'-methylenebis(2,6-diethylaniline) with TFBA.....	23
3.2.1.6. Reaction of 4,4'-methylenebis(2,6-diisopropylaniline) with PFB.....	23
3.2.1.7. Reaction of 4,4'-methylenebis(2,6-diisopropylaniline) with TFBA.....	24
3.2.1.8. Reaction of 2,2'-diaminobibenzyl with PFB.....	24
3.2.1.9. Reaction of 2,2'-diaminobibenzyl with TFBA.....	25

3.2.2. Preparation of spin coated 4,4'-methylenebis(2,6-diethylaniline) surfaces	26
3.2.2.1. Substrates and chemicals used	26
3.2.2.2. Cleaning procedure for silicon wafers	26
3.2.2.3. Spin coating of 4,4'-methylenebis(2,6-diethylaniline) on Si	27
3.2.2.4. Reaction set-up for gas-phase surface derivatizations	27
3.2.3. Preparation of self-assembled monolayers (SAMs)	28
3.2.3.1. Chemicals used	28
3.2.3.2. Procedure for the preparation of SAMs	28
3.2.3.3. Gas-phase derivatization of SAMs	28
3.2.4. Preparation of plasma polymerized allylamine samples	29
3.2.4.1. Chemicals used	29
3.2.4.2. Plasma deposition equipment	29
3.2.4.3. Preparation and derivatization of plasma deposited allylamine films	30
4. Derivatization of primary amines	31
4.1. Liquid phase derivatization reactions	31
4.2. Test samples	33
4.2.1. Spin coated samples of 4,4'-methylenebis(2,6-diethylaniline)	33
4.2.1.1. XPS and NEXAFS characterization before derivatization	33
4.2.1.2. XPS and NEXAFS after derivatization with PFB	37
4.2.1.3. XPS and NEXAFS after derivatization with TFBA	46
4.2.2. Self-assembled monolayers (SAMs)	55
4.2.2.1. Introduction	55
4.2.2.2. Characterization of SAMs	57
4.2.2.3. XPS and NEXAFS characterization of aliphatic SAMs	59
4.2.2.4. XPS and NEXAFS characterization of aromatic SAMs	63
4.2.2.5. Derivatization and characterization of the amino terminated SAMs	66
4.2.2.6. Radiation damage effects	72
4.3. Plasma polymerized allylamine samples	74
4.3.1. Introduction	74
4.3.2. Characterization of plasma polymerized allylamine films	75
4.3.3. Effects of external plasma parameters on amino group retention	81
4.3.4. NEXAFS characterization of plasma polymerized allylamine films	85

4.4. Quantification of surface amino groups on plasma polymerized allylamine surfaces.....	88
4.5. C-F bond cleavage during derivatization reactions of plasma polymerized allylamine surfaces.....	93
5. Derivatization of OH groups on plasma surfaces.....	98
5.1. An interlaboratory comparison	98
5.2. Plasma modification procedure of poly(propylene) and chemicals used	99
5.3. Derivatization protocol	99
5.4. XPS analysis and data evaluation.....	100
5.5. Results and discussion.....	102
6. Conclusions – Zusammenfassung.....	106
7. References.....	112

Abbreviations

AcCl	Acetylchloride
AES	Auger electron spectroscopy
ATR	Attenuated reflection spectroscopy
at%	Atomic percent
a.u.	Atomic units
BE	Binding energy
CDCl ₃	Deuterated chloroform
CD-ToF-SIMS	Chemical derivatization time-of-flight secondary ion mass spectrometry
CD-XPS	Chemical derivatization X-ray photoelectron spectroscopy
CLSM	Confocal laser scanning microscopy
DAE	Diaminoethane
DHy	Dansyl hydrazine
DMSO-D ₆	Deuterated dimethylsulfoxide
EK	Kinetic energy
EtOH	Ethanol
Fluram	Flourescamin
FTIR	Fourier transform infrared spectroscopy
¹ H-NMR	¹ H - Nuclear magnetic resonance spectroscopy
MIR	Multiple internal reflection spectroscopy
NEXAFS	Near-edge X-ray absorption fine structure
PFA	Peak fit analysis
PFB	Pentafluorobenzaldehyde
PIC	Phenyl isocyanate
PPEDA	Plasma polymerized ethylenediamine
PE	Polyethylene
PP	Polypropylene
ppm	Parts per million
r.f.	Radio frequency
rpm	Rounds per minute
SAM	Self-assembled monolayer

scm	Standard cubic centimetres per minute
SIMS	Secondary ion mass spectrometry
TAA	Titanium di-isopropoxide-bis(2,4-pentandionate)
TDFS	Tridecafluoro-1,1,2,2-tetrahydrooctyl-1-trichlorosilane
TFAA	Trifluoroaceticanhydride
TFBA	4-(trifluoromethyl)-benzaldehyde
TMS	Trimethylsilane
TOF-SIMS	Time-of-flight secondary ion mass spectrometry
QEA	Quantitative elemental analysis
XPS	X-ray photoelectron spectroscopy

1. Introduction

All solid materials interact with their surroundings through their surfaces. The nature of the interactions is determined by the physical and chemical compositions of these surfaces. The surface chemistry will influence factors such as contact potential, catalytic activity, corrosion rates, adhesive properties, wettability and failure mechanisms. Consequently, surfaces influence many important properties of the solid [1]. Controlling the surface density and selectivity of specific functional groups that exist on the surface is therefore crucial. Active functionalities dispersed over surfaces are used as bonding agents for specific molecules and are essential in various biomedical applications [2].

Aminated surfaces are reported to be useful in a vast number of applications such as immobilization of biomolecules and cell growth [3-5], preparation of enzyme electrode sensors [6] and modification of carbon nanotubes [7]. Additionally, in the field of adhesion, amino groups on surfaces can improve the interfacial bonding between fibers and polymer matrices [8]. These functions play also a role in biocompatibility of artificial biomaterials or can be used for covalent bonding of bioactive molecules [9].

Amino group determination on surfaces is a challenging task and X-ray photoelectron spectroscopy (XPS or ESCA) is one of the most widely used methods, also in combination with FTIR [10,11], TOF-SIMS [12], and mass spectroscopy [13]. XPS along with NEXAFS was used by Swaraj et al. [12]. The authors focused their investigation on the in situ characterization of plasma deposited allylamine films.

Direct identification and quantification of amino groups at an aminated surface by XPS is not possible when the amino groups coexist with a manifold of other nitrogen-containing species with similar chemical shifts [12,14,15]. A workaround which is often used in this case is Chemical Derivatization XPS (CD-XPS). Amino groups are reactively tagged with molecular entities, comprising elements not originally present on the surface of the samples, e.g. fluorine. In applying CD-XPS on plasma deposited aminated surfaces, (4-trifluoromethyl)benzaldehyde (TFBA) and pentafluorobenzaldehyde (PFB) are often used as derivatization reagents for primary amino groups. Fluorescence labelling is also successfully applied to determine surface amino groups. Dansyl hydrazine and fluorogenic pyrylium are examples of possible fluorescent markers [11, 16]. However, the characterization and quantification of fluorescently labelled surface functionalities is still complicated. Non-specific adsorption and binding result in enhanced background

fluorescence and quenching phenomena. While fluorescence techniques have the advantage of a higher sensitivity than CD-XPS, they require calibration before quantitative analysis.

Plasma polymers with amino functional groups are important in adhesion science and biotechnology. In the latter case aminated surfaces are a preferred template for the development of cell culture substrates or diagnostic tools such as micro assays [2,17]. Plasma technology might be a solution for a cost effective mass production of those templates [18]. Among other approaches, low-pressure plasma polymerized allylamine films are of potential interest because relatively high concentrations of nitrogen-containing moieties can be obtained and a considerable fraction of them are amino groups [3].

Effects of various external plasma parameters on the chemical character of the plasma polymers have been widely investigated. Most of them have been focused on Yasuda factor [19] (defined as W/FM where W is the power, F is the flow rate and M is the molecular weight of the respective monomer), power and duty cycle. Generally, low values of power and Yasuda factor have shown a greater retention of structures from the monomer in the plasma polymers. Inagaki et. al published similar results in terms of high monomer retention at low power, using a mixture of carbon dioxide with acrylic acid for depositing plasma polymers [20]. Swaraj et al. used allylamine monomer in order to apply plasma polymerization and studied the effect of power, pressure and duty cycle on the monomer retention. They reported that milder plasma conditions show a greater degree of monomer retention on the polymer surface.

When amino groups are considered, it is inevitable to use derivatization techniques in order to study the effects of external plasma parameters. Meanwhile, an optimal derivatization procedure should be developed in order to get a high specificity, a low cross-talk and the maximum yield from the reactions. Thus, CD-XPS should be applied to different functional groups in order to compare the reactions and procedures.

This work has the following aims:

1. To examine surface derivatization reactions of amino groups using TFBA and PFB, and hydroxyl groups using TFAA.
2. Amino group determination on different surfaces (e.g. spin coated surfaces, SAMs, plasma polymerized thin films) and their comparison.

3. To investigate effects of external plasma parameters on amino groups at plasma deposited poly allylamine surfaces.
4. To show the efficient use of XPS and NEXAFS as complimentary tools in surface analysis

2. Chemical derivatization X-ray photoelectron spectroscopy (CD-XPS)

2.1. Introduction

XPS is one of the most widely used surface analytical techniques. It allows a quantitative elemental analysis of surfaces, however its ability to detect and quantify a number of functional groups is limited [21]. In several cases, relative chemical shifts of different groups are below the energy resolution attainable, even by the new generation XP spectrometers, due to the existence of significant intrinsic peak widths [22]. Therefore, the data has only limited value for the determination of the concentration of a particular functional group. For instance, binding energy (BE) shifts of oxygen- or nitrogen-containing surface functional groups are smaller due to their similar electronegativity. The chemical shifts from a large variety of such species are present in a narrow BE window, and many of the peaks indicating these species overlap [23]. Moreover, small BE shifts induced by double bonds are also present in this region, further complicating the analysis of the C 1s spectral envelope. Carbon atoms can be distinguished according to the number of bonds to neighboring oxygen atoms. For instance, a C-O will give a different shift than a C-C or a O-C-O. However, the differentiation of hydroxyl groups from ethers, peroxides and epoxides due to their C1s binding energies is not possible [24]. Similarly, the chemical shifts for nitrogen containing functionalities, such as amine, imine, nitrile or amide on the C 1s or N 1s core levels, are very small.

Table 2.1 is an XPS reference table, displaying C 1s and N 1s binding energy intervals, which are established using literature data. Some of these species, such as aliphatic thiol SAMs, are investigated in this study and results will be discussed.

High resolution XP C 1s and N 1s binding energies obtained from aromatic species may show differences from their aliphatic counterparts. Table 2.2 displays XP C 1s and N 1s binding energy intervals established from literature data of aromatic species.

All samples investigated in this study are analyzed by near-edge X-ray photoelectron spectroscopy (NEXAFS) in conjugation with XPS. NEXAFS spectra of amino groups on surfaces revealed that there is a broad range of spectral data and interpretations. To summarize the status, NEXAFS data are listed in the present chapter for various amine compounds, taken from dedicated measurements of this study and from the literature.

Table 2.1. XPS reference table with N 1s and C 1s binding energies for aliphatic species. BE intervals are established using literature data together with those of our own measurements.

	Binding energy	
N=C	397.8-399.0	[25,26]
N≡C	398.0	
N=C=C	398.8	[26]
NH₂	399.1-399.6	[25]
NHC=O	400.3-400.7	
---NH₂/NH₃⁺	400.9-401.7	
C-Si	284.4	[27]
C-C, C-H	285	
C-COOH (β-COOH)	285.2	[28]
C-N, C-O, C=N/C≡N	C-N 285.7-286.0 [25, 28, 29] C=N/C≡N 286.5-286.7 [25, 29] C-O 286.2-286.7 [25, 27, 28, 29]	
C=O	287.6-287.9 [25] amide: 287.9-288.3 [28,29]	
COOH	289.3-290.5	[28]
COOR	289.4	

Table 2.2. XPS reference table with N 1s and C 1s binding energies for aromatic species investigated in this study. BE intervals are established using literature data together with those of our own measurements.

	Binding energy	
N=C	397.8-399	[30]
NH₂	399.0-399.3	[30]
NHC=O	400.3-400.7	
---NH₂/NH₃⁺	400.6-401.9	
C-Si	284.4	
C-C, C-H + C_{arom}	285 + 284.3	
C-N, C-O, C=N/C≡N	C-N 285.7-286.0 [29] C=N/C≡N 286.5-286.7 [25,29] C-O 286.2-286.7 [29]	
C=O	287.6-287.9 amide: 287.9-288.3	
COOH	289.3-290.5	

Table 2.3 displays the NEXAFS reference table with C and N K-edge resonance energy intervals for aliphatic species. Energy intervals are established using literature data and those of our own measurements. Table 2.4 displays NEXAFS and N K-edge resonance energy intervals of aromatic species, which are investigated in this study or found in literature.

Table 2.3. NEXAFS reference table with N and C K-edge resonance energies for aromatic species investigated in this study. BE intervals are established using literature data together with those of our own measurements.

	Resonance energies	
	Data from literature	
N1s → π^* (N=C, N-C=C)	N=C 397.5-399.1 [12,15,26,29,31] N-C=C 398.7 [29]	
N1s → π^* (N≡C, N=C=C)	N≡C 399.0-8/400.0/402.0 [29,31,32] N=C=C 398.7-8/401.5-402.0 [26,32]	
N1s → σ^* (N-H) of NH ₃ ⁺	398/406.0 [31,33]	
N1s → σ^* (N-H)	400.6-401.5 [33]	
N1s → π^* (NHC=O)	401.0/405.1 [31]	
N1s → σ^* (N-C)	405.0-406.7 [29]	
N1s → σ^* (N=C)	411.1 [29]	
N1s → σ^* (N≡C)	423.3 [29]	
C1s → π^* (C=C, C=N, C≡N)	C=C 284.9-285.5 [15,29,34] C=N 285.5-9 [15,29,34] C≡N 286.6-9 [15,29,34,35] C=C-NH ₂ 286.5-8	
C1s → σ^* (C-H)	287.5-288.5 [29,34]	
C1s → π^* (C=O)	288.2-288.7 [29,34,35]	
C1s → σ^* (C-C, C-N)	292.0-292.9 [29,34]	
C1s → σ^* (C=C, C=N)	301.5-302.5 [29]	

Table 2.4. NEXAFS reference table with N and C K-edge resonance energies for aliphatic species derived from literature data together with those of our own measurements.

	Resonance energies	
	Data from literature	
N1s → π^* (N=C, N-C=C)	N=C 397.5-399.1 [12,15,26,29-31] N-C=C 398.7 [31] aromatic π^* 398.4 [29]	
N1s → π^* (N≡C, N=C=C)	N≡C 399.0-8/400.0/402.0 [12,15,29,31] N=C=C 398.7-8/401.5-402.0 [26,32]	
N1s → σ^* (N-H) of NH ₃ ⁺	406.0 [31]	
N1s → σ^* (N-H)	400.6-401.6 [29-31]	
N1s → π^* (NHC=O)	401.0/405.1 [31]	
N1s → σ^* (N-C)	405.4-407.9 [29]	
N1s → σ^* (N=C)	411.1 [29]	
N1s → σ^* (N≡C)	423.3 [29]	
C1s → π^* (C=C, C=N, C≡N)	C=C 284.9-285.4 [15,29,34] C=N 285.5-9 [15,29,34] C≡N 286.6-9 [15,29,34,36] C=C-NH ₂ 286.5-8 C=C _{ring} 289.0 [33]	
C1s → σ^* (C-H)	287.5-288.5 [29,34]	
C1s → π^* (C=O)	288.2-288.7 [29,34,35,36]	
C1s → σ^* (C-C, C-N)	292.0-292.9 [29,34]	
C1s → σ^* (C=C, C=N)	301.5-302.5 [29]	

The identification and quantification of functional groups can be improved significantly by chemical derivatization. The method is based on a specific reaction between the targeted functional group and a reagent containing a tag atom (e.g. fluorine), which is not

part of the studied surface. Quantitative analysis of the tag is then fulfilled by XPS where derivatization may offer a significant decrease in the detection limit of the derivatization reagent. Since the selected reagent usually contains more than one tag atom, the sensitivity is increased due to the enhanced stoichiometry of the reagent and through the high cross-section of the tag element.

The particular requirements for the successful development of a derivatization reaction involve:

1. The selection of a reagent with an element having a high photoionization cross section.
2. Stability under analysis conditions (X-rays and vacuum in XPS).
3. Selectivity, where the reagent tags only the desired functional group quantitatively, over the entire sampling depth of the technique [24].
4. A high yield of the reaction between desired surface functional group and the derivatization reagent.

2.2. Chemical derivatization methods and reagents used for amino and hydroxyl group derivatizations

Liquid-phase or gas-phase reactions are the two derivatization modes, which have been used prior to XPS analysis. In liquid-phase reactions, the surface contacts the solvent often for extended period of time, which can lead to a reorganization of the polymer surface. Rasmussen et al. investigated and characterized the functional groups presence in the surface region of chemically oxidized polyethylene (PE) [37]. They showed that the surface groups were highly mobile and migrate into the subsurface region (depth ≥ 1 nm) under certain conditions. Since XPS only samples the top 100 Å, the migration of surface functional groups into the subsurface region – below the sampling depth of XPS – complicates the quantitative estimation of the functional group of interest. Using solvents in order to induce the considerable functional group mobility can cause leaching of low molecular weight components. The reaction solvent may also influence the surface by swelling, dissolution or extraction. Such disadvantages complicate the use of liquid-phase derivatization reactions for the quantitative estimation of surface functional groups. Consequently, vapour-phase derivatization reactions seem more advantageous due to their less restructuring of the polymer surface. However, they are difficult to implement successfully because of the additional requirement of volatility of the imposed liquid reagents. Consequently, the reagent must be

restricted to liquids of low boiling points or to gases. Mostly reactions are applied under vacuum in order to work at room temperature. If the derivatization chambers are needed to be heated, a great care must be taken in order to prevent disturbances, such as dissolution of thin films under direct contact to the heated chamber walls.

The most frequently used solution media in the liquid-phase derivatization reactions are pentane and nonhydrous EtOH. The samples are introduced to the boiling solvents in a reflux condenser containing the reagents. Reaction times are 2-4 hours depending on the reagent and the solvent. After derivatization, the sample is washed carefully in order to remove the unreacted and adsorbed reagents. Sonicated baths with different solvents or the clean hot reaction solvent are used for washing. However, most commonly Soxhlet extraction is applied for around 12 h to the derivatized samples.

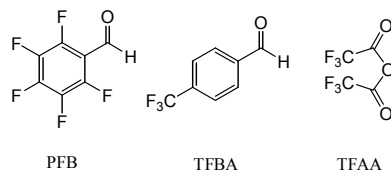


Figure 2.1. The structures of pentafluorobenzaldehyde (PFB), (4-trifluoromethyl)benzaldehyde (TFBA) and trifluoroacetic anhydride (TFAA)

Up to now, the accessibility and the reactivity of the amino groups are studied by means of tagging reactions mostly with reagents, such as pentafluorobenzaldehyde (PFB), (4-trifluoromethyl)benzaldehyde (TFBA) and with trifluoroacetic anhydride (TFAA) in liquid and in vapour phases [2,10,38-41]. The structures of the derivatization reagents are shown in the Fig. 2.1.

Both PFB and TFBA are solely reactive towards primary amines where TFAA reacts with primary and secondary amines. Consequently, the reagents are specific against amines. Other nitrogen functional groups, such as amides, imines and nitriles, do not react with the derivatization reagents. The expected reactions during derivatization are shown in the Fig. 2.2.

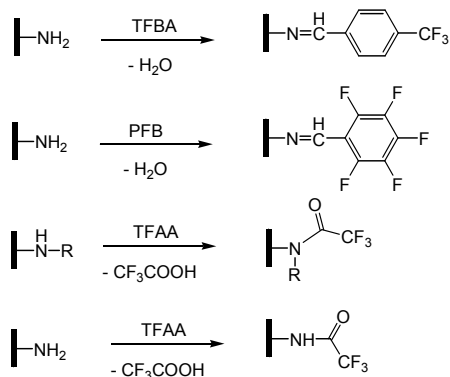


Figure 2.2. A scheme of surface gas phase derivatization reactions of both primary and secondary amino groups.

Boiling points of all three reagents are (PFB: 164-166 °C, TFBA: 180 °C and TFAA: 40 °C) suitable for both liquid and gas phase reactions. Only a few reports discuss the use of TFAA as an amino group tag [22,42,43] since the hydroxyl groups present on the surface are compatible with the reagent. When $-\text{OH}$ and $-\text{NH}_x$ groups are expected in a sample, it is challenging to distinguish these groups by the elemental composition. The reagent can be bonded to $-\text{OH}$ or $-\text{NH}$ - or $-\text{NH}_2$. Another disadvantage of TFAA is its air-sensitivity. The reaction should be done with great care in order to prevent or minimize a possible hydrolyzation. Due to the disadvantages and the possible side reactions, TFAA was only used for the derivatization of hydroxyl groups which is explained in the following chapters.

TFAA is by far the most applied derivatization reagent for $-\text{OH}$ group determinations either in the gas [44,45] or liquid phase [46]. Its high vapour pressure makes it perfectly suitable for gas phase reactions. The reactions are fast and usually lead to a high yield [45]. However, when TFAA is applied to a surface containing exclusively oxygen-carrying functional groups, few side reactions may occur. For instance, the epoxy group may give a similar reaction. As already mentioned, TFAA is able to react with other nucleophilic functional groups, such as amines or thiols. Ratner et al. carried out an X-ray photoelectron spectroscopic investigation of the selectivity of hydroxyl derivatization reactions [47]. TFAA, acetylchloride (AcCl) and heptafluorobutyl-chloride (HFBuCl) were used in order to derivatize surface hydroxyl groups. The results showed that none of the three reagents were hydroxyl selective in the presence of other oxygen carrying functional groups, especially epoxides. Additionally, HFBuCl is reactive towards unsaturated groups. The reactions are shown in Fig. 2.3.

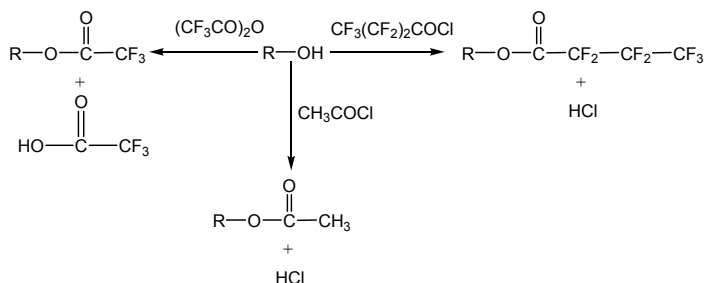


Figure 2.3. Hydroxyl derivatization reactions with $(\text{CF}_3\text{CO})_2\text{O}$ (TFAA), $\text{CH}_3\text{C}(\text{O})\text{Cl}$ (AcCl) and $\text{CF}_3(\text{CF}_2)_2\text{C}(\text{O})\text{Cl}$ (HFBuCl).

There are some alternative derivatization reagents for surface hydroxyl groups when it is necessary to avoid side reactions. Malitesta et al. used titanium di-isopropoxide-bis(2,4-pentandionate) (TAA) in order to detect -OH groups on the surfaces of electrosynthesized polypyrroles (Fig. 2.4). The area of the high resolution Ti 2p spectrum was correlated to the number of derivatized -OH groups [21].

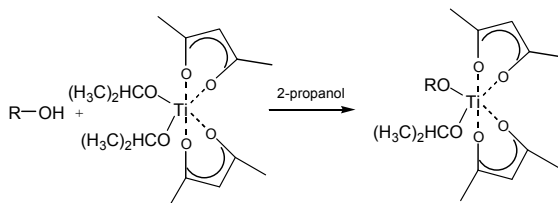


Figure 2.4. Titanium di-isopropoxide-bis(2,4-pentandionate) derivatization of surface hydroxyl groups.

Dang et al. achieved the labelling of -OH groups through silylation with tridecafluoro-1,1,2,2-tetrahydrooctyl-1-trichlorosilane (TDFS). This allows the detection of -OH groups on glass since they cannot be identified by XPS directly when glass is used as substrate. Its presence does not result in any significant change in binding energy of either Si or O. The Si content could be estimated by calculating the fluorine content due to the reaction shown in Fig. 2.5 [38].

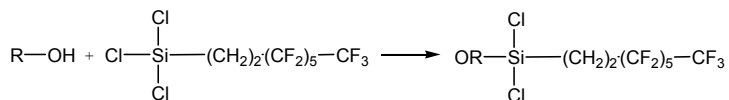


Figure 2.5. Silylation of surface -OH groups. Although all three labile chlorine groups of the silane molecule are available for silylation with the -OH groups in glass, only one bond is generally formed from each silicon of the silane to the glass substrate.

Ivanov et al. used fluorescence labelling for surface hydroxyl groups on plasma polymerized polyethylene films (Fig. 2.6). Dansyl chloride was coupled to -OH groups. Although the reaction procedure is long and complicated, fluorescence labelling is a sensitive tool for quantitative determination of surface hydroxyl groups [48].

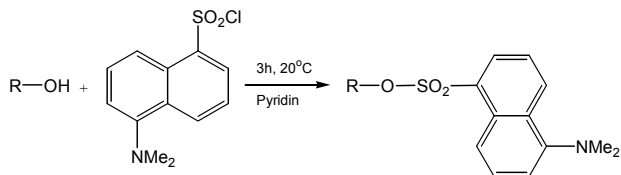


Figure 2.6. Derivatization of hydroxyl groups by dansyl chloride.

Hollaender et al. studied fluorescence labelling in order to detect carbonyl and primary amino groups [16]. They reported that dansyl hydrazine (DHy) and fluorescamin (fluram) label carbonyl and amino groups, respectively. As with all fluorescence markers, tagging reactions were carried out in liquid phase. Oxygen plasma treated polyethylene films, which carry carboxyl groups ($>C=O$) were used. These groups form a Schiff base ($>C=N-CH_2-CH_2-NH_2$) with diaminoethane (DAE). The nitrogen concentration represents the carbonyl concentration. DHy reacts in a similar way to DAE. Coupling of fluorescamin to the $-NH_2$ groups of DAE functionalized surface was done in another experiment. Fig. 2.7 displays the functionalities on the surface after the reaction with DAE (a), DHy (b) and fluorescamin (c), respectively. It is reported that the fluorescence yield of fluram is considerably higher than the dansyl fluorophore and the resulting spectrum is more intense. They concluded that the detection limit of fluorescence labelling is much lower than the detection limit of XPS, even if it is considered that the XPS sensitivity of nitrogen is small.

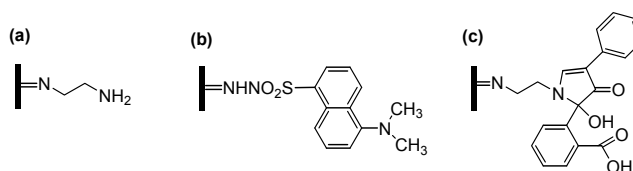


Figure 2.7. Oxygen plasma treated polyethylene after reaction with DAE (a), DHy (b), and fluorescamin (c).

2.3. Characterization of derivatized surfaces by other analytical methods

Derivatization techniques have been extensively used in conjunction with a wide variety of analytical techniques, such as Fourier transform infrared spectroscopy (FTIR), near

edge X-ray absorption fine structure (NEXAFS) spectroscopy, time-of-flight secondary ion mass spectrometry (TOF-SIMS) and fluorescence spectroscopy.

Before XPS, the only technique available for studying polymer surfaces was reflection infra-red spectroscopy (either attenuated reflection (ATR) or multiple internal reflection (MIR) spectroscopy). This technique requires fairly large samples with flat or easily deformable surfaces and typically gives information pertaining to » 1 mm into the material. In the recent years, improved FT-IR techniques allow an increased surface sensitivity and a decreased sample size. Due to its ease of use, high chemical bonding information and indestructibility, FT-IR became one of the most widely used analytical techniques to identify specific chemical functional groups in numerous types of organic and biological samples [17]. In particular, the surfaces of organic thin layers [2,49], including plasma deposited films [2,50] have been characterized using attenuated total reflection [2,51] and reflection-absorption FT-IR [52-55]. Despite the advantages, FT-IR has played an ancillary role in the quantification of specific surface chemical compositions. Functional groups are usually analyzed using better quantitative surface analysis techniques, such as XPS, mainly because the extinction coefficients for organic thin layers are unknown in FT-IR and even in the most favourable cases, FT-IR cannot match the sensitivity of XPS. For compensation, several studies have quantified organic thin layers by using FT-IR spectroscopy with another technique, such as XPS [2,56].

The application of Auger electron spectroscopy (AES) in this field has commonly been discounted on the grounds of unacceptably high rates of radiation damage.

Another vibrational spectroscopy with much potential in this area is Raman spectroscopy. Spectra from thin polymer films have been described and with the Raman microprobe it is possible to analyse polymeric materials at high spatial resolution (» 1 mm) while sampling the first few micrometers. The great advantage of the vibrational spectroscopies is their ability to comment on morphology, which is a very important aspect of polymeric structures.

In parallel with the growth and development of XPS over the last three decades, the technique of secondary ion mass spectrometry (SIMS) has also been evolving. The basic principle of SIMS is the bombardment of a surface with a beam of energetic ions and subsequent mass analysis of the sputtered ions and cluster ions. SIMS has much higher elemental sensitivity than XPS and all elements including hydrogen, can be detected by this method. Additionally, as the analysis is based on the mass separation of the secondary particles, it has both, isotopic and molecular specificity. The time-of-flight (TOF) mass

spectrometer is ideal for static SIMS applications. Using this instrument, the ion beam is operated in a pulsed mode, which minimizes the number of incident ions and therefore maximizes the available information. CD-ToF-SIMS was also used by Lee et al. in order to quantify surface amino groups [17]. Characteristic molecular secondary ions of chemical tags are detected by TOF-SIMS. The surface amino groups on plasma polymerized ethylenediamine (PPEDA) films were quantified using UV-visible absorption spectroscopy compared to FT-IR, XPS and TOF-SIMS. In order to determine the surface amine density on PPEDA by UV-visible spectroscopy, the non-absorbing amine groups were converted into nitrobenzyl-substituted imines [39]. Then, a correlation correlated between surface amine densities and normalized TOF-SIMS, XPS and FT-IR intensities is applied. It is published that TOF-SIMS revealed a good correlation between surface amine density and the secondary ion signal of the chemical tag molecules. Quantifications by SIMS can be carried out accurately by comparison of the specimen being examined with standards of very close composition. However, for routine analysis of unknown specimens, quantification will not usually be attempted.

Since often used surface sensitive methods (e.g. FT-IR and XPS) are costly and often fail at low concentrations, the use of simple and sensitive fluorometric methods in conjunction with labelling techniques are very attractive. Although the detection of characteristic emission bands of surface-linked fluoropores have been often reported [48,57], the potential of fluorometry to identify and quantify reactive groups and intermediates at surfaces is still under discussion [58].

Steady-state spectrofluorometry and confocal fluorescence microscopy were applied by Resch-Genger et al. in order to monitor the amino functionalities on plasma coated polypropylene (PP) [11]. They used a chromogenic and fluorogenic pyrilium label Py-1. The corresponding derivatization reaction is shown in Fig. 2.8.

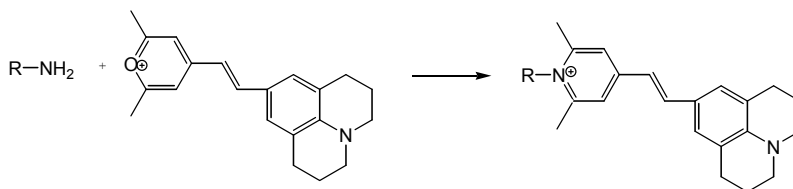


Figure 2.8. The marker reaction of the blue fluorescent reporter Py-1 with surface amino functionalities, yielding a red polymer conjugate.

Steady-state spectrofluorometry, although commonly applied for fluorometric surface analysis, is a bulk measurement technique that cannot differentiate between surface-attached dye molecules and dye molecules diffused into the support material. On the other hand, the confocal laser scanning microscopy (CLSM) yield the emission intensity as a function of the z-axis from the top of the polymer support, within the film and from its bottom, enabling the distinction between the dye molecules attached to amino groups localized at the PP surface and fluoropores diffused into deeper layers of the substrates. The authors published that Py-1 is a suitable fluorescent marker to monitor primary amino groups since the reaction takes place at room temperature and it is relatively easy compared to the same kind of marker reactions when markers have bulky groups in ortho positions.

3. Experimental

3.1. Surface characterization techniques

3.1.1. X-Ray Photoelectron Spectroscopy (XPS)

X-ray photoelectron spectroscopy was developed in the mid-1960s by Siegbahn and his co-workers at the University of Uppsala, Sweden [59]. In XPS, electrons are liberated from the specimen as a result of a photoemission process. An electron is ejected from an atomic energy level or a valence band by an X-ray photon, mostly from an Al-K α or Mg-K α primary source, and its kinetic energy is analysed by the spectrometer (Fig.3.1). Then the data presented as a graph of intensity (usually expressed as counts or counts/s or atomic units) versus electron energy is the X-ray induced photoelectron spectrum [1].

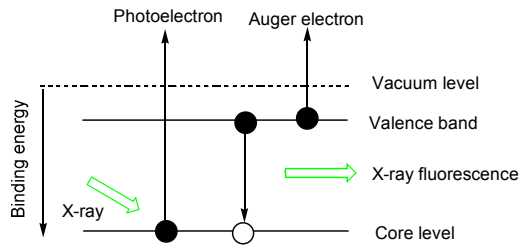


Figure 3.1. Schematic representation of photoionization process and a possible relaxation mechanism.

XPS not only allows to identify and quantify the constituting elements of a sample, but makes it also possible to obtain information on their chemical state. The core level peaks in XPS show a clear shift in binding energy, the so-called chemical shift, related with differences in the chemical environment of the emitting element.

The kinetic energy of the measured electron depends on the energy $h\nu$ of the primary X-ray source. The characteristic parameter for the electron is its binding energy. The relation between these parameters is given by the Equation 3.1 where BE and EK are respectively the binding and the kinetic energy of the emitted photoelectron, $h\nu$ is the photon energy, and ϕ_s is the spectrometer work function.

$$BE = h\nu - EK - \phi_s \quad \text{(Equation 3.1)}$$

3.1.1.1. Surface analysis by XPS

The primary beam of XPS has a penetration depth of a few micrometers. The photoelectron can only travel a limited distance of nanometer scale. Since the mean free path of the electrons in solids is very small, a majority of the detected electrons originate from the top few atomic layers. The distance, electrons travel without undergoing an inelastic collision, is known as the inelastic mean free path. It is typically of the order of 2 to 3 nm for the C1s, O1s, and N1s core levels of organics when electrons have a kinetic energy between 100 to 1000 electron volts (eV). This distance corresponds to around 10 atomic layers in most materials, and thus, the technique is surface sensitive.

3.1.1.2. Qualitative analysis

The qualitative analysis identifies the elements that are present in the specimen. For this purpose, a survey or wide energy scan spectrum is recorded. Each element has a characteristic XPS spectrum and a chemical shift, which can vary from a fraction of an electron volt up to several eVs. The instrumentation of XPS is equipped with data treatment systems running automatic peak identification tools. The computer curve fitting of a high resolution XPS is now a routine application. The identification of composing elements of a sample under investigation is in most cases straightforward, except unless peaks are overlapping.

The shifts observed in XPS are due to both, initial-state and final-state effects. In the case of initial-state effects, the charge on the atom before photoemission is responsible from the value of the chemical shift. Consequently, when the number of bonds to electronegative atoms increases, XPS chemical shift increases. For instance, the binding energy of C1s in a C-F group is shifted by 2.9 eV where CF₂ and CF₃ carrying groups are shifted by 5.9 eV and 7.7 eV respectively.

Final-state effects occur after photoionization. These effects are core hole screening, relaxation of electron orbitals and the polarization of surrounding ions. They play the major role in the determination of chemical shift value. In most metals, a positive shift between the elemental form, mono-, di-, and trivalent ions is expected. Cerium shows an exception by a negative shift of nearly 2 eV between Ce and CeO₂ due to large final-state effects.

3.1.1.3. Quantitative analysis

The intensity (I) of a photoelectron is given by the Equation 3.2.

$$I = n \cdot J \cdot \sigma(E_{kin}) \cdot D(E_{kin}) \cdot T \cdot L \cdot A \cdot \lambda(E_{kin}) \cdot \cos\theta \quad \text{(Equation 3.2)}$$

where n is the number of atoms of the element per cm^3 of the sample, J is the X-ray flux in photons/ $\text{cm}^2 \cdot \text{sec}$, $\sigma(E_{kin})$ is the photoelectric ionization cross-section for the atomic orbital of interest in cm^2 , $D(E_{kin})$ is the detection efficiency for each electron transmitted by the electron spectrometer, T is the analyzer transmission, L is the angular asymmetry of the intensity of the photoemission from each atom, A is the area of the sample from which photoelectrons are detected, $\lambda(E_{kin})$ is the inelastic mean free path of the photoelectrons in the sample, θ is the angle of emission of the electrons measured from the surface normal.

The equation 3.2 leads to

$$n = I / (J \cdot \sigma(E_{kin}) \cdot D(E_{kin}) \cdot T \cdot L \cdot A \cdot \lambda(E_{kin}) \cdot \cos\theta) \quad \text{(Equation 3.3)}$$

The denominator in the Equation 3.3 can be defined as the atomic sensitivity factor, S . If a peak from each of two elements is considered, the Equation 3.4 is obtained:

$$n_1/n_2 = (I_1/S_1)/(I_2/S_2) \quad \text{(Equation 3.4)}$$

This expression may be used for all homogenous samples. Thus, for any spectrometer, it is possible to develop a set of relative values of S for all of the elements. Multiple sets of values are necessary for instruments with multiple X-ray sources at different angles relative to the analyzer and different X-ray energies.

3.1.1.4. Instrumentation of XPS

XPS measurements were carried out with an AXIS Ultra DLD electron spectrometer manufactured by Kratos Analytical, UK. XPS spectra were recorded using monochromated Al $K\alpha$ excitation at a pass energy of 80 eV for survey spectra and 20 eV for core level spectra. The electron emission angle was 0° and the source-to-analyzer angle was 54° . The binding

energy scale of the instrument was calibrated following a Kratos Analytical procedure, which uses ISO 15472 binding energy data [60]. Spectra were taken by setting the instrument to the hybrid lens mode and the slot mode providing approximately a $300 \times 700 \mu\text{m}^2$ analysis area. In case of insulating samples the charge neutralizer was used. The binding energy scale was corrected for charging using an electron binding energy BE of 285.0 eV for the aliphatic hydrocarbon C1s component [61, 62].

3.1.2. Near-edge X-ray absorption fine structure (NEXAFS)

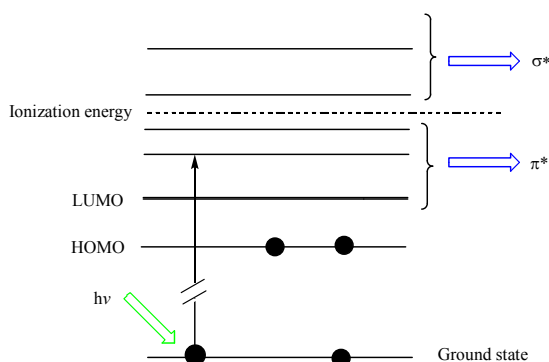


Figure 3.2. Schematic representation of an X-ray absorption process.

Near-edge X-ray absorption fine structure (NEXAFS) spectroscopy, in addition to being surface-sensitive in the electron yield, can provide molecular information that is complementary to XPS, in particular regarding unsaturated moieties. Using polarized, high intensity synchrotron X-rays, NEXAFS also supplies information on functional group orientation [6]. The spectra are obtained by monitoring the absorption of X-rays as a function of energy, close to a core level excitation energy. Absorption is found to occur when the photon energy can promote the core electron to an unoccupied valence orbital [29]. Strong absorption occurs when the symmetry of the valence orbital is optimal, and sharp absorptions occur when the valence orbital energy corresponds to a bound state. In organic polymers, these conditions are best met when there is a π^* orbital, associated with the atom (e.g. when it displays sp or sp^2 hybridization). Fig 3.2 shows a schematic representation of an X-ray absorption process.

3.1.2.1. Instrumentation of NEXAFS

NEXAFS spectroscopy was carried out at the HE-SGM monochromator dipole magnet beam line at the synchrotron radiation source BESSY II (Berlin, Germany). Spectra were acquired at the C, N and F K-edges in the TEY (total energy electron yield) mode [33]. The resolution $E/\Delta E$ of grid 1 at the carbonyl π^* resonance of CO ($h\nu = 287.4$ eV) was found to be in the order of 2500. The slit-width used was 150 μm . Spectra were recorded at an angle of 55° measured between the surface plane of the sample and the direction vector of the incident linearly polarized light beam. In case of thiol SAMs spectra were recorded also at angles of 30° and 90° . Energy alignment of the energy scales were achieved by using an I_0 feature referenced to a $\text{C}1s \rightarrow \pi^*$ resonance measured with a fresh surface of a HOPG (Highly Ordered Pyrolytic Graphite, Advanced Ceramic Corp., Cleveland, USA) at 285.4 eV [63]. Spectra are shown with the pre-edge count rate subtracted and after normalization in units of the absorption edge jump [33].

3.1.3. Error estimations

The reported XPS values for N/C and O/C ratios or component areas after peak fittings in this work have an estimated statistical error of 5%. For the cases where an error bar is shown, the method of calculation is explained in the corresponding chapter. For NEXAFS studies, no error estimation is done since the data is not used for quantification.

3.1.4. ^1H - Nuclear magnetic resonance spectroscopy (^1H -NMR)

NMR spectroscopy is one of the principal techniques used to obtain chemical and structural information about molecules. NMR exploits the magnetic properties of nuclei and measures their radio frequency absorptions. Depending on the local chemical environment, different protons in a molecule each resonate at slightly different frequencies. Since this frequency is dependent on the strength of the magnetic field, it is converted into a field-independent value, known as the chemical shift. By understanding different chemical environments, the chemical shift can be used to obtain structural information about the investigated molecule to assign signals to an atom or a group of atoms [64].

3.1.4.1. Instrumentation of NMR

The NMR spectra were measured with a 400 MHz multicore spectrometer from the company Joel. CDCl_3 and DMSO-D_6 were used as solvent. Trimethylsilane (TMS) was used as reference.

3.2. Preparation of test samples

3.2.1. Liquid-phase derivatization reactions of PFB and TFBA

3.2.1.1. Chemicals used

4,4'-methylenebis(2,6-dimethylaniline) (CAS 4073-98-7) was purchased from Aldrich, 4,4'-methylenebis(2,6-diethylaniline) (CAS 13680-35-8), 4,4'-methylenebis(2,6-diisopropylaniline) (CAS 19900-69-7) and 2,2'-diaminobibenzyl (CAS 34124-14-6) were supplied from Acros Organics.

The derivatization reagents of 4-(trifluoromethyl)-benzaldehyde (TFBA) (CAS455-19-6) and pentafluorobenzaldehyde (PFB) (CAS 653-37-2) were supplied from Alfa Aesar. Ethanol (CAS 64-17-5) used as the solvent was purchased from Merck KGaA.

3.2.1.2. Reaction of 4,4'-methylenebis(2,6-dimethylaniline) with PFB

1 mmol (0.25 g) of 4,4'-methylenebis(2,6-dimethylaniline) was refluxed with 2 mmol (0.39 g) of PFB in 10 ml of ethanol for 2 h. The colour of the solution turned into yellow immediately after the addition of PFB. Very fast formation of a white precipitate was observed. The reaction displayed in Fig. 3.3. The product kept in the fridge overnight and the powder was filtrated the next day and dried under vacuum.

Yield: 0.54 g, 89%, $^1\text{H-NMR}$ (400 MHz, CDCl_3) δ [ppm] = 1.13 (s, 12H, $[\text{CH}_3]$), 3.94 (s, 2H, $[\text{CH}_2]$), 6.91 (s, 4H, aromatic), 8.37 (s, 2H, $[\text{CH}=\text{N}]$).

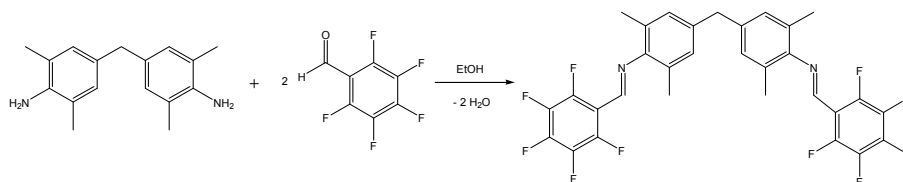


Figure 3.3. Reaction between 4,4'-methylenebis(2,6-dimethylaniline) and PFB.

3.2.1.3. Reaction of 4,4'-methylenebis(2,6-dimethylaniline) with TFBA

1 mmol (0.25 g) of 4,4'-methylenebis(2,6-dimethylaniline) was refluxed with 2 mmol (0.35 g) of TFBA in 10 ml of ethanol for 2 h. The light pink colour of the 4,4'-methylenebis(2,6-dimethylaniline) – ethanol solution turned into yellow after the addition of TFBA. A clear yellow solution formed during reflux. The solution was reduced and kept in the fridge overnight. A yellow powder formed until the next day which was filtered off and dried under vacuum.

Yield: 0.48 g, 86%, $^1\text{H-NMR}$ (400 MHz, CDCl_3) δ [ppm] = 1.13 (s, 12H, $[\text{CH}_3]$), 3.95 (s, 2H, $[\text{CH}_2]$), 6.98 (s, 4H, aromatic), 7.73 and 8.02 (d, 8H, aromatic), 8.26 (s, 2H, $[\text{CH}=\text{N}]$).

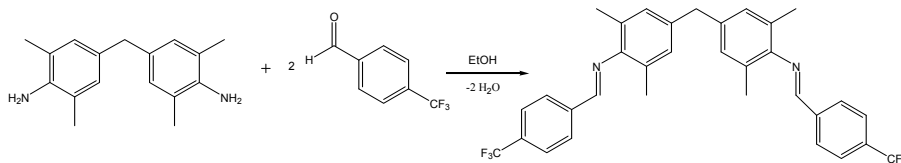


Figure 3.4. Reaction between 4,4'-methylenebis(2,6-dimethylaniline) and TFBA.

3.2.1.4. Reaction of 4,4'-methylenebis(2,6-diethylaniline) with PFB

1 mmol (0.31 g) of 4,4'-methylenebis(2,6-diethylaniline) was refluxed with 2 mmol (0.39 g) of PFB in 10 ml of ethanol for 2 h (Fig. 3.5). The reaction formed a clear green solution and kept in the fridge overnight. The yellow precipitate was filtered and dried under vacuum.

Yield: 0.57 g, 87%, $^1\text{H-NMR}$ (400 MHz, CDCl_3) δ [ppm] = 1.14 (tr, 12H, $[\text{CH}_3]$), 2.47 (q, 8H, $[\text{CH}_2]$), 3.91 (s, 2H, $[\text{CH}_2]$), 6.93 (s, 4H, aromatic), 8.36 (s, 2H, $[\text{CH}=\text{N}]$).

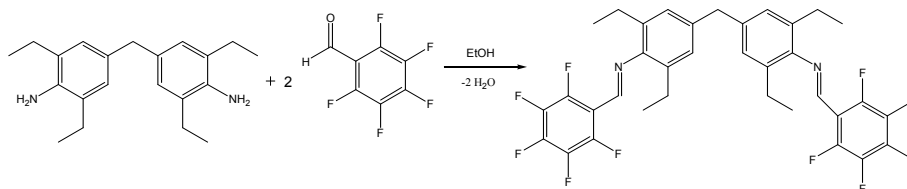


Figure 3.5. Reaction between 4,4'-methylenebis(2,6-diethylaniline) and PFB.

3.2.1.5. Reaction of 4,4'-methylenebis(2,6-diethylaniline) with TFBA

1 mmol (0.31 g) of 4,4'-methylenebis(2,6-diethylaniline) was refluxed with 2 mmol (0.35 g) of TFBA in 10 ml of ethanol for 2 h (Fig. 3.6). The reaction formed a clear yellow solution and kept in the fridge. After a couple of hours, the formation of a precipitate was observed but the solution cooled overnight. Then the yellow powder is filtered and dried under vacuum.

Yield: 0.52 g, 87%, $^1\text{H-NMR}$ (400 MHz, CDCl_3) δ [ppm] = 1.10 (tr, 12H, $[\text{CH}_3]$), 2.47 (q, 8H, $[\text{CH}_2]$), 3.92 (s, 2H, $[\text{CH}_2]$), 6.95 (s, 4H, aromatic), 7.75 and 8.01 (d, 8H, aromatic), 8.28 (s, 2H, $[\text{CH}=\text{N}]$).

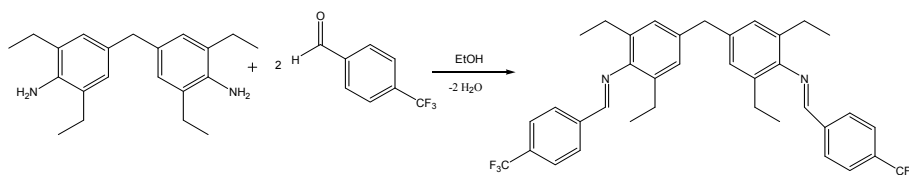


Figure 3.6. Reaction between 4,4'-methylenebis(2,6-diethylaniline) and TFBA.

NMR data shows that the product is clean. The yield can be improved by evaporating more solvent from the mother solution.

3.2.1.6. Reaction of 4,4'-methylenebis(2,6-diisopropylaniline) with PFB

4,4'-methylenebis(2,6-diisopropylaniline) has a purity of 85%, which has to be taken into considerations during the calculations.

1 mmol (0.43 g, 85% purity) of 4,4'-methylenebis(2,6-diisopropylaniline) was refluxed with 2 mmol (0.39 g) of TFB in 10 ml of ethanol for 2 h. The clear reaction solvent kept in the fridge overnight and the powder was filtered the next day and dried under vacuum. The reaction between 4,4'-methylenebis(2,6-diisopropylaniline) and PFB is shown in Fig. 3.7.

Yield: 0.62 g, 80%, $^1\text{H-NMR}$ (400 MHz, CDCl_3) δ [ppm] = 1.14 (d, 24H, $[\text{CH}_3]$), 2.92 (sep, 4H, $[\text{CH}]$), 3.98 (s, 2H, $[\text{CH}_2]$), 6.87 (s, 4H, aromatic), 8.32 (s, 2H, $[\text{CH}=\text{N}]$).

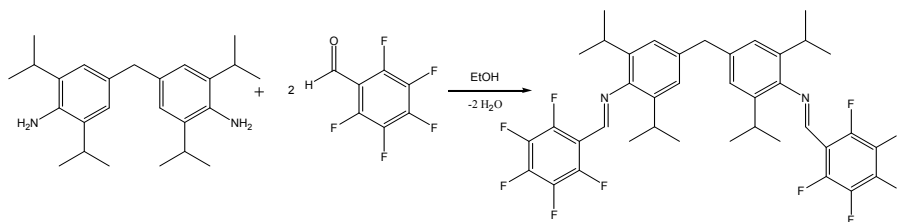


Figure 3.7. Reaction between 4,4'-methylenebis(2,6-diisopropylaniline) and PFB.

3.2.1.7. Reaction of 4,4'-methylenebis(2,6-diisopropylaniline) with TFBA

1 mmol (0.43 g, 85% purity) of 4,4'-methylenebis(2,6-diisopropylaniline) was refluxed with 2 mmol (0.35 g) of TFBA in 10 ml ethanol for 2 h. The clear yellow solution was kept in the fridge overnight, filtered the next day and dried under vacuum. The reaction between 4,4'-methylenebis(2,6-diisopropylaniline) and TFBA is displayed in Fig. 3.8.

Yield: 0.53 g, 78 %, $^1\text{H-NMR}$ (400 MHz, CDCl_3) δ [ppm] = 1.12 (d, 24H, $[\text{CH}_3]$), 2.91 (sep, 4H, $[\text{CH}]$), 3.99 (s, 2H, $[\text{CH}_2]$), 7.00 (s, 4H, aromatic), 7.74 and 8.01 (d, 8H, aromatic), 8.24 (s, 2H, $[\text{CH}=\text{N}]$).

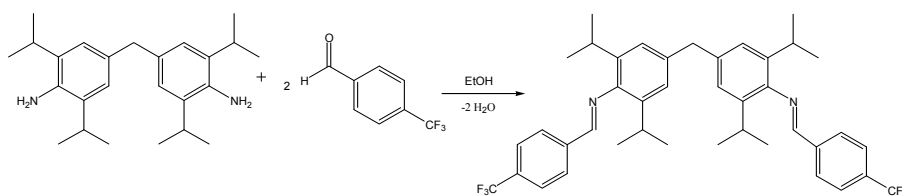


Figure 3.8. Reaction between 4,4'-methylenebis(2,6-diisopropylaniline) and TFBA.

3.2.1.8. Reaction of 2,2'-diaminobibenzyl with PFB

1 mmol (0.21 g) of 2,2'-diaminobibenzyl was refluxed with 2 mmol (0.39 g) of TFB in 10 ml of ethanol for 2 h. The product formed immediately. The colourless powder was filtered and dried in the oven. Yield: 0,47 g, 83%.

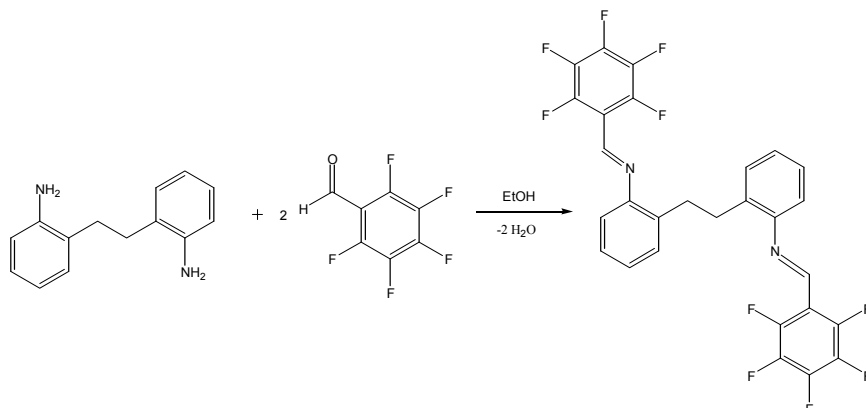


Figure 3.9. Reaction between 2,2'-diaminobibenzyl and PFB.

Due to its insolubility in chloroform, hot DMSO was used where the product was slightly soluble. Because of the high signal to noise ratio, the integration could not be applied. However, the absence of the aldehyde signal and the intensive peak at 8.39 ppm shows the formation of the Schiff base. The reaction is displayed in Fig. 3.9.

3.2.1.9. Reaction of 2,2'-diaminobibenzyl with TFBA

1 mmol (0.21 g) of 2,2'-diaminobibenzyl was refluxed with 2 mmol (0.35 g) of TFBA in 10 ml of ethanol for 2 h. The yellow solution was kept in the fridge overnight. A colourless powder was formed and filtered. The reaction is displayed in Fig. 3.10.

Yield: 0,45 g, 88%, $^1\text{H-NMR}$ (400 MHz, CDCl_3) δ [ppm] = 3.10 (s, 4H, $[\text{CH}_2]$), 6.76 – 7.17 (m, 8H, aromatic), 7.66 and 7.87 (d, 8H, aromatic), 8.00 (s, 2H, $[\text{CH}=\text{N}]$).

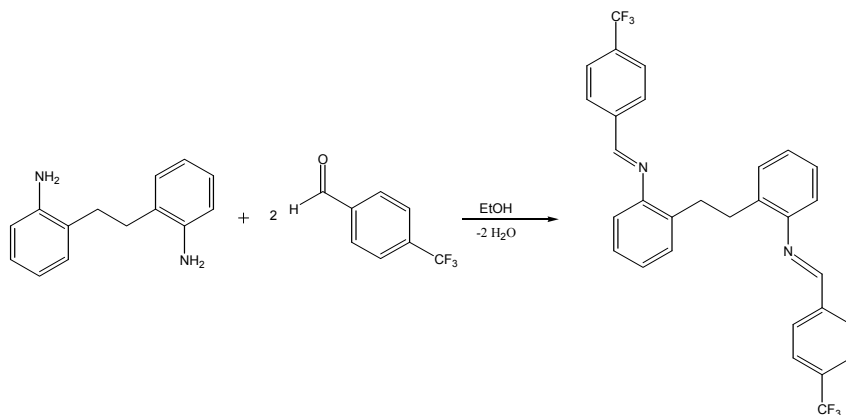


Figure 3.10. Reaction between 2,2'-diaminobibenzyl and TFBA.

3.2.2. Preparation of spin coated 4,4'-methylenebis(2,6-diethylaniline) surfaces

3.2.2.1. Substrates and chemicals used

Silicon (Si) wafers were purchased from Crys Tech GmbH, Germany and were used as substrates for the spin coating. Si wafers were cut to approximately 1 cm by 1 cm square pieces before use. Sulfuric acid (CAS 7664-93-9) and hydrogen peroxide (CAS 7722-84-1) were supplied from Fluka and used in order to clean the Si surfaces. Toluene (CAS 108-88-3) was supplied from Fluka. 4,4'-methylenebis(2,6-diethylaniline) (CAS 13680-35-8) was obtained from Acros Organics.

3.2.2.2. Cleaning procedure for silicon wafers

Si wafers were cleaned three times in an ultrasonic bath with acetone. After rinsing with water, they were dried using a N₂ stream. Then Piranha solution, which typically consists of a 30:70 v/v solution of 30% hydrogen peroxide (H₂O₂) and concentrated sulfuric acid (H₂SO₄), was prepared. The wafers were cleaned in an ultrasonic bath using the following procedure:

1. Heating the Piranha solution to 60°C.
2. Placing the substrates into the Piranha solution for 30 s. The samples should begin bubbling furiously. Prolonged exposure to Piranha solution may result in sample surface roughening.
3. Removing the substrates and rinsing them in a beaker, filled with ultra pure water.
4. Rinsing several times with ultra pure water.
5. Drying with a stream of N₂.

Piranha solution should be handled with extreme care. It is a strong oxidant and reacts violently with many organic materials.

3.2.2.3. Spin coating of 4,4'-methylenebis(2,6-diethylaniline) on Si

Si wafers are used as substrates for spin coated samples of 4,4'-methylenebis(2,6-diethylaniline). A 3% v/v toluene solution of 4,4'-methylenebis(2,6-diethylaniline) was prepared and applied as a droplet onto the Si wafers. Samples were spin coated by the CONVAC TSR 110 spin coater at 3000 rpm for 1 min.

The films were checked with an optical microscope in order to prove their fully coverage.

The prepared surfaces were investigated before and after derivatization by XPS and NEXAFS in order to perform quantitative analysis of the primary amino groups on the surface.

3.2.2.4. Reaction set-up for gas-phase surface derivatizations

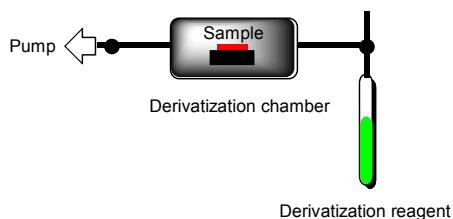


Figure 3.11 Set-up of the derivatization chamber.

Fig. 3.11 shows a scheme of the derivatization set-up. Derivatization reactions were carried out in separate chambers and each chamber was attached to a tube, carrying the correspondent derivatization reagent. The samples were fixed on a metal sample holder and then introduced to the chamber. When the chamber was pumped out, the valve was opened and the reagent penetrated to the chamber. During the derivatization of the spin coated samples, the chamber was heated to 50°C by a hot wire.

3.2.3. Preparation of self-assembled monolayers (SAMs)

3.2.3.1. Chemicals used

The Au substrates, which were used for the deposition of self-assembled monolayers, were purchased from Georg Albert PVD (Germany) prepared by thermal evaporation of 30 nm of Au (purity 99.99%) onto polished single-crystal Si (100) wafers that had been pre-coated with a 9 nm titanium adhesion layer.

1-Undecanethiol, 11-hydroxyundecanethiol and 11-amino-1-undecanethiol hydro-chloride were supplied from Asemblon INC, U.S.A, with a purity of 99%. 4-Amino-phenylbutane-1-thiol was supplied from Terfort et al. and the synthesis has been published [65].

NEt₃, acetic acid, ethanol, poly(allylamine) solution (20% w/w in H₂O, MW ~65,000 g/mol) were purchased from Sigma-Aldrich and were of highest available purity. The Si wafers were purchased from CrysTec Berlin (Germany).

3.2.3.2. Procedure for the preparation of SAMs

For the preparation of SAMs, the substrates were cleaned with piranha solution (dipping for less than 30 s), rinsed with water and ethanol, then immersed into a 1 mM ethanolic solution of thiol monomers, respectively. SAMs were prepared according to a procedure published by Wang et al. [66] where 3% NEt₃ was added to ethanolic solutions of thiols. Reactions took place at room temperature for 24 h in a sealed container which was purged with nitrogen. After immersion, samples were rinsed with ethanol, an ethanolic solution with 10% v/v acetic acid and again ethanol and blown dry with nitrogen.

3.2.3.3. Gas-phase derivatization of SAMs

Gas-phase derivatization of amino terminated SAMs (11-amino-1-undecanethiol hydrochloride and 4-aminophenylbutane-1-thiol) were performed in order to quantify free amino groups on the surface. TFBA and PFB were used as derivatization reagents. Both experiments were applied for 90 min. at room temperature. Surfaces were characterized with XPS and NEXAFS before and after surface derivatizations.

3.2.4. Preparation of plasma polymerized allylamine samples

3.2.4.1. Chemicals used

1cm x 1cm square pieces of silicon wafers were used as substrates. These substrates were cleaned first by isopropanol and then by acetone in an ultrasonic bath for 15 min. each. The substrates were dried by a stream of N₂. All solvents necessary were purchased from Sigma-Aldrich and were of highest available purity. Allylamine was purchased from Merck (CAS 107-11-9),

3.2.4.2. Plasma deposition equipment

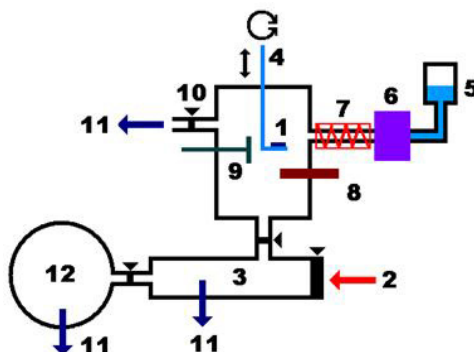


Figure 3.12. The scheme of plasma deposition chamber.

Fig. 3.12 displays the scheme of the plasma deposition chamber. The sample (1) is introduced through a gate (2) to the transfer chamber (3). The sample will be moved by the sample manipulator (4) in the plasma chamber (the chamber on top, without a number). Liquid monomer (5) passes the flow controller (6) and evaporates through a tube (7), heated by a hot wire. Plasma will be produced by an RF plasma generator (8). The film thickness is measured by an oscillating quartz crystal (9). The pressure will be controlled by the valve (10) in front of the vacuum pump (11). After deposition, the sample can be transferred to the XPS chamber (12) and measured in-situ.

3.2.4.3. Preparation and derivatization of plasma deposited allylamine films

Plasma deposited allylamine films were obtained at varying duty cycle, power and pressure. The monomer flow rate was kept constant using a gas flow controller (MÄTTIG, Germany). The thicknesses of the films were kept at 40 nm, which was measured by a water-cooled quartz crystal set to 6 MHz oscillation. As the allylamine introduced to the system, the oscillating frequency was changed and the thickness was monitored. A 13.65 MHz radio frequency (r.f) plasma generator (CESARTM 136), combined with a matching unit (VM1500) made by Dressler, Stolberg, Germany, was used to establish the plasma in the reactor. The pulse frequency can be adjusted in a range of 10 to 10⁴ Hz and the duty cycle of the pulses can be varied between 0.01 and 0.99. The power can be adjusted in a range between 1 and 650W.

Two sets of samples were prepared for XPS and NEXAFS studies. Both sets were derivatized by TFBA and PFB before XPS and NEXAFS measurements. Again, a set of derivatization reactions containing 1, 5, 20, 45, 90 and 180 min. were performed in order to define the saturation time of the reaction.

4. Derivatization of primary amines

4.1. Liquid phase derivatization reactions

It is known that amino groups in general are quite reactive against aldehydes in order to form imines via condensation reactions. Fig. 4.1 demonstrates the reaction mechanism. Surface derivatization reactions are based on the same procedure.

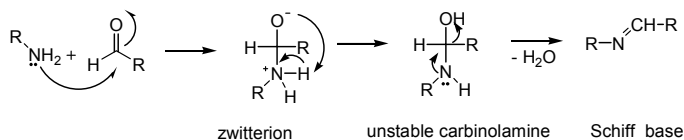


Figure 4.1. Reaction mechanism of the condensation reaction between a primary amino group and an aldehyde.

Before starting with gas phase surface derivatizations, a set of CD-XPS reactions was performed in liquid phase in order to observe the reactivity of the derivatization reagents and to detect reaction yields. Yields of liquid phase reactions are accepted to be the upper limit of gas phase surface derivatizations. Since surface derivatization reactions are rather complicated and may suffer from functional group migration, yields are not accepted to be higher than reactions in liquid phase.

Different compounds carrying primary amino groups with a different sterical hindrance were chosen. Pentafluorobenzaldehyde (PFB) and 4-(trifluoromethyl)-benzaldehyde (TFBA) were reacted with the selected compounds in ethanolic solution under the same conditions. Fig. 4.2 shows three derivatives of 2,6-dimethylaniline, carrying different branching groups. The bulkiness of the groups may have a direct effect on reactivity of the active site and can influence reaction yields, or even reaction completion. A decrease in the yield was expected as the sterical hindrance increases. Because of its size, the isopropyl group in ortho position to the amino functionality shields the amino groups more and was expected to have the highest effect on the reactivity of the compound.

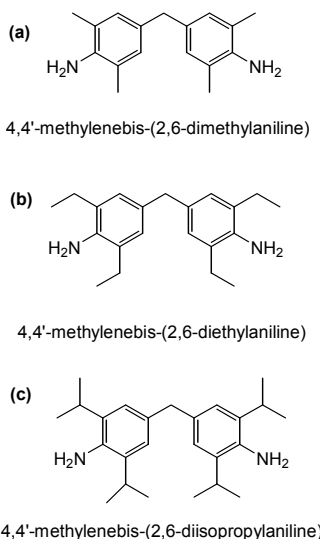


Figure 4.2. Primary amino group carrying compounds: 4,4'-methylenebis(2,6-dimethylaniline) (a), 4,4'-methylenebis(2,6-diethylaniline) (b) and 4,4'-methylenebis(2,6-diisopropylaniline) (c).

However, in all the reactions a high yield (78-89%) is observed. $^1\text{H-NMR}$ s of the products do not show starting material. It is obvious that the reactions are not affected by the steric hindrances of the three compounds. In addition to that, TFBA and PFB do not show any superiority to each other.

Liquid phase derivatization reactions of TFBA and PFB were also applied to 2,2'-diaminobenzyl (Fig. 4.3) in order to investigate the reaction yields.

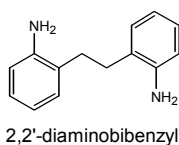


Figure 4.3. Structure of 2,2'-diaminobenzyl

2,2'-diaminobenzyl reacts also readily with PFB and TFBA in order to form the Schiff base with yields of 83% and 88%, respectively.

A reaction time of 2 hours in the boiling solvent was enough for the complete conversion. $^1\text{H-NMR}$ spectra of the residues show no starting material. Because of the fair solubilities of the products in ethanol, quantitative yields are not achieved. Related reactions with yields are shown in Table 4.1.

Table 4.1. Yields (%) of the reactions between the derivatization reagents and the compounds carrying primary amino groups.

	TFBA	PFB
4,4'-methylenebis(2,6-dimethylaniline)	86	89
4,4'-methylenebis(2,6-diethylaniline)	87	87
4,4'-methylenebis(2,6-diisopropylaniline)	78	80
2,2'-diaminobibenzyl	88	83

The gas-phase surface reactions are more challenging than wet chemical reactions due to the possible migration of compounds, unpredictable surface concentrations or contaminations in case of plasma deposited surfaces. Thus, the yield achieved in wet chemical reactions can only be the upper limit when a gas-phase surface reaction is performed.

4.2. Test samples

4.2.1. Spin coated samples of 4,4'-methylenebis(2,6-diethylaniline)

Before starting with the applications of plasma polymerization, a set of spin coated samples were derivatized with TFBA and PFB, in order to study the gas phase surface derivatization reactions. For that purpose, the compound reacting with the highest yield in the liquid phase reactions is chosen (4,4'-methylenebis(2,6-diethylaniline)). A 3% v/v toluene solution of 4,4'-methylenebis(2,6-diethylaniline) was prepared and applied as a droplet onto Si wafers. Samples were then spin coated at 3000 rpm for 1 min. The films were checked with an optical microscope to prove a fully coverage. The prepared surfaces were investigated before and after derivatization by XPS and NEXAFS in order to perform quantitative analysis of the primary amino groups on the surface.

4.2.1.1. XPS and NEXAFS characterization before derivatization

A spin coated surface of 4,4'-methylenebis(2,6-diethylaniline) (Fig. 4.2b) was measured by XPS and NEXAFS before derivatization in order to assign the new peaks due to C-F groups introduced by TFBA and PFB.

The $C_{\text{aromatic}}/C_{\text{aliphatic}}$ and N/C ratios obtained from the XPS data of 4,4'-methylenebis(2,6-diethylaniline) match with the calculated stoichiometry. The ratio of the aromatic carbons to the aliphatic carbons of the compound is 1.33. The value obtained from

the high resolution XP C1s spectra is 1.52. The nitrogen to carbon ratio of the compound is 0.095. The ratio obtained from the survey scan is 0.081. Table 4.2 displays the calculated stoichiometry and atomic percent [at%] obtained from XP survey and high resolution XP C1s spectra of the spin coated 4,4'-methylenebis(2,6-diethylaniline) film.

Table 4.2. Calculated stoichiometry and atomic percent [at%] from XP survey spectra of the spin coated underivatized 4,4'-methylenebis(2,6-diethylaniline) film.

4,4'-methylene bis(2,6-diethyl aniline)	calculated stoichiometry [at%]						obtained from XPS results [at%]					
	[C _{aromatic}]	[C _{aliphatic}]	[N]	[O]	[C _{ar}]/[C _{al}]	[N]/[C]	[C]	[N]	[O]	[Si]	[C _{ar}]/[C _{al}]	[N]/[C]
	12	9	2	-	1.33	0.095	74	6	11	9	1.51	0.081

Aromatic and aliphatic carbons can be differentiated by highly resolved C1s spectra [62]. In this case, the energy difference between aliphatic and aromatic carbons is 0.6 eV. The C-N peak appears at 285.7 eV whereas the C-O peak appears at 286.7 eV. The feature at 288.3 eV is assigned to amide groups [65].

Binding energies [BE(eV)] and area percentages [area%] of carbon functionalities of the spin coated underivatized 4,4'-methylenebis(2,6-diethylaniline) film are displayed in Table 4.3. Binding energies and area percentages are obtained from high resolution XP C1s spectrum.

Table 4.3. Binding energies [BE(eV)] and area percentages [area%] of carbon functionalities of spin coated underivatized 4,4'-methylenebis(2,6-diethylaniline) film. The values are obtained from high resolution XP C1s spectra.

4,4'-methylene bis(2,6-diethyl aniline)	high resolution XP C1s spectra					
	C _{aromatic}	C _{aliphatic}	C-N	C-O	NHC=O	
	284.4	285.0	285.7	286.7	288.3	BE(eV)
53	35	6	2	1	[area%]	

Fig. 4.4 shows the survey scan and the high resolution XP C1s spectra of the underivatized sample

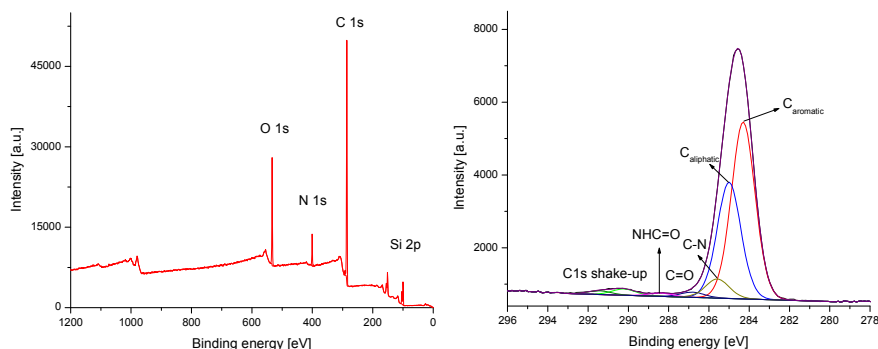


Figure 4.4. XP survey scan and high resolution C1s spectrum of 4,4'-methylenebis(2,6-diethylaniline) spin coated on Si wafer.

The high resolution XP N1s spectrum of the underivatized 4,4'-methylenebis(2,6-diethylaniline) sample shows two sub-peaks. 97% of the nitrogen are assigned to primary amino groups (BE=399.6 eV), 3% is in the form of protonated or hydrogen-bonded amine (BE=401.3 eV). The spectrum is shown in Fig. 4.5. Binding energies [BE(eV)] and area percentages [area%] of nitrogen functionalities of the spin coated underivatized 4,4'-methylenebis(2,6-diethylaniline) film are displayed in Table 4.4. Binding energies and area percentages are obtained from the high resolution XP N1s spectrum.

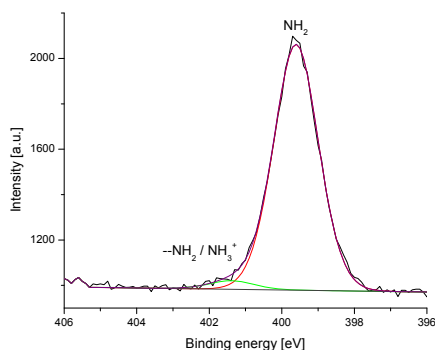


Figure 4.5. High resolution XP N1s spectrum of the spin coated underivatized 4,4'-methylenebis(2,6-diethylaniline) film.

4. Derivatization of primary amines

Table 4.4. Binding energies [BE(eV)] and area percentages [area%] of nitrogen functionalities of the spin coated underivatized 4,4'-methylenebis(2,6-diethylaniline) film. The values are obtained from high resolution XP N1s spectra.

4,4'-methylenebis(2,6-diethylaniline)	high resolution N1s spectrum		
	NH ₂	--NH ₂ / NH ₃ ⁺	
	399.6	401.4	BE(eV)
97	3	[area%]	

A spin coated surface of 4,4'-methylenebis(2,6-diethylaniline) was also characterized by NEXAFS before derivatization in order to assign the new peaks due to C-F groups introduced by TFBA and PFB.

Fig. 4.6 gives the NEXAFS C K-edge (a) and N K-edge (b) of an underivatized spin coated 4,4'-methylenebis(2,6-diethylaniline) film. The C K-edge spectrum displays features at 285.4 eV due to a C1s $\rightarrow\pi^*$ (C=C) resonance and at 288.7 eV corresponding to C1s $\rightarrow\pi^*$ (C=O) resonance. The feature at 286.5 eV is due to amino groups attached to unsaturated bond systems (C=C-NH₂). There are also various σ^* resonances above 292 eV [12]. For further information we rely on the NEXAFS N K-edge spectrum of the spin coated 4,4'-methylenebis(2,6-diethylaniline) film. Several prominent features can be seen in this spectrum. Features at 401.4 and 405.9 eV are widely accepted to be σ^* (N-H) and σ^* (C-N) resonances respectively [29]. The feature at 398.3 eV is assigned as π^* (N-C=C) resonances [29,31,65].

Table 4.5 summarizes C and N K-edge resonance energies for 4,4'-methylene-bis(2,6-diethylaniline).

Table 4.5. C and N K-edge resonance energies obtained from NEXAFS measurements of the spin coated underivatized 4,4'-methylenebis(2,6-diethylaniline) film.

	C K-edge resonance energies (eV)			N K-edge resonance energies (eV)		
	π^* (C=C)	π^* (C=C-NH ₂)	π^* (C=O)	π^* (C=C-NH ₂)	σ^* (N-H)	σ^* (N-C)
4,4'-methylene bis(2,6-diethyl aniline)	285.4	286.5	288.7	398.3	401.4	405.9

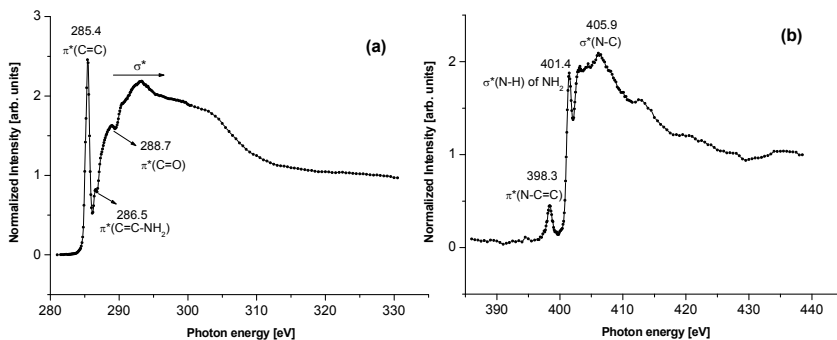


Figure 4.6. NEXAFS C K-edge and N K-edge spectra of the spin coated underderivatized 4,4'-methylene-bis(2,6-diethylaniline) film.

When a reaction takes place between 4,4'-methylenebis(2,6-diethylaniline) and the derivatization reagents, a new peak formation in lower BE compared to $\pi^*(\text{C}=\text{C}-\text{NH}_2)$ is expected in the N K-edge, indicating $\pi^*(\text{N}=\text{C})$.

4.2.1.2. XPS and NEXAFS after derivatization with PFB

Spin coated samples of 4,4'-methylenebis(2,6-diethylaniline) were derivatized with PFB and XPS spectra were measured. The reaction between 4,4'-methylenebis(2,6-diethylaniline) and PFB is presented in Fig. 4.7. A set of derivatization reactions with different reaction times (1, 5, 10, 15 and 45 min. at 50 °C) were performed in order to determine the reaction time required for saturation. XPS measurements were taken with and without charge neutralizer but no difference was observed. The following spectra were measured with charge neutralizer.

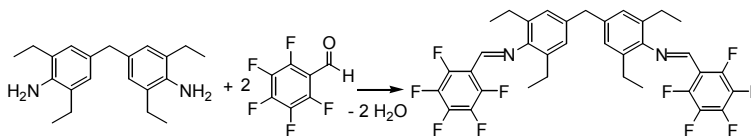


Figure 4.7. The derivatization reaction between 4,4'-methylenebis(2,6-diethylaniline) and PFB.

Unlike the underderivatized sample, all PFB - derivatized samples show an expected additional C1s peak at around 287.9 eV indicating the C-F bond. The intensity of the peak is high and the shift is characteristic for the C1s spectra of all derivatized samples.

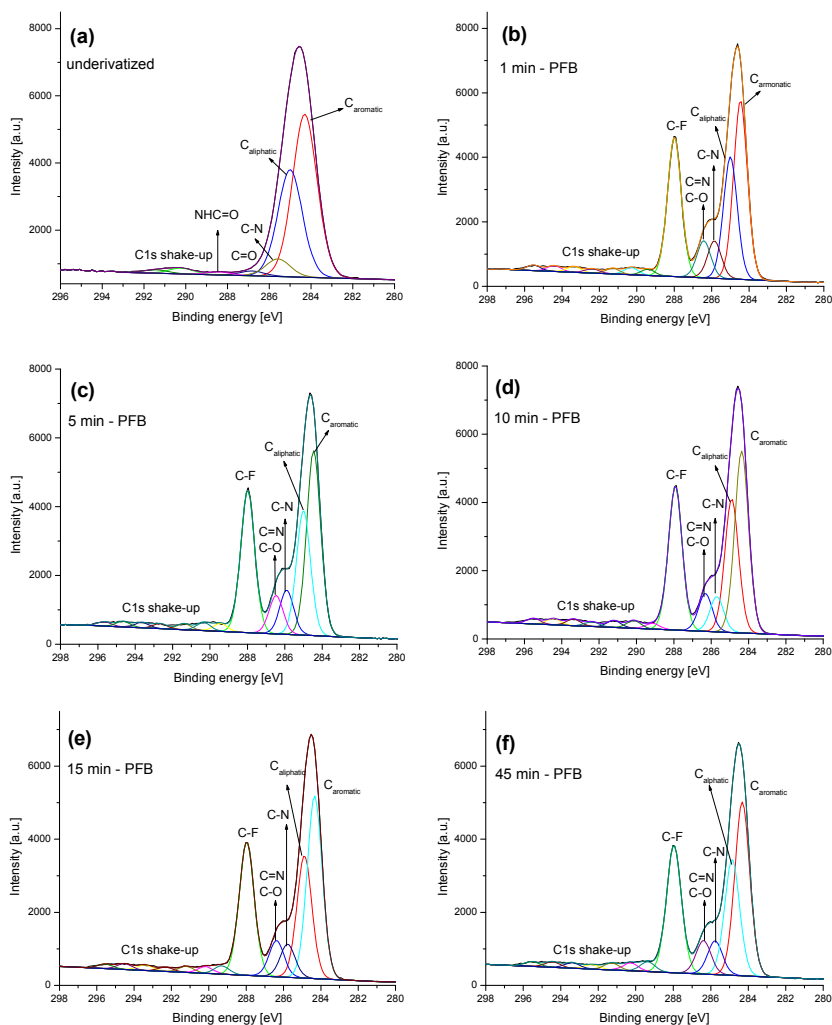


Figure 4.8. XP C1s spectra of spin coated 4,4'-methylenebis(2,6-diethylaniline) surfaces of (a) underivatized, (b) 1 min., (c) 5 min., (d) 10 min., (e) 15 min, and (f) 45 min. PFB derivatized samples, respectively.

Fig. 4.8 shows XP C1s spectra of PFB derivatized 4,4'-methylenebis(2,6-diethylaniline) samples with different reaction times. The XP C1s spectrum of the underivatized sample is also displayed for comparison. The C-N peak is observed at 285.9 eV, matching with the literature data [65]. The peak at around 286.4 eV in all derivatized samples is assigned to the imine groups. However, the binding energy of imines intersects with the binding energy of C-O groups [31,25,27,28]. Due to the oxygen contamination on the surface,

an amino group quantification relying on C=N binding energies is not possible. Table 4.6 summarizes the binding energies and the relative component peak areas of the PFB derivatized 4,4'-methylenebis(2,6-diethylaniline) samples.

Table 4.6. XPS data table of C 1s binding energies and relative component peak areas for PFB derivatized 4,4'-methylenebis(2,6-diethylaniline) samples. Data of underivatized sample is also displayed for comparison. The BE intervals are established by our own measurements matching with literature values. Relative component peak areas represent atomic fractions per total C content.

	Binding energy [eV]	Relative component areas [%] for sample					
		underivatized	1 min	5 min	10 min	15 min	45 min
C_{aromatic}	284.4	53.0	32.2	32.0	37.9	33.3	32.8
C_{aliphatic}	285.0	35.0	22.0	21.6	18.9	22.3	22.0
C-N	285.7-285.9	6.0	6.7	7.7	7.3	6.0	6.4
C=N, C-O	286.4-286.7	2.2	6.7	6.7	3.9	6.6	6.3
NHC=O,	288.1-288.3	1.1	-	-	-	-	-
C-F	287.9	-	23.3	24.0	24.3	24.8	24.6

The high resolution XP N1s spectrum of the underivatized sample shows an NH₂ peak at 399.6 eV. This peak shifts to lower energies as the reaction takes place and C=N forms. It is not possible to differentiate between C-NH₂ and C=NH peaks from the high resolution XP N1s spectra of the 1 and 5 minute reactions where both peaks appear at 399.0 eV. This peak is assigned as a combination of unreacted primary amino groups and imine groups that are formed by derivatization. Fig. 4.9 shows XP N1s spectra of PFB derivatized 4,4'-methylenebis(2,6-diethyl-aniline) samples with different reaction times. The XP N1s spectrum of the underivatized sample is also displayed for comparison.

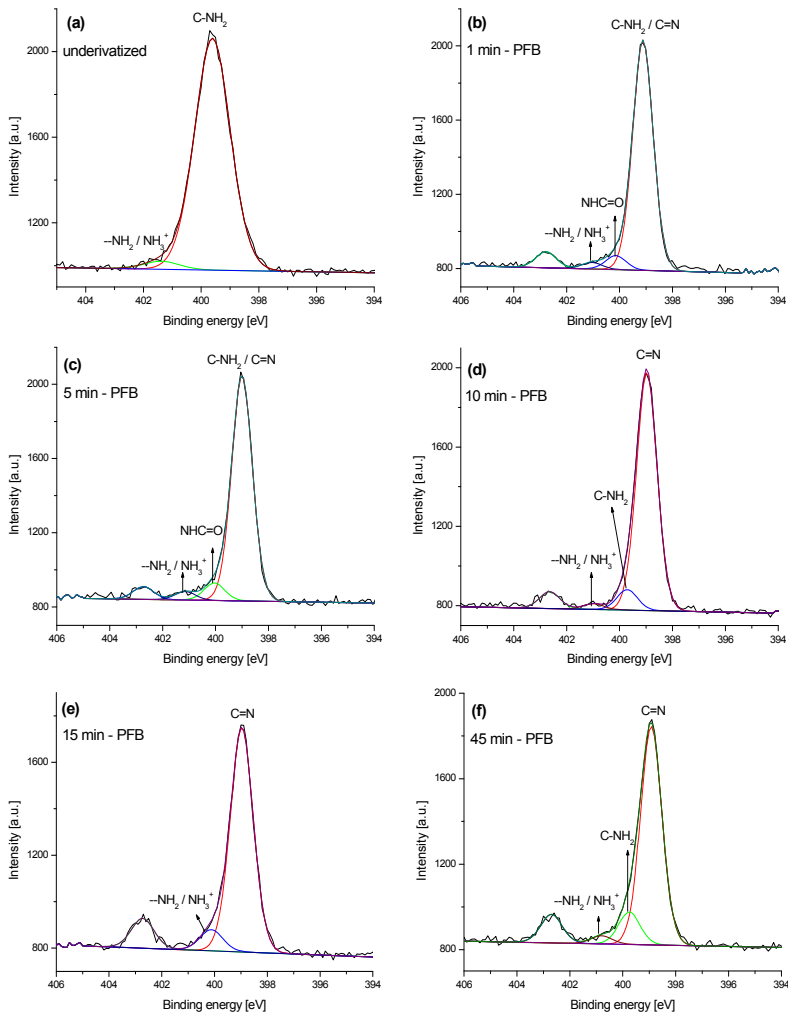


Figure 4.9. XP N1s spectra of spin coated 4,4'-methylenebis(2,6-diethylaniline) surfaces of (a) underivatized, (b) 1 min., (c) 5 min., (d) 10 min., (e) 15 min., and (f) 45 min. PFB derivatized samples, respectively. $\text{RH}_2\text{N}^+\text{-O}^-$ peak which appears at 402.8 eV in the N1s spectra of the derivatized samples (b-f) is not assigned.

The peak, which appears between 400.3-400.7 eV in the high resolution XP N1s spectra of 1 and 5 min. PFB derivatized 4,4'-methylenebis(2,6-diethylaniline) films, is due to amide functionalities present on the surface. This explains the oxygen contamination found by XP survey scans.

An additional peak appears at around 402.8 eV in all high resolution XP N1s spectra of the PFB derivatized samples. Hollaender et al. recently published an XPS study of the

model compounds poly(allylamine) and poly(diallylamine). The samples were derivatized with trifluoroacetic anhydride (TFAA) in order to study the amine functionalities on the surface. Some oxidation products were observed in the XPS spectra. The feature at 402.8 eV in the high resolution XP N1s spectrum is attributed to amine oxide which is defined as a reasonable intermediate in the oxidation of amines [67].

Table 4.7 summarizes the binding energies and the relative component peak areas of PFB derivatized 4,4'-methylenebis-(2,6-diethylaniline) samples.

Table 4.7. XPS data table of N 1s binding energies and relative component peak areas for PFB derivatized 4,4'-methylenebis(2,6-diethylaniline) samples. Data of underivatized sample is also displayed for comparison. The BE intervals are established by our own measurements matching with literature values. Relative component peak areas represent atomic fractions per total N content.

	Binding energy [eV]	Relative component areas [%] for sample					
		underivatized	1 min	5 min	10 min	15 min	45 min
C=N	398.9	-	86 (399.0 eV)	85 (399.0 eV)	85	83	76
C-NH ₂	399.6	96.6			7	-	11
NHC=O	400.3-400.7	-	5	7	-	-	-
--NH ₂ / NH ₃ ⁺	400.6-401.9	3.4	2	3	2	6	3
RH ₂ N ⁺ -O ⁻	402.8	-	6	5	6	11	9

In order to detect the time of reaction completion, N/C and F/C values vs. time graphs are plotted and displayed in Fig. 4.10. [C-F] area percentage, obtained from high resolution C1s spectra vs. time graph is also displayed for comparison. A correction must be carried out for both ratio diagrams due to additional atoms introduced to the surface (7 C atoms and 5 F atoms pro amino group) after the derivatization. The correction of F/C is defined by Equation 4.1 whereas the correction of N/C ratio is defined by Equation 4.2.

$$[F]/[C]^{\text{corrected}} = \frac{[F]_{\text{at}\%}}{[C]_{\text{at}\%} - 7/5[F]_{\text{at}\%}} \quad (\text{Equation 4.1})$$

$$[N]/[C]^{\text{corrected}} = \frac{[N]_{\text{at}\%}}{[C]_{\text{at}\%} - 7/5[F]_{\text{at}\%}} \quad (\text{Equation 4.2})$$

4. Derivatization of primary amines

Spin coated 4,4'-methylenebis(2,6-diethylaniline) films were derivatized with PFB at 50°C for 1, 5, 10, 15 and 45 min. $[F]/[C]^{\text{corrected}}$, $[N]/[C]^{\text{corrected}}$ and [C-F] area % vs. time graphs indicate a 15 min. reaction time for saturation.

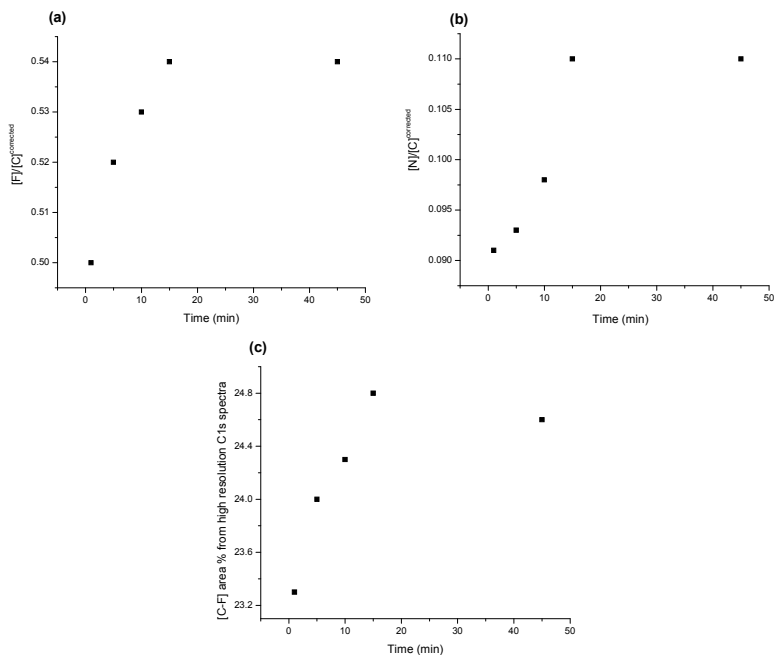


Figure 4.10. Spin coated 4,4'-methylenebis(2,6-diethylaniline) surfaces were derivatized with PFB for 1, 5, 10, 15 and 45 minutes to determine the time required for reaction completion. The reactions were carried out at 50°C. $[F]/[C]^{\text{corrected}}$ (a) and $[N]/[C]^{\text{corrected}}$ (b) vs. time graphs as well as [C-F] area % vs. time graph (c) indicate a 15 min. saturation reaction time. [F], [N] and [C] values are obtained from XP survey scan. [C-F] area % values are obtained from high resolution XP C1s spectra.

From the analysis of the N1s high resolution spectrum of the saturated case (Fig.4.9 e), we obtain 83 area% for the C=N component versus 17 area% for amino species (6 area% hydrogen bonded or protonated amine + 11 area% $\text{RH}_2\text{N}^+-\text{O}^-$). This result can be interpreted as a yield of 82% for the coupling reaction ($83 \text{ area\%} / (83+17) \text{ area\%}$). The yield calculated from the N1s spectrum is independently cross-checked by the $[F]/[N]$ ratio obtained from the survey scan which result in 96%. In order to quantify the $[\text{NH}_2]$ groups, an equation (Equation 4.3) should be derived concerning the reaction between 4,4'-methylenebis(2,6-diethylaniline) and PFB.



where x and y values can be defined by

$$y = [\text{F}]/5 \text{ and } x = [\text{C}] - 7y$$

$$[\text{NH}_2]_s = \frac{y}{x} \cdot 100 [\text{at}\%] \Rightarrow [\text{NH}_2]_s = \frac{[\text{F}]}{5[\text{C}] - 7[\text{F}]} \cdot 100 [\text{at}\%] \quad (\text{Equation 4.3})$$

The $[\text{NH}_2]_s$ value is calculated by using stoichiometrical data and XP survey scan of the PFB derivatized 4,4'-methylenebis(2,6-diethylaniline) film. [F] and [C] values are obtained from theoretical data (Fig. 4.7) and from XP survey scan, respectively.

Table 4.8 displays [at%] calculated from stoichiometry and obtained XP survey scan, including $[\text{NH}_2]_s$ values obtained from Equation 4.3.

Table 4.8. [at%] values calculated from stoichiometry and obtained from XP survey scan for PFB derivatized 4,4'-methylenebis(2,6-diethylaniline) surfaces at saturation. $[\text{NH}_2]_s$ values calculated from Equation 4.3 are also displayed.

PFB derivatization	calculated stoichiometry [at%]					obtained from XP survey scan [at%]				
	[C]	[N]	[F]	[F]/[N]	$[\text{NH}_2]_s$	[C]	[N]	[F]	[F]/[N]	$[\text{NH}_2]_s$
	35	2	10	5	9.5	73	4	20	4.8	9.3

Table 4.9 summarizes the PFB derivatization results of spin coated 4,4'-methylenebis(2,6-diethylaniline). The coupling reaction was applied at 50°C for 15 min.

Table 4.9. Summary of derivatization results of the reaction between 4,4'-methylenebis(2,6-diethylaniline) and PFB. Reaction yields and surface $[\text{NH}_2]$ group concentrations are displayed.

	Yield obtained from N1s	Yield obtained from [F]/[N]	$[\text{NH}_2]$ obtained from stoichiometry	$[\text{NH}_2]$ obtained from survey scan
PFB derivatized 4,4'-methylenebis(2,6-diethylaniline)	83	96	9.5	9.3

Fig. 4.11 displays the NEXAFS C K-edge (1) and N K-edge (2) spectra of all PFB derivatized 4,4'-methylenebis(2,6-diethylaniline) samples.

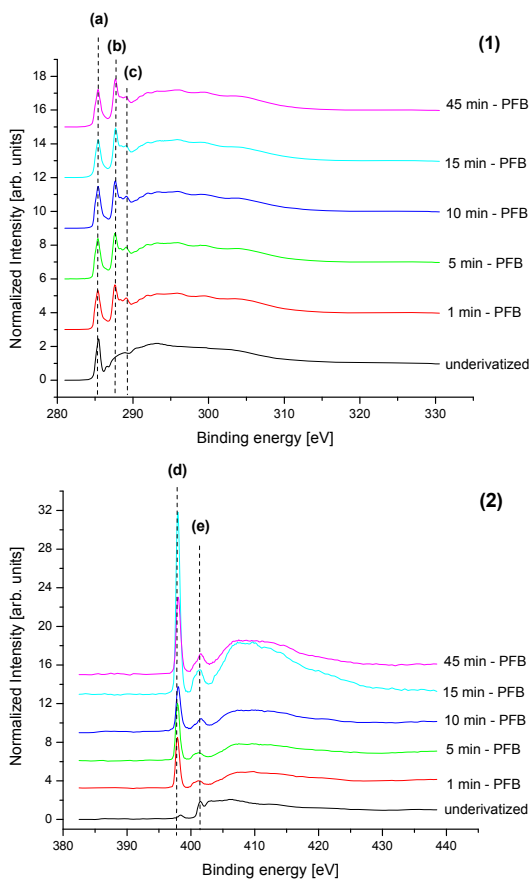


Figure 4.11. NEXAFS C K-edge (1) and N K-edge (2) spectra of the underivatized and PFB derivatized (1, 5, 10, 15 and 45 min.) spin coated 4,4'-methylenebis(2,6-diethylaniline) film

The feature (a) in the C K-edge spectra of all derivatized samples appear at 285.5 eV. This sharp peak shows a shoulder at 285.0 eV. $C1s \rightarrow \pi^*_{(C=C)}$ and $C1s \rightarrow \pi^*_{(C=N)}$ resonances are expected between 284.9-285.4 eV and 285.5-285.9 eV, respectively [15,29,35]. Thus feature (a) is assigned for a combination of π^* resonances of (C=C) and (C=N) bonds. The peak at 278.7 eV is due to $C1s \rightarrow \sigma^*_{(C-H)}$ resonances (b). PFB coupling of 4,4'-methylenebis(2,6-diethylaniline) forms a highly conjugated system with 4 phenyl rings (Fig. 4.7), resulting in the feature at 289.0 eV (c). The peak is due to the π^* resonances of (C=C_{ring}) [33].

$\pi^*_{(N-C=C)}$ resonance appears at 398.3 eV in the NEXAFS N K-edge spectrum of the underivatized spin coated 4,4'-methylenebis(2,6-diethylaniline) film (Fig. 4.6b). This peak shifts to 397.8 eV in the case of derivatized samples indicating imine formation. N1s $\rightarrow\pi^*_{(C=N)}$ (d) resonances are sharp and reaches to the highest intensity at saturation (15 min. reaction). The feature (e) appears at 401.5 eV with a shoulder at 400.6 eV due to N1s $\rightarrow\pi^*_{(C=C=N)}$ [14,15] and N1s $\rightarrow\sigma^*_{(N-H)}$, respectively.

Table 4.10 summarizes C and N K-edge resonance energies for underivatized and PFB derivatized 4,4'-methylenebis(2,6-diethylaniline) films. Samples were derivatized for 1, 5, 10, 15 and 45 min at 50°C.

Table 4.10. C and N K-edge resonance energies obtained from NEXAFS measurements of the spin coated underivatized and PFB derivatized 4,4'-methylenebis(2,6-diethylaniline) films. Corresponding spectra are shown in Fig. 4.11.

4,4'-methylene bis(2,6-diethyl) aniline)	C K-edge resonance energies (eV)			N K-edge resonance energies (eV)	
	$\pi^*_{(C=C)}$ $\pi^*_{(C=N)}$	$\sigma^*_{(C-H)}$	$\pi^*_{(C=C_{imp})}$	$\pi^*_{(C=N)}$	$\pi^*_{(C=C=N)}$
	(a)	(b)	(c)	(d)	(e)
	285.5	278.7	289.0	397.8	401.5

There are also various σ^* resonances above 292 eV in the NEXAFS C K-edge spectra. Features at 292.0 and 299.0 eV are due to C1s $\rightarrow\sigma^*_{(C-F)}$ resonances [16] and observed only in derivatized samples. The peak at 293.1 eV is due to C1s $\rightarrow\sigma^*_{(C-C, C-N)}$ resonances [15,29,65].

Fig. 4.12 shows in detail all resonance features obtained from C K-edge spectrum of PFB derivatized sample in saturation.

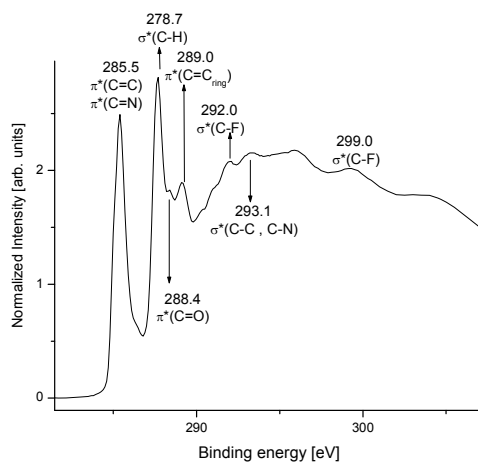


Fig. 4.12. Detailed overview of the NEXAFS C K-edge spectrum PFB derivatized 4,4'-methylenebis(2,6-diethylaniline) film (15 min. reaction time).

4.2.1.3. XPS and NEXAFS after derivatization with TFBA

Spin coated samples of 4,4'-methylenebis(2,6-diethylaniline) were derivatized with TFBA and XPS spectra were measured.

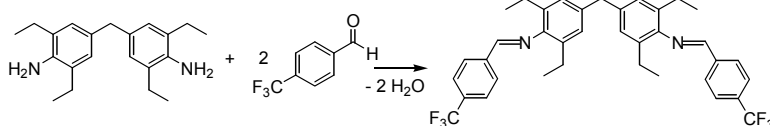


Figure 4.13. Derivatization reaction between 4,4'-methylenebis(2,6-diethylaniline) and TFBA.

The reaction between 4,4'-methylene-bis(2,6-diethylaniline) and TFBA is presented in the Fig. 4.13. A set of derivatization reactions with different reaction times (1, 5, 10, 15 and 45 min. at 50 °C) were performed in order to determine the reaction time required for saturation. XPS measurements were taken with and without charge neutralizer but no difference was observed. The spectra presented in the following were measured with charge neutralizer.

Unlike the underivatized sample, the TFBA - derivatized samples show an additional peak in the high resolution XP C1s spectra at around 292.5 eV, indicating the C-F binding energy of the trifluoromethyl group (CF₃). This characteristic peak superimposes with the C1s shake-up region for the 1 min. derivatization.

Since the fluorine content of the 1 min. reaction is just 0.64% on the surface, it is not possible to detect an intensive CF_3 peak. In addition, the C-N binding energy appears at around 285.8 eV. Due to the oxygen content on the surface of the spin coated films, C=N peaks superimpose with C-O peaks and are observed at around 286.6 eV. As a result, carbonyl groups (C=O) are also observed in the high resolution XP C1s spectra. The shake-up region is noticeable at 290-291 eV in all spectra due to the aromatic character of the compound. Table 4.11 summarizes the binding energies and the relative component peak areas of the PFB derivatized 4,4'-methylenebis(2,6-diethylaniline) samples.

Table 4.11. XPS data table of C 1s binding energies and relative component peak areas for TFBA derivatized 4,4'-methylenebis(2,6-diethylaniline) samples. Data of the underivatized sample is also displayed for comparison. The BE intervals are established by our own measurements matching with literature values. Relative component peak areas represent atomic fractions per total C content.

	Binding energy [eV]	Relative component areas [%] for sample					
		underivatized	1 min	5 min	10 min	15 min	45 min
$\text{C}_{\text{aromatic}}$	284.4	53.0	51.3	41.2	42.2	42.8	48.3
$\text{C}_{\text{aliphatic}}$	285.0	35.0	37.7	37.6	36.0	36.6	35.9
C-N	285.7-285.9	6	6.7 (286.2 eV)	11.7	8.4	10.6	8.3 (286.0 eV)
C=N, C-O	286.4-286.7	2.1		3.14	4.4	2.4	
C=O	287.6-287.9		1.7	1.2	2.8	-	1.2
NHC=O,	288.1-288.3	1.1	-	-	-	1.0	-
CF_3	292.6-292.7	-	-	2.0	2.98	3.75	3.14

Figure 4.14 shows the high resolution XP C1s spectra of TFBA derivatized 4,4'-methylenebis(2,6-diethylaniline) samples with different reaction times. The XP C1s spectrum of the underivatized sample is also displayed for comparison.

4. Derivatization of primary amines

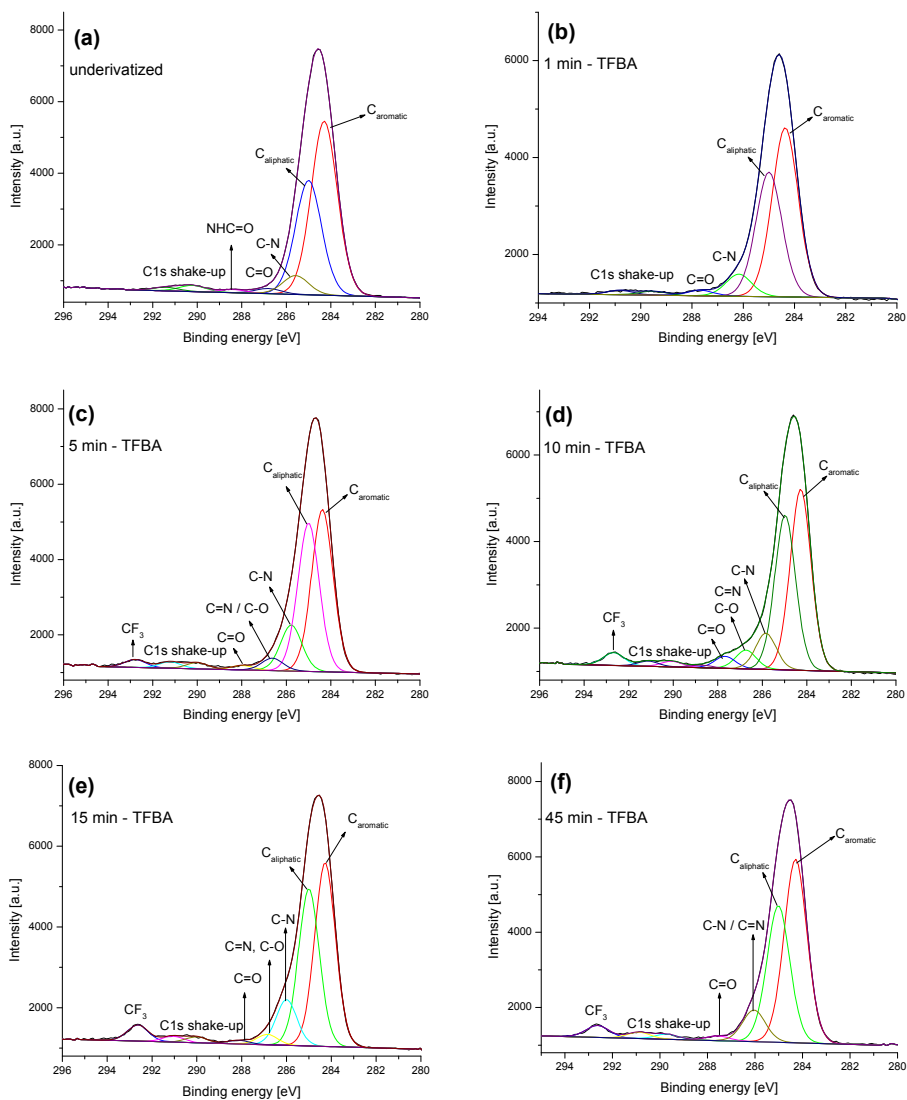


Figure 4.14. XP C1s spectra of spin coated 4,4'-methylenebis(2,6-diethylaniline) surfaces of (a) underivatized, (b) 1 min., (c) 5 min., (d) 10 min., (e) 15 min., and (f) 45 min. TFBA derivatized samples, respectively.

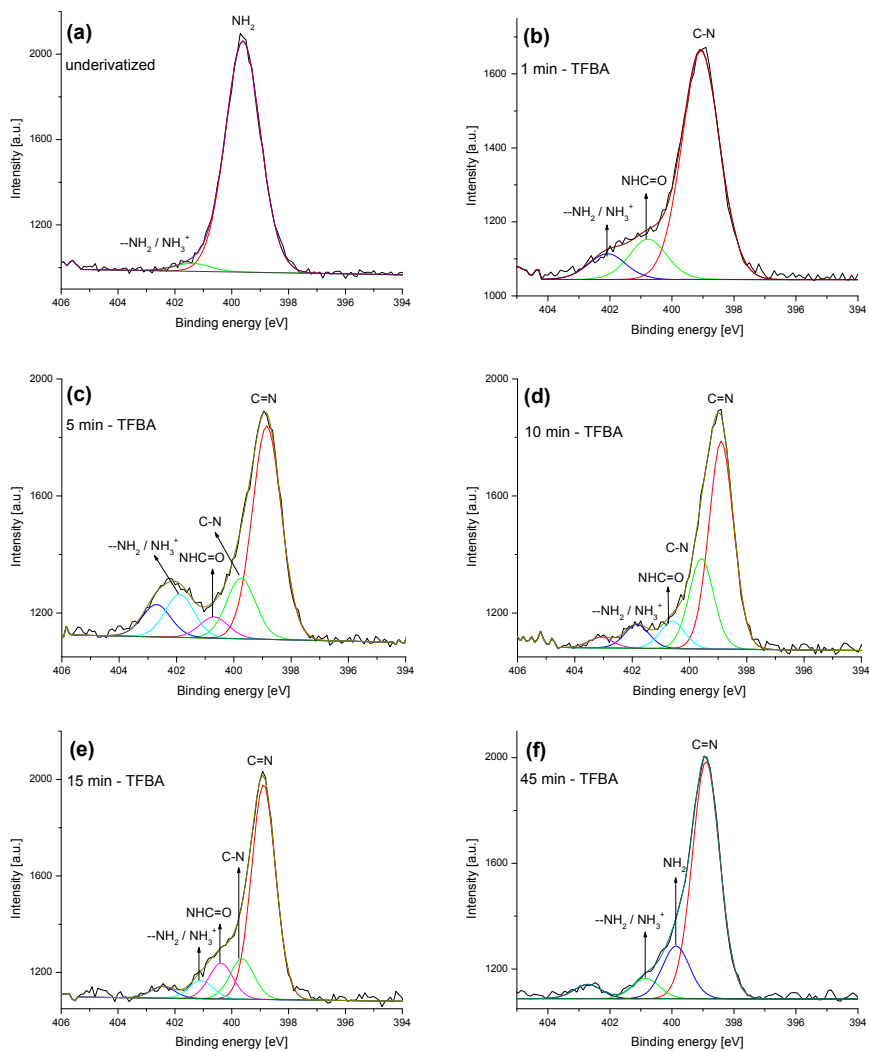


Figure 4.15. XP N1s spectra of spin coated 4,4'-methylenebis(2,6-diethylaniline) surfaces of (a) underivatized, (b) 1 min., (c) 5 min., (d) 10 min., (e) 15 min., and (f) 45 min. TFBA derivatized samples, respectively.

Figure 4.15 shows the high resolution XP N1s spectra of TFBA derivatized 4,4'-methylenebis(2,6-diethylaniline) samples with different reaction times. The XP N1s spectrum of the underivatized sample is also displayed for comparison.

In the high resolution XP N1s spectra of the TFBA derivatized films, the imine binding energy (C=N) is observed at 398.9 eV. The N1s spectrum of the 1 min. TFBA

4. Derivatization of primary amines

derivatized film, however, shows a major NH_2 peak at 399.1 eV due to the insufficient reaction time. In some cases amide groups are also observed in the XP N1s spectra at around 400.6 eV. Hydrogen bonded and protonated amino groups are present between 400.8 eV and 401.7 eV. Similar to the XP high resolution N1s spectra of PFB derivatized films, the oxidation intermediate of amines (amine oxides, $\text{RH}_2\text{N}^+\text{-O}^-$) is observed between 402.5 - 402.9 eV.

Table 4.12 summarizes the binding energies and the relative component peak areas in the XP N1s spectra of PFB derivatized 4,4'-methylenebis(2,6-diethylaniline) samples.

Table 4.12. XPS data table of the N1s binding energies and relative component peak areas for the TFBA derivatized 4,4'-methylenebis(2,6-diethylaniline) samples. Data of the underivatized sample is also displayed for comparison. The BE intervals are established by our own measurements matching with literature values. Relative component peak areas represent atomic fractions per total N content.

	Binding energy [eV]	Relative component areas [%] for sample					
		underivatized	1 min	5 min	10 min	15 min	45 min
C=N	398.9	-	-	57.7	57.7	67	73.1
C-NH ₂	399.1-399.6	96.6	77.7	16.4	25.13	12.6	16.23
NHC=O	400.3-400.7	-	13.6	5.7	7.6	11.1	-
--NH ₂ / NH ₃ ⁺	400.6-401.9	3.4	8.7	12.4	6.6	5.6	6.2
RH ₂ N ⁺ -O ⁻	402.8	-	-	8.7	2.9	3.6	4.4

In order to detect the time of reaction completion, N/C and F/C values vs. time graphs are plotted and displayed in Fig. 4.16. $[\text{CF}_3]$ area percentage obtained from high resolution

$$[\text{F}]/[\text{C}]^{\text{corrected}} = \frac{[\text{F}]_{\text{at}\%}}{[\text{C}]_{\text{at}\%} - 8/3[\text{F}]_{\text{at}\%}} \quad (\text{Equation 4.4})$$

C1s spectra vs time graph is also displayed for comparison. A correction must be carried out for both ratio diagrams due to additional atoms, introduced to the surface (8 C atoms and 3 F atoms pro amino group) after the derivatization. The correction of F/C is defined by the Equation 4.4 whereas the correction of N/C ratio is defined by the Equation 4.5.

$$[\text{N}]/[\text{C}]^{\text{corrected}} = \frac{[\text{N}]_{\text{at}\%}}{[\text{C}]_{\text{at}\%} - 8/3[\text{F}]_{\text{at}\%}} \quad (\text{Equation 4.5})$$

Spin coated 4,4'-methylenebis(2,6-diethylaniline) films were derivatized with TFBA at 50°C for 1, 5, 10, 15 and 45 min. $[F]/[C]^{\text{corrected}}$, $[N]/[C]^{\text{corrected}}$ and $[CF_3]$ area % vs. time graphs (Fig. 4.16 (a), (b) and (c), respectively) indicate a 15 min. reaction time for saturation.

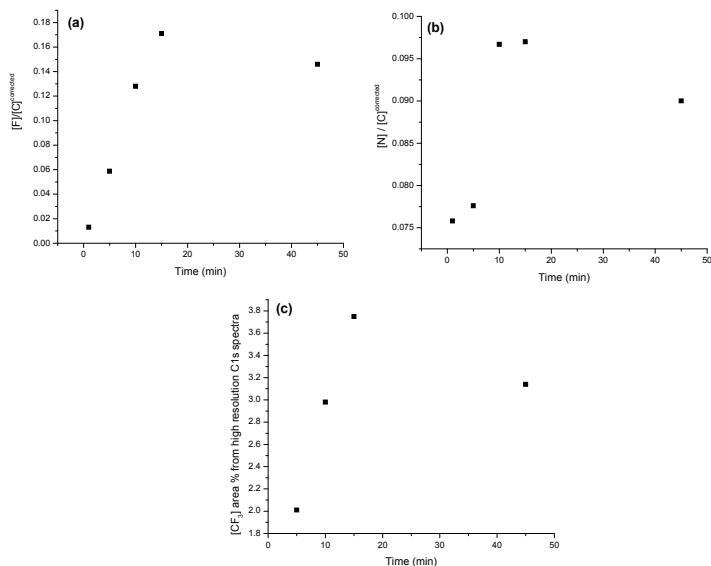


Figure 4.16. Spin coated 4,4'-methylenebis(2,6-diethylaniline) surfaces were derivatized with TFBA for 1, 5, 10, 15 and 45 min. to determine the time required for reaction completion. The reactions were carried out at 50°C. $[F]/[C]^{\text{corrected}}$ (a) and $[N]/[C]^{\text{corrected}}$ (b) vs. time graphs as well as $[CF_3]$ area % vs. time graph (c) indicate a 15 min. reaction time. $[F]$, $[N]$ and $[C]$ values are obtained from XP survey scan. $[CF_3]$ area % values are obtained from high resolution XP C1s spectra.

From the analysis of the N1s high resolution spectrum of the saturated sample (Fig. 4.15 e), 67 area% for the C=N component versus 33 area% for amino species (13 area% unreacted amines + 11 area% amide + 6 area % hydrogen bonded or protonated amine + 3 area% $RH_2N^+-O^-$) is obtained. This result can be interpreted as a yield of 67% for the coupling reaction (67 area% / (67+33) area%). The yield calculated from the N1s spectrum is independently cross-checked by the $[F]/[N]$ ratio (60%) obtained from the survey scan. In order to quantify the $[NH_2]$ groups from the XP spectra, Equation 4.6 is derived concerning the reaction between 4,4'-methylenebis(2,6-diethylaniline) and TFBA.

4. Derivatization of primary amines



where x and y values can be defined by

$$y = [F]/3 \text{ and } x = [C] - 8y$$

$$[NH_2]_s = \frac{y}{x} \cdot 100 [\text{at}\%] \Rightarrow [NH_2]_s = \frac{[F]}{3[C] - 8[F]} \cdot 100 [\text{at}\%] \quad (\text{Equation 4.6})$$

[F] and [C] values are obtained from theoretical data (Fig. 4.13) and the XP survey scan of the TFBA derivatized 4,4'-methylenebis(2,6-diethylaniline) film in order to determine the $[NH_2]_s$ values of the calculated stoichiometry and the XPS data, respectively.

Table 4.13 displays [at%] calculated from stoichiometry and obtained from the XP survey scan, including $[NH_2]_s$ values from Equation 4.6.

Table 4.13. [at%] values calculated from stoichiometry and obtained from XP survey scan for TFBA derivatized 4,4'-methylenebis(2,6-diethylaniline) surfaces at saturation. $[NH_2]_s$ values calculated from Equation 4.6 are shown.

TFBA derivatization	calculated stoichiometry [at%]					obtained from XP survey scan [at%]				
	[C]	[N]	[F]	[F]/[N]	$[NH_2]_s$	[C]	[N]	[F]	[F]/[N]	$[NH_2]_x$
	37	2	6	3	9.5	64	4	8	2	6

Table 4.14 summarizes the TFBA derivatization results of spin coated 4,4'-methylenebis(2,6-diethylaniline). The coupling reaction was applied at 50°C for 15 min.

Table 4.14. Summary of the derivatization results of the reactions between 4,4'-methylenebis(2,6-diethylaniline) and TFBA. Reaction yields and surface $[NH_2]$ group concentrations are displayed.

	Yield obtained from N1s	Yield obtained from [F]/[N]	$[NH_2]$ obtained from stoichiometry	$[NH_2]$ obtained from survey scan
TFBA derivatized 4,4'-methylenebis(2,6-diethylaniline)	67	60	9.5	6

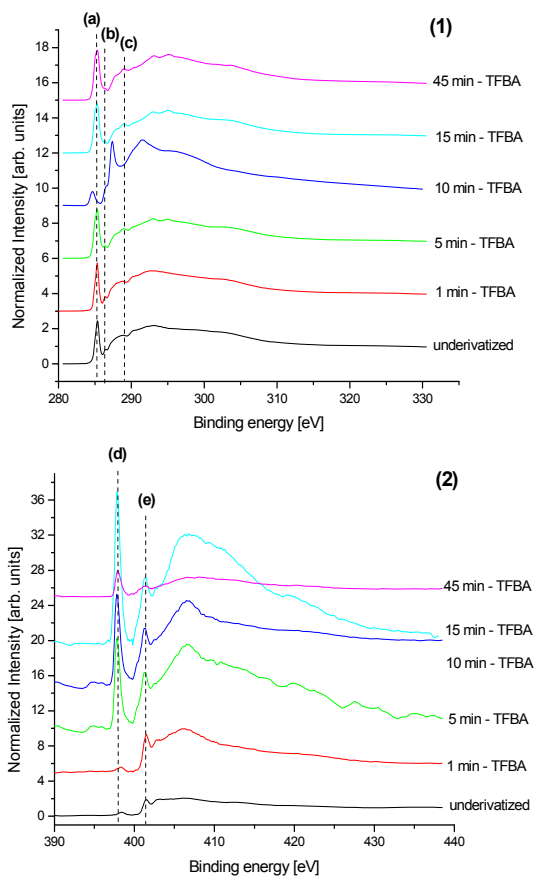


Figure 4.17. NEXAFS C K-edge (1) and N K-edge (2) spectra of the underivatized and TFBA derivatized (1, 5, 10, 15 and 45 min.) spin coated 4,4'-methylenebis(2,6-diethylaniline) films.

Fig. 4.17 displays the NEXAFS C K-edge (1) and N K-edge (2) spectra of all TFBA derivatized 4,4'-methylenebis(2,6-diethylaniline) samples. Unlike the 10 min. TFBA derivatized sample, the feature (a) in C K-edge spectra of all samples appear at 285.5 eV. This sharp peak shows a small shoulder at 285.1 eV. As explained in 4.2.1.2, feature (a) is assigned to a combination of π^* resonances of (C=C) and (C=N) bonds. The peak at 286.4 eV (b) is due to $C1s \rightarrow \pi^*(C-C-NH_2)$ resonances [65]. $\sigma^*(C-H)$ resonances are only observed as a small shoulder at 287.7 eV. TFBA coupling of 4,4'-methylenebis(2,6-diethylaniline) forms a highly conjugated system with 4 phenyl rings (Fig. 4.13) resulting in the feature at 289.0 eV (c) which can be explained by the π^* resonances of (C=C_{ring}). In the N K-edge spectrum of the

10 min. derivatized sample, $C1s \rightarrow \pi^*_{(C=C)}$ appears at 284.9 eV. $C1s \rightarrow \pi^*_{(C=C-NH_2)}$ resonance (b) is observed as a small shoulder at 286.6 eV. Different from other derivatized samples, σ^* resonances of (C-H) are observed as a sharp peak at 287.7 eV for 10 min. derivatized sample.

The $\pi^*_{(N-C=C)}$ resonance appears at 398.3 eV in the NEXAFS N K-edge spectrum of the underivatized spin coated 4,4'-methylenebis(2,6-diethylaniline) film (Fig. 4.6b). This peak shifts to 397.9 eV in case of derivatized samples indicating imine formation. $N1s \rightarrow \pi^*_{(C=N)}$ (d) resonances are sharp and reach to the highest intensity at saturation (15 min. reaction). The feature (e) appears at 401.5 eV ($N1s \rightarrow \pi^*_{(C=C=N)}$).

Table 4.15 summarizes C and N K-edge resonance energies for underivatized and TFBA derivatized 4,4'-methylenebis(2,6-diethylaniline) films. The samples were derivatized for 1. 5. 10, 15 and 45 min. at 50°C.

Table 4.15. C and N K-edge resonance energies obtained from NEXAFS measurements of the spin coated underivatized and TFBA derivatized 4,4'-methylenebis(2,6-diethylaniline) films. Corresponding spectra are shown in Fig. 4.17.

4,4'-methylene bis(2,6-diethyl aniline)	C K-edge resonance energies (eV)			N K-edge resonance energies (eV)	
	$\pi^*_{(C=C)}$ $\pi^*_{(C=N)}$	$\pi^*_{(C=C-NH_2)}$	$\pi^*_{(C=C_{ring})}$	$\pi^*_{(C=N)}$	$\pi^*_{(C=C=N)}$
	(a) 285.5	(b) 286.4	(c) 289.0	(d) 397.9	(e) 401.5

There are also various σ^* resonances observed above 292 eV in the NEXAFS C K-edge spectra. $C1s \rightarrow \sigma^*_{(C-F)}$ resonances are observed at 295.1 eV and as a small shoulder at 291.9 eV [68]. The peak at 293.0 eV is due to $C1s \rightarrow \sigma^*_{(C-C, C-N)}$ resonances whereas the feature at 303.0 eV is assigned to $C1s \rightarrow \sigma^*_{(C=C, C=N)}$ [65]. Fig. 4.18 shows in detail all resonance features obtained from the C K-edge spectrum of the saturated TFBA derivatized sample.

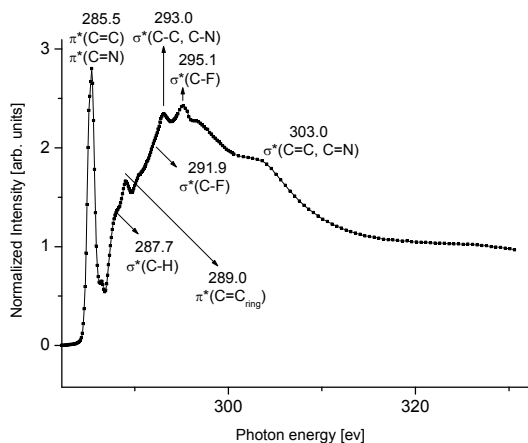


Figure 4.18. A detailed overview of the NEXAFS C K-edge spectrum of the 15 min. TFBA derivatized 4,4'-methylenebis(2,6-diethylaniline) film.

4.2.2. Self-assembled monolayers (SAMs)

4.2.2.1. Introduction

Self-assembled monolayers (SAMs) are surfaces consisting of a single layer of molecules on a substrate. SAMs with different terminal groups have potential applications in several areas of bioengineering, including biosensors, bio-mimetic processes, and biomaterials due to their well-defined, organized structure and stability [69]. Outermost terminal groups of a SAM can be functionalized and chemically modified to create well-defined surfaces for the study of interactions with bio-molecules and cells. Some examples of those functionalities are $-\text{CH}_3$, $-\text{OH}$, $-\text{COOH}$, $-\text{NH}_2$, and $-(\text{C}=\text{O})\text{OCH}_3$. An understanding of the accessibility and reactivity of the outermost groups is a critical step in developing systematic control of the chemical composition of the surfaces.

A common example of SAMs is an alkane thiol on gold. Sulfur has an affinity for gold, with a binding energy in the range of 20–35 kcal/mol. An alkane with a thiol head group will stick to the gold surface and form an ordered assembly with the alkyl chains packing together due to van der Waal forces. The initial stage of the SAM formation usually takes minutes or less, under normal conditions of 0.1-10 mmol/L thiol concentrations in a solvent.

However, it is necessary to use adsorption times of 15h or more to obtain well-ordered, defect-free SAMs.

A variety of other self-assembled monolayers can be formed. Alkyl thiols are known to assemble on many metals including silver, copper, palladium and platinum. Alkyl silane molecules are another well-known example of self-assembly on silicon oxide surfaces. All these systems have been reviewed in great detail in the book "An Introduction to Ultrathin Organic Films From Langmuir-Blodgett to Self-Assembly" by U. Alman [70].

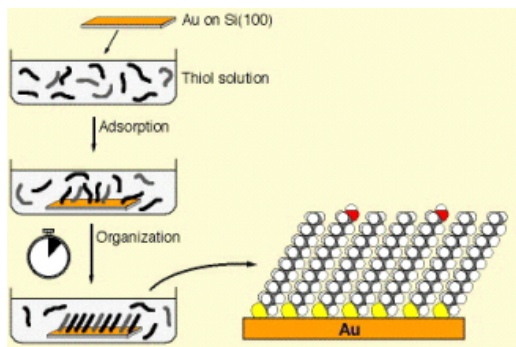


Figure 4.19. Preparation of SAMs. The substrate Au on Si is immersed into an EtOH solution of the desired thiols. Initial absorption is fast (seconds); then an organization phase follows regarding head and tail groups, which should be allowed to continue overnight for better results [71].

For the preparation of SAMs on gold substrates (Fig. 4.19), the preferred crystal face is the (111) direction, which can be obtained either by using single crystal substrates or by evaporation of thin Au films on flat supports, typically glass or silicon. The most common used solvent at the low thiol concentrations is ethanol.

It becomes more and more important to precisely control chemical, structural and biological surface properties of mixed SAMs of alkane thiols on Au(111) due to their usage as a model of bio-mimetic [72]. However, it is still difficult to prepare and characterize mixed SAMs with controlled chemical, structural, and biological properties. By using two differently terminated thiols in the preparation solution, the preparation of mixed SAMs is possible. The relative proportion of the two functionalities in the assembled SAM will then depend upon several parameters, like the mixing ratio in solution, the alkane chain lengths, the solubilities of the thiols in the solvent used and the properties of the chain-terminating groups. In general, the composition will not be the same in the SAM as in the preparation solution. For instance, co-adsorption from a solution containing two components onto a surface may lead to surface

segregation when two components have a difference in chain length. Shevade et al. carried out a configurational-bias Monte Carlo simulation study for the preferential absorption and the phase segregation of alkane thiol mixed SAMs on Au(111) and found out that phase segregation occurs when two components have a chain length difference of more than three carbon atoms [73]. However, in cases where the two thiol molecules are of equal alkyl chain length and no special circumstances (e.g. bulky tail groups), the SAM composition will be almost identical to the composition of the solution (eg. $\text{HS}(\text{CH}_2)_{15}\text{CH}_3$ and $\text{HS}(\text{CH}_2)_{16}\text{OH}$).

The ability to adjust the end group makes SAMs very attractive for surface reactions. -OH or -COOH terminated SAMs were investigated by several groups. On polymer surfaces, TFAA reacts with surface hydroxyl groups nearly quantitatively. This effect was also studied for -OH terminated SAMs [69,74,75]. In all cases, the same reaction was applied but different results were obtained. Bertilsson et al. studied the distribution of hydroxyl groups in a mixed SAM of 16-mercapto-1-hexadecanol and alkane thiols by reacting it with TFAA in THF solution. The yield was estimated as 80-90% and it is assumed that the steric hindrance affected the yield. For vapor phase derivatization performed by Legget et al., it was published that there were not sufficient degrees of freedom for the CF_3 groups to pack at the same density as the underlying monolayer. Then Castner et al. published a nearly complete surface reaction and concluded that the steric hindrance of the CF_3 groups was not significant.

Himmel et al. [76] investigated the surface derivatization of -OH and -COOH terminated SAMs by phenyl isocyanate ($\text{C}_6\text{H}_5\text{NCO}$, PIC). In both cases, the reactivity to gas phase PIC was very low at room temperature. However, reaction yields of more than 80% could be achieved by depositing multilayers on a sample cooled down to 120 K and subsequently heating it up to 290 K.

SAMs of different terminal groups were prepared. TFBA and PFB derivatization on NH_2 terminated SAMs of alkane thiols were performed. The results will be displayed in this chapter.

4.2.2.2. Characterization of SAMs

Fig. 4.20 displays the aliphatic and aromatic thiols with different head groups attached to Au surfaces along with reference samples. In the following, the numbers **1-6** refer to the chemical structures displayed in this figure. After the formation of SAMs, XPS analysis were performed for surface characterization. NEXAFS was used along with XPS to obtain information about the surface orientation of the monolayers.

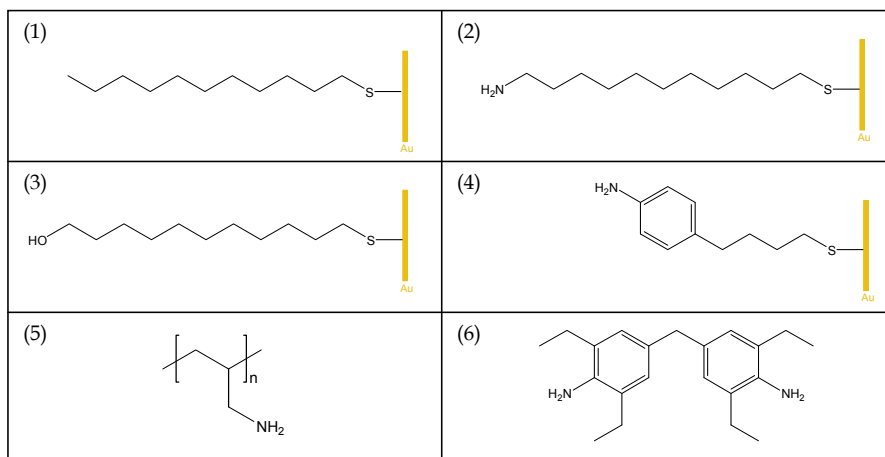


Figure 4.20. Aliphatic and aromatic thiolates on Au: 1-undecanethiol **(1)**, 11-amino-1-undecanethiolate **(2)**, 11-hydroxyundecanethiol **(3)**, 4-aminophenylbutane-1-thiolate **(4)**. Chemical structures of reference samples: poly(allylamine) **(5)** and 4,4'-methylenebis(2,6-diethylaniline) **(6)**.

Organothiolate SAMs are formed from organothiols by binding the thiol group on one end to an Au substrate. A midchain segment, normally relatively long, connects to a terminal group like amine, which forms the outermost surface of the monolayers. In Fig. 4.21, several possibilities for the conformation of aliphatic thiol SAMs made from 11-amino-1-undecanethiol **(2)** and 11-hydroxyundecanethiol **(3)** are shown: The ideal case of upright alkyl chains with free amine or hydroxyl groups and a sulphur bound to Au is shown in Fig. 2a and 2e. Connected by hydrogen bonds between the amino functionalities two molecules can form a bilayer (Fig. 2b and 2f). When oxidation of the sulphur atom occurs, sulfonate (Fig. 2c and 2g) and sulfinate (Fig. 2d and 2h) are present. In those cases the organothiol molecule is not participating in the ordered SAM structure, but might be attached to the amino-terminated or hydroxy-terminated surface via hydrogen bonding or ionic interactions.

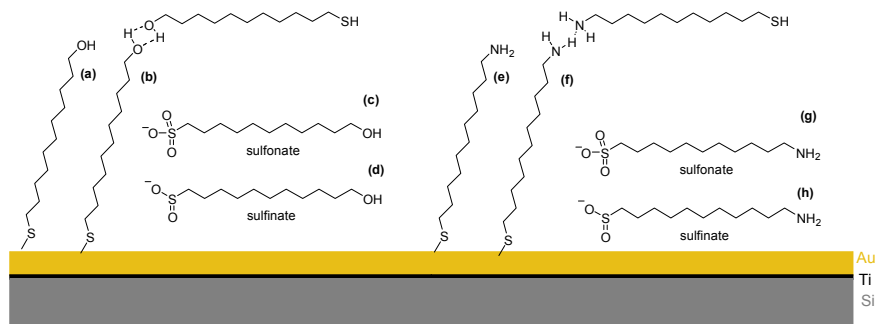


Figure 4.21. Bonding possibilities of 11-hydroxyundecanethiol (3) and 11-amino-1-undecanethiol (2) on Au respectively.

4.2.2.3. XPS and NEXAFS characterization of aliphatic SAMs

For sample **(1)** elemental analysis reveals an enhanced [C] fraction ($[C]/[S] = 16:1$ instead of 11:1, expected from the stoichiometry). This may be due to an aliphatic carbon contamination that originates from incomplete substrate cleaning. The highly resolved S2p spectrum shows a single doublet from S 2p_{3/2} and S 2p_{1/2} with a relative peak area ratio (1.6:1) close to real value of 2:1 and a difference in BE of 1.2 eV as expected from literature for Au-thiol bond formation [77].

For sample **(2)** the measured XPS [N]/[S] ratio (0.8:1) is consistent with the stoichiometry of the sample. The highly resolved S2p spectrum shows a single doublet from S2p_{3/2} and S2p_{1/2} with a relative peak area ratio 2:1 and a difference in BE of 1.2 eV. Aliphatic carbon contamination, which is also revealed by the high resolution XP C 1s spectrum, may again be the reason for increased [C] value. On bare Au surfaces, O and C were found also after cleaning, although the samples were stored in vacuum before the analysis. The substrate's Au signal intensities in the XP survey spectrum and the angle dependence of the NEXAFS underpin the character of sample **(2)** to be a regular monolayer.

For sample **(3)** elemental analysis shows a reduced ratio for [C]/[O] of 9:1 instead of 11:1. However, the highly resolved S2p spectrum shows a single doublet with a relative peak area ratio 1.7:1 and a difference in BE of 1.2 eV. The Au signal intensities in the XP survey spectrum and the angle dependence of the NEXAFS show an ordered monolayer.

4. Derivatization of primary amines

Reference sample (5) shows atomic ratios expected from the stoichiometry. No substrate signals have been detected, pointing to closed layer at a thickness > ~20 nm. A rather small O contamination was observed.

Information on elemental composition of the samples, obtained from XP survey spectra are summarized in Table 4.16.

Table 4.16. Results of XPS elemental analysis in at%. Samples are described in Fig. 4.21.

Element	sample(1) [at%]	sample(2) [at%]	sample(3) [at%]	sample(4) [at%]	sample(5) [at%]	sample(6) [at%]
C	48	65	45	55	80	75
N	-	4	-	3	19	5
O	-	9	5	3	1	11
S	3	5	2	2	-	-
Au	49	16	47	37	-	9

Fig. 4.22 displays the XPS spectrum of SAM sample (**2**) as an example. Although the sample was kept under vacuum, an oxygen peak of 9% is observed in XP survey scan. Consequently, the highly resolved XP C1s spectrum displays oxygen-bound carbon species. The XP N1s spectrum shows two amine species. The peak at higher BE corresponds to hydrogen-bonded or protonated amines and the peak at low BE to free amines. Due to the preparation of amine terminated SAMs including a final acid rinsing step, a majority of protonated amine species is expected. The highly resolved XP S2p spectrum shows the main doublet component S 2p_{3/2} at 162.1 eV which is gold-bound thiolate, indicating monolayers well bound to the substrate.

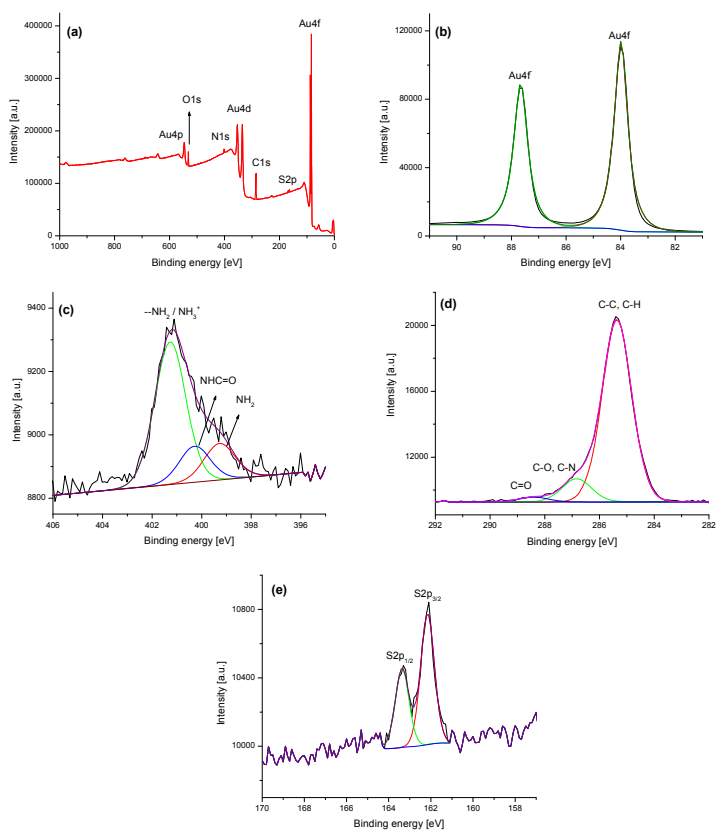


Figure 4.22. XPS spectrum of 11-amino-1-undecanethiol (**2**) on Au. Survey spectrum (a), XP Au 4f (b), XP N 1s (c), XP C1s (d), and XP S 2p (e) are displayed respectively.

In order to prove a successful SAM deposition in the case of different terminated thiols on Au, angle resolved NEXAFS was applied at the C K-edge. Fig. 4.23 displays the C K-edge NEXAFS spectrum of 11-amino-1-undecanethiol (**2**) on Au as an example. NEXAFS is well known to be a powerful technique to determine orientations of molecules adsorbed on surfaces. Intense peaks in the difference spectra are indicative of polarization dependence in the orbital, responsible for the NEXAFS resonance and, therefore, of well-defined bond/functional group orientation [26,29,31-34,36,63,77-81]. The mean tilt angle of the carbon chain in SAM (**2**) relative to the surface normal was estimated to be 48° following a procedure described in [82]. This is in agreement with previously published data [34,83].

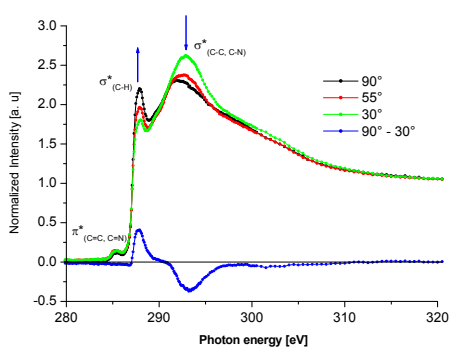


Figure 4.23. C K-edge NEXAFS at three different angles of incident linear polarized synchrotron light (30° , 55° and 90°) and the difference spectrum ($90^\circ - 30^\circ$) for 11-amino-1-undecanethiolate on Au (**2**).

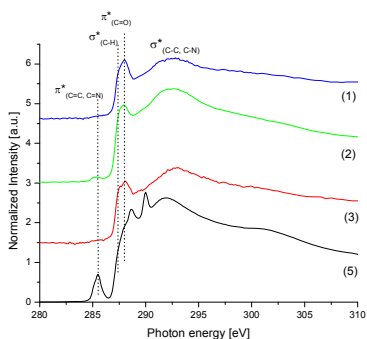


Figure 4.24. C K-edge NEXAFS of 1-undecanethiol (**1**), 11-amino-1-undecanethiolate (**2**), 11-hydroxyundecanethiol (**3**) on Au and poly(allylamine) (**5**) on oxidized Si.

NEXAFS spectra at the C K-edge (Fig. 4.24) reveal $C1s \rightarrow \sigma^*(C-H)$ resonances at 287.7 eV and $\sigma^*(C-C)/\sigma^*(C-N)$ resonances at around 292 eV. It can be speculated that the

feature ~ 0.8 eV above the $\sigma^*(\text{C-H})$ resonance, which was observed exclusively for poly(allylamine), could be a small amide π^* resonance, which was also observed by Shard et al. [29] and Dhez et al. [36] with polymer references at around 288.2 eV. Resonances at 285.0 and 285.6 eV represent transitions from C 1s to $\pi^*(\text{C=C})$ and $\pi^*(\text{C=N})$ orbitals. Their appearance in the spectra of nominally saturated systems may be due to radiation damage. Because a certain number of spectra had to be acquired to reach reasonable S/N ratios, a considerable danger of beam damage in the NEXAFS experiments occurs.

4.2.2.4. XPS and NEXAFS characterization of aromatic SAMs

Fig. 4.25 displays the XPS spectrum of SAM sample (**4**).

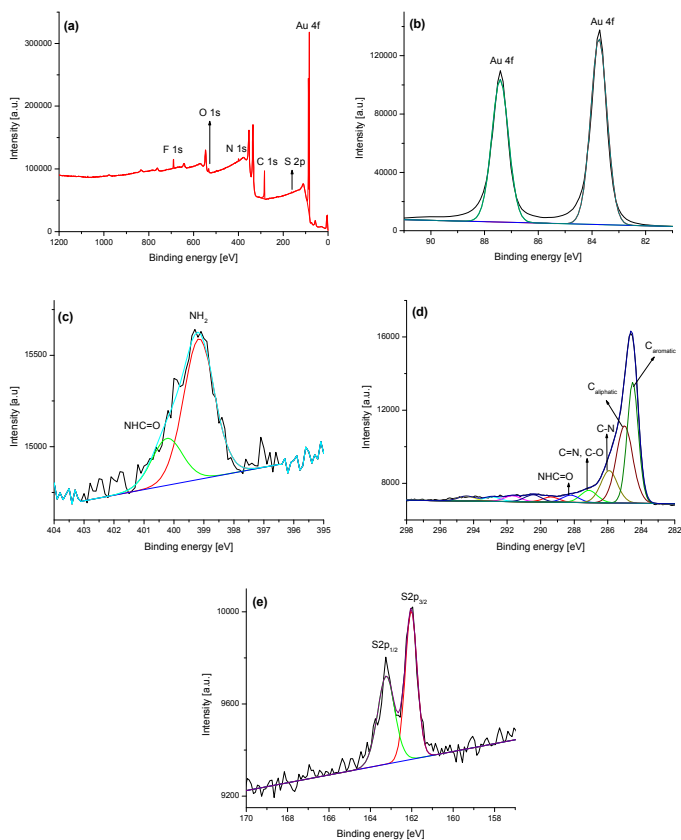


Figure 4.25. XPS spectrum of 4-aminophenylbutane-1-thiolate (**4**) on Au. Survey spectrum (a), XP Au 4f (b), XP N 1s (c), XP C 1s (d) and XP S 2p (e) are displayed respectively.

As for the aliphatic SAM sample **(2)**, the N:S ratio is approximately 1:1 for the aromatic SAM sample **(4)**. The increased [C] value is probably due to unspecific adsorption of aliphatic and oxidized hydrocarbons, also revealed by high resolution XP C1s. Contamination by substantial amounts of NHC=O species have been ruled out. The substrate's Au signal intensities in the XP survey spectrum and the angle dependence of the NEXAFS underpin the character of sample **(4)** to be a regular monolayer. Highly resolved XP S2p spectrum shows the expected doublet as observed for sample **(2)**. XP survey scan of underivatized SAM **(4)** shows a fluorine contamination. This may be caused by grease which was used to seal the glass apparatus. Fig. 4.25 displays the XPS spectrum of SAM sample **(4)**.

The reference sample **(6)** shows atomic ratios expected from the stoichiometry. Small substrate signals, expressed as [Si] and [O], have been detected pointing to layer at a thickness $< \sim 10$ nm.

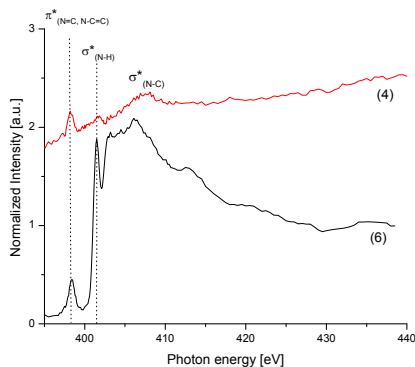


Figure 4.26. N K-edge NEXAFS of 4-aminophenylbutane-1-thiol on Au **(4)** and 4,4'-methylenebis(2,6-diethylaniline) **(6)** on oxidized Si. Due to the low N surface concentration, the N K-edge electron yield is small for the SAM **(4)** sample and the normalization of the spectrum is strongly influenced by the C K-edge decay background at the N K-edge.

NEXAFS N K-edge (Fig. 4.26) spectra show N-H resonances, which are more pronounced for the aromatic aniline derivative **(6)** in comparison to the N K-edges, measured with aliphatic samples. For the reference sample **(6)** the spectrum shows more σ^* features in the range of above ~ 403 eV which can be explained by its highly conjugated character. The quality of the N K-edge spectra of the aromatic thiol on Au **(4)** suffer from the low N content of the film and an enhanced radiation damage risk due to longer acquisition times has to be assumed.

In the C K-edge NEXAFS spectra of aromatic films, displayed in Fig. 4.27, $\pi^*(\text{C}=\text{C})$ and $\pi^*(\text{C}=\text{N})$ resonances at 285.0-4 eV and 285.5-6 eV are distinctive. For sample (4), the $\pi^*(\text{C}=\text{C})$ resonance intensity is considerably higher, whereas for the aniline derivative (6) the $\pi^*(\text{C}=\text{N})$ resonance intensity is more striking.

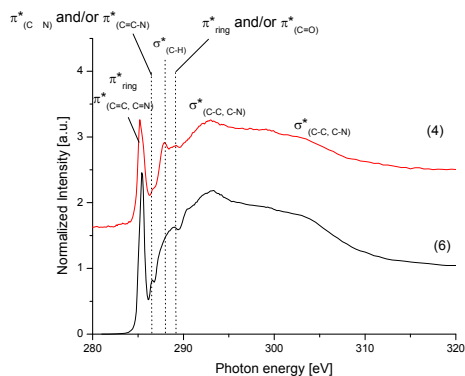


Figure 4.27. The C K-edge NEXAFS spectra of 4-aminophenylbutane-1-thiol on Au (4) and 4,4'-methylenebis(2,6-diethylaniline) (6) on oxidized Si.

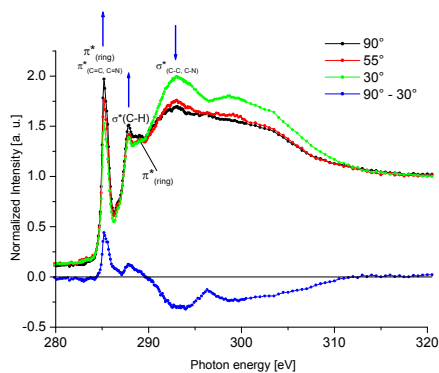


Figure 4.28. C K-edge NEXAFS at three different angles of incidence of linearly polarized synchrotron light (30°, 55° and 90°) and the difference spectrum (90°-30°) for 4-aminophenylbutane-1-thiol on Au (4).

In contrast to the NEXAFS spectra of aliphatic species there is one more feature (~289 eV) that is attributed to another π^* resonance of the ring [33]. Amides which give rise to resonances at around 288.7 eV for $\pi^*(\text{C}=\text{O})$ may also contribute to this peak, but there is no clear evidence for such species obtained from the N1s XP spectra. Similar to the aliphatic analogues there is an evidence for C=O bonds in the C1s XP spectra of the aromatic samples, but these species contribute to less than 6% of the total C1s intensity.

For SAM (**4**) the C K-edge NEXAFS spectra were found to be angle dependent (Fig.4.28), proving its orientation. The mean tilt angle of the aromatic ring in SAM (**4**) relative to the surface normal was estimated to be $\sim 31.5^\circ$ following a procedure described in [84].

4.2.2.5. Derivatization and characterization of the amino terminated SAMs

Gas-phase derivatization of amino terminated SAMs were performed in order to quantify free amino groups on the surface. SAM (**4**) was derivatized by TFBA whereas SAM (**2**) was coupled with PFB. TFBA and PFB were used as derivatization reagents since they react selectively with primary amino groups and are easily detectable by XPS and NEXAFS due to their high fluorine content. Both experiments were applied at room temperature for 90 min.

Fig. 4.29 displays the coupling reaction between TFBA and SAM (**4**).

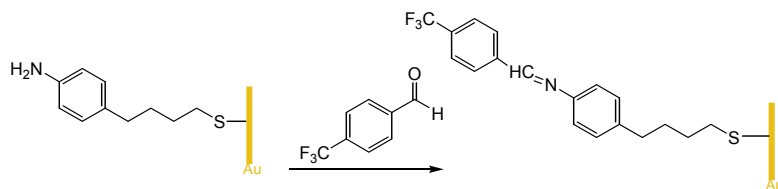


Figure 4.29. A scheme of the derivatization reaction between 4-aminophenylbutane-1-thiolate (**4**) and TFBA.

Table 4.17 summarizes the calculated stoichiometry and atomic percent [at%] obtained from XP survey spectra. The fluorine contamination of SAM (**4**) (4-aminophenylbutane-1-thiolate), (supplied from Terfort et al.) was mentioned before. In order to obtain $[\text{F}]/[\text{C}]$ ratio from XPS results, fluorine contamination of underivatized sample is subtracted from the fluorine content of TFBA derivatized sample. The $[\text{C}]/[\text{N}]$ ratios of both underivatized and TFBA derivatized SAM (**4**) are consistent with the stoichiometry of the sample. The $[\text{F}]/[\text{N}]$ ratio is close to the theoretical value.

Table 4.17. Calculated stoichiometry and atomic percent [at%] from the XP survey spectra of underivatized and 90 min. TFBA derivatized SAM (**4**) on Au.

	underivatized SAM(4)		TFBA derivatized SAM(4)	
	calculated stoichiometry [at%]	obtained from XPS results [at%]	calculated stoichiometry [at%]	obtained from XPS results [at%]
[C]	10	54.9	18	58.4
[N]	1	3.0	1	2.9
[S]	1	2.1	1	2.0
[F]	-	5	3	12.5
[C]/[N]	10 : 1	18 : 1	18 : 1	20 : 1
[N]/[S]	1 : 1	1.4 : 1	1 : 1	1.4 : 1
[F]/[N]	-	-	3 : 1	2.6 : 1

The surface spectra of underivatized 4-aminophenylbutane-1-thiolate (**4**) on Au were discussed in 4.2.2.4. After derivatization, a CF₃ peak at 292.8 eV is observed in the high resolution XP C1s spectrum. Imine binding energy is observed at 398.9 eV in the N1s spectrum of the derivatized sample. Table 4.18 summarizes the binding energies and area percentages of carbon and nitrogen components of underivatized and TFBA derivatized SAM (**4**).

Table 4.18. Binding energies [BE (eV)] and area percentages [area%] of carbon and nitrogen functionalities of underivatized and TFBA derivatized 4-aminophenylbutane-1-thiolate (**4**) on Au. TFBA derivatization was carried out at room temperature for 90 min. Binding energies and area percentages are obtained from high resolution XP C1s and N1s spectra.

	high resolution XP C1s spectra						high resolution XP N1s spectra				
	C _{aromatic}	C _{aliphatic}	C-N	C=N C-O	C=O HNC=O	CF ₃	NH ₂	C=N	NHC=O	--NH ₂ NH ₃ ⁺	
SAM (4)	284.4	285.0	285.7	286.3	287.8	-	399.2	-	400.4	-	BE(eV)
	43.1	19.2	13.1	6.4	2.7	-	88.2	-	11.8	-	[area%]
TFBA SAM (4)	284.4	285.0	285.7	286.5	287.5	292.8	-	398.9	-	401.0	BE(eV)
	60.2	14.1	10.2	4.6	3.04	5.6	-	78.5	-	21.5	[area%]

Fig. 4.30 displays XP survey scans, C1s and N1s spectra of the underivatized (a-1,2,3) and the TFBA derivatized (b-1,2,3) SAM (**4**).

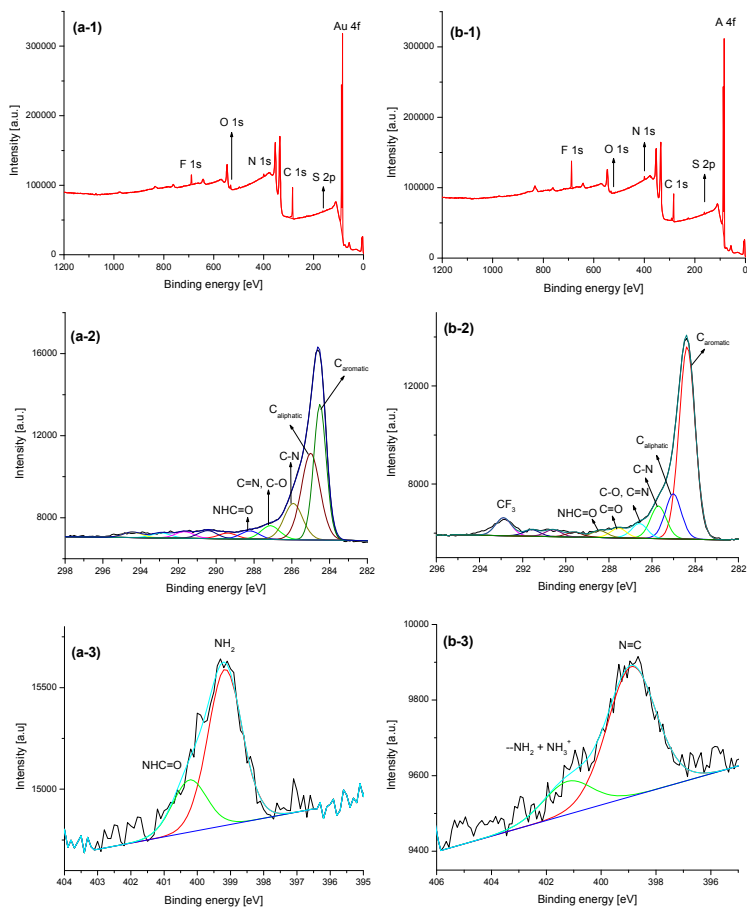


Figure 4.30. XP survey scan (a-1), high resolution XP C1s (a-2) and N1s (a-3) of 4-aminophenylbutane-1-thiolate (**4**) on Au. (b-1), (b-2) and (b-3) represent the XP survey scan and the high resolution XP C1s, XP N1s of TFBA derivatized SAM (**4**), respectively. Surface is derivatized for 90 min at r.t.

From the analysis of the N1s high resolution spectrum, 78.5 area% of C=N component versus 21.5 area% for hydrogen bonded or protonated amines was observed. This result can be interpreted as a yield of 78% for the coupling reaction (78 area% / (78.5+21.5) area%). Yields of derivatization reactions carried out in liquid phase are in the range of 78% - 88% (4.1) and are expected to be the upper limit of gas-phase surface derivatization reactions. 78% yield of TFBA derivatization reaction of SAM (**4**) is in this range. For the TFBA derivatized SAM (**4**), the C K-edge NEXAFS spectra were found to be angle dependent (Fig. 4.31), proving its orientation. Table 4.19 summarizes the C K-edge resonance energies for TFBA derivatized 4-aminophenylbutane-1-thiolate (**4**).

Table 4.19. C K-edge resonance energies obtained from NEXAFS measurements of TFBA derivatized 4-aminophenylbutane-1-thiolate (**4**) on Au. TFBA derivatization was carried out at r.t. for 90 min.

	C K-edge resonance energies					
TFBA derivatized SAM(4)	π^* (C=C)				σ^* (C-C)	
	π^* (C=N)	σ^* (C-H)	π^* (ring)	σ^* (C-F)	σ^* (C-N)	σ^* (C-F)
	285.1	287.7	289.0	291.9	292.9	295.0

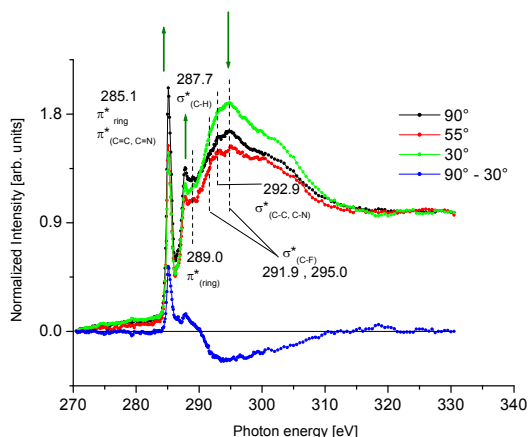


Figure 4.31. C K-edge NEXAFS at three different angles of incidence of linear polarized synchrotron light (30°, 55° and 90°) and the difference spectrum (90°-30°) for TFBA derivatized 4-aminophenylbutane-1-thiol on Au (**4**).

The mean tilt angle of the aromatic ring in TFBA derivatized SAM (**4**) relative to the surface normal was calculated to be 60.5° [84].

11-amino-1-undecanethiol (**2**) on Au was derivatized with PFB at r.t. for 90 min. XPS and NEXAFS analysis of the underivatized surface was discussed in 4.2.2.3. After derivatization, XPS and NEXAFS measurements were applied to the surface in order to quantify amino groups and prove the orientation of the monolayer.

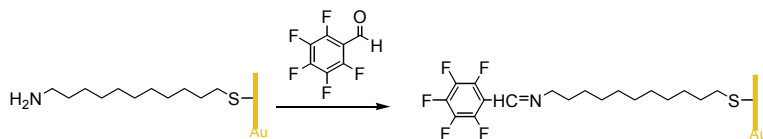


Figure 4.32. A scheme of the derivatization reaction between 11-amino-1-undecanethiol (**2**) and PFB.

Figure 4.32 displays the coupling reaction between SAM (**2**) and PFB. Table 4.20 summarizes calculated stoichiometry and atomic percent [at%] of underivatized and 90 min. PFB derivatized SAM (**2**). Atomic percentages are obtained from XP survey scans.

4. Derivatization of primary amines

Table 4.20. Calculated stoichiometry and atomic percent [at%] from XP survey spectra of underivatized and 90 min. PFB derivatized SAM (2) on Au.

	underivatized SAM(2)		TFBA derivatized SAM(2)	
	calculated stoichiometry [at%]	obtained from XPS results [at%]	calculated stoichiometry [at%]	obtained from XPS results [at%]
[C]	10	65.3	18	65.5
[N]	1	4.2	1	1.9
[S]	1	5.4	1	2.2
[F]	-	-	5	8.7
[C]/[N]	10 : 1	15 : 1	18 : 1	34 : 1
[N]/[S]	1 : 1	0.8: 1	1 : 1	0.9 : 1
[F]/[N]	-	-	5 : 1	4.6 : 1

The [C]/[N] ratios of both underivatized and PFB derivatized SAM (2) is somewhat higher than expected. This may be due to a carbon contamination that originates from incomplete substrate cleaning. [N]/[S] ratios as well as [F]/[N] ratio are consistent with the stoichiometry of the sample.

Table 4.21. Binding energies [BE (eV)] and area percentages [area%] of carbon and nitrogen functionalities of underivatized and PFB derivatized 11-amino-1-undecanethiol (2) on Au. PFB derivatization was carried out at room temperature for 90 min. Binding energies and area percentages are obtained from high resolution XP C1s and N1s spectra.

	high resolution XP C1s spectra					high resolution XP N1s spectra				
	C-C C-H	C-N	C=N C-O	C=O	C-F	NH ₂	C=N	NHC=O	--NH ₂ NH ₃ ⁺	
SAM (2)	285.0	286.4		287.7	-	399.3	-	400.3	401.3	BE(eV)
	87.3	19.2	13.1	6.4	-	18.6	-	8.8	72.6	[area%]
PFB	285.0	285.7	286.2	287.6	288.5	-	398.9	400.3	401.7	BE(eV)
SAM (2)	37	23.6	12.2	3.0	11.7	-	65.0	21.0	14.0	[area%]

Table 4.21 summarizes the binding energies and area percentages of carbon and nitrogen components of the underivatized and the PFB derivatized SAM (2). In the high resolution XP C1s spectrum of the underivatized SAM (2) (Fig. 4.22), the C-N peak, which is expected between 285.7-286.0 eV, superimposes with broad C-C, C-H peak and a C-O peak at 285.0 and 286.4 eV respectively. After derivatization, a sharp C-F peak is observed at 288.5 eV the in high resolution XP C 1s spectrum of the PFB derivatized SAM (2).

From the analysis of the N1s high resolution spectrum of the PFB derivatized SAM (2), 65 area% of C=N component versus 35 area% for hydrogen bonded or protonated amines

and amides. This result can be interpreted as a yield of 65% for the coupling reaction (65 area% / (65+14+21) area%). Yields of derivatization reactions were discussed in 4.1. 65% yield obtained for PFB derivatization of SAM (**2**) is in expected range (max. 87% from liquid phase).

Figure 4.33 displays XP survey scan (a), C1s (b) and N1s (c) spectra of PFB derivatized 11-amino-1-undecanethiol (**2**) on Au.

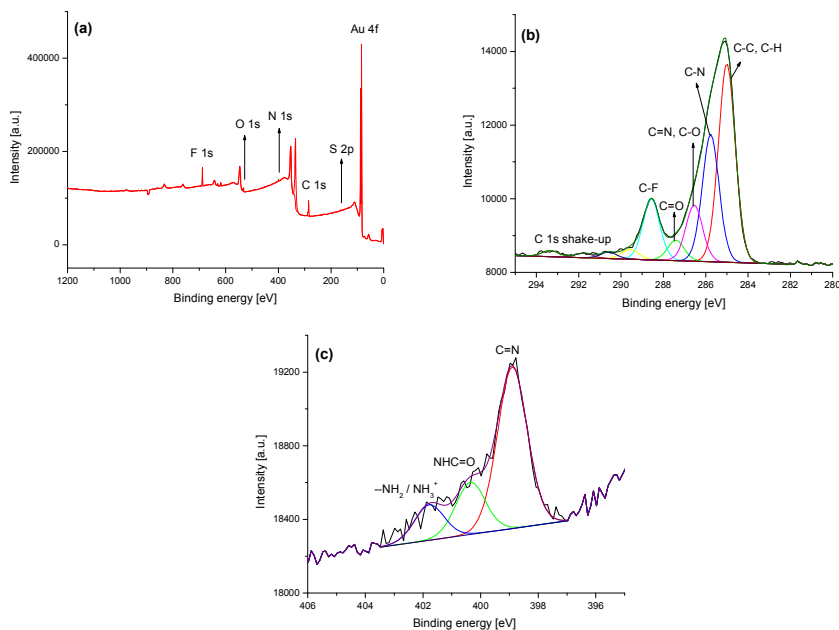


Figure 4.33. XP survey scan (a), high resolution XP C1s (b) and N1s (c) of PFB derivatized 11-amino-1-undecanethiol (**2**) on Au. PFB derivatization was carried out at room temperature for 90 min.

The C K-edge NEXAFS spectra of PFB derivatized SAM (**2**), were found to be angle dependent (Fig. 4.34). Table 4.22 summarizes the C K-edge resonance energies for PFB derivatized 11-amino-1-undecanethiol (**2**).

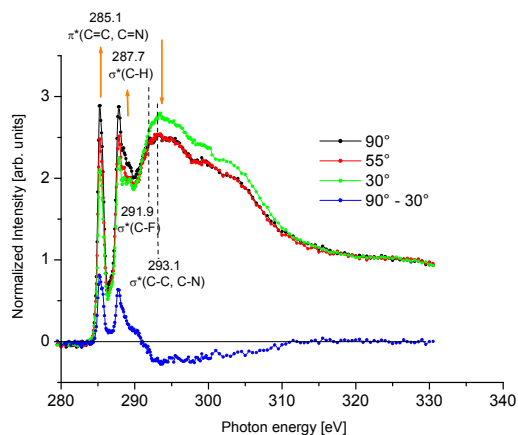


Figure 4.34. C K-edge NEXAFS at three different angles of incidence of linear polarized synchrotron light (30°, 55° and 90°) and the difference spectrum (90°-30°) for PFB derivatized 11-amino-1-undecanethiol (**2**) on Au.

Table 4.22. C K-edge resonance energies obtained from NEXAFS measurements of PFB derivatized 11-amino-1-undecanethiol (**2**) on Au. PFB derivatization was carried out at r.t. for 90 min.

		C K-edge resonance energies			
TFBA derivatized SAM(4)	π^* (C=C)				σ^* (C-C)
	π^* (C=N)				σ^* (C-N)
		285.1	287.7	291.9	292.9

The mean tilt angle of the aromatic ring in PFB derivatized SAM (**2**) relative to the surface normal was $\sim 64^\circ$ [84].

4.2.2.6. Radiation damage effects

The application of XPS as a tool for quality control of aminated surfaces as for instance microarray slides requires a knowledge on potential radiation damage originating from the use of X-rays during analysis. Kristensen et al. [85] reported in an XPS study of an amino siloxane sample that the radiation damage effect at their experimental conditions was minimal. In agreement with that, the influences of radiation damage effects are supposed to be negligible for all samples investigated in this study.

Though NEXAFS spectroscopy will not be a standard tool for quality control of aminated templates, it can provide valuable information for the development of new functional surfaces. Radiation damage potentially occurring during this kind of analysis is a point of interest. The NEXAFS C K-edge spectra of the aliphatic amino thiol film (**2**) is

shown in Figure 4.35 before and after 1 h radiation exposure at 295 eV at increased slit width. In that way, the samples were exposed to photon fluxes much higher as in a typical NEXAFS analysis in this study, in order to find changes in the spectra unequivocally due to radiation damage. The result of this test are increased intensities of resonances related to unsaturated species such as C=C and C=N.

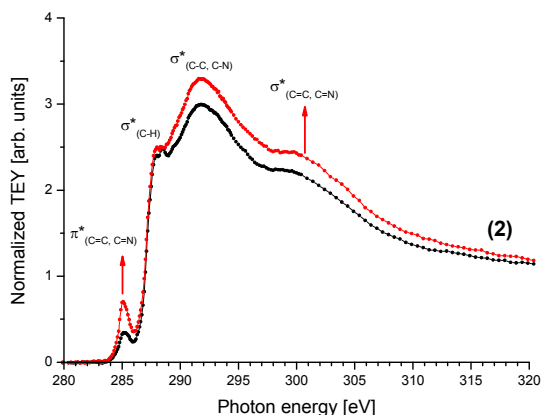


Figure 4.35. NEXAFS spectra at the C K-edge of 11-amino-1-undecanethiol on Au (**2**). The sample was analyzed in fresh state (black lines) and after extended X-ray exposure (samples irradiated at 295 eV for 1 hour using the HE-SGM grid 1 and an enhanced slit width of 500 μm).

The related NEXAFS spectra at the N K-edge are shown in Figure 4.36. Resonance intensities for unsaturated species such as N=C, N-C=C and N \equiv C show no significant irradiation effect in the N K-edge NEXAFS of SAM (**2**). It means for the SAM (**2**) beam damage preferentially leads to the formation of unsaturated carbon bonds as known from other alkane SAM NEXAFS studies [86]. Probably it is important here that there are 10 C-C bonds but only one C-N bond per molecule in the thiol film.

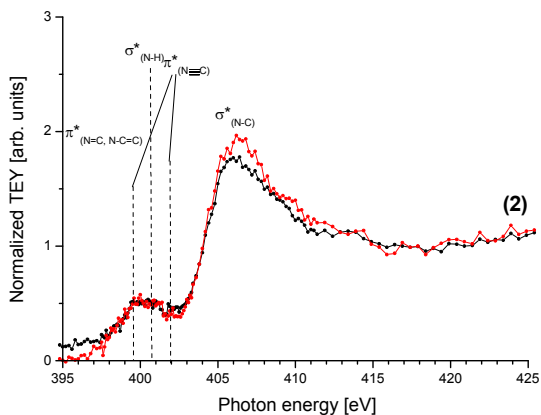


Figure 4.36. NEXAFS spectra at the N K-edge of 11-amino-1-undecanethiol on Au **(2)**. The sample was analyzed in fresh state (black lines) and after extended X-ray exposure (samples irradiated at 295 eV for 1 hour using the HE-SGM grid 1 and an enhanced slit width of 500 μm).

4.3. Plasma polymerized allylamine samples

4.3.1 Introduction

Plasma polymerization is a thin film forming process onto surfaces of substrates under the influence of plasma. Here, conversion of low-molecular weight molecules (monomers) into high-molecular weight molecules (polymers), occurs with the assistance of the plasma energy. Plasma polymerization mechanisms are generally very complex and involve multiple reaction pathways ending up in the formation of a broad range of species. Ultra-thin film forming capability of plasma polymerization is a unique and valuable asset and plasma polymers are generally chemically inhomogeneous, branched and cross-linked.

The nature of the deposited films depends on the internal (plasma density, plasma temperature, electron energy distribution, mean free paths, Debye length and sheath potential) and external (reactor geometry, type of excitation, applied power, monomer pressure, gas flow rate or duty cycle) plasma parameters. Several studies of the effect of these parameters have been done over the past years [87-91]. Although it is possible to directly control the internal plasma parameters, it is a highly complex and difficult task. However, as it is performed in this work, it is possible to exercise an indirect control on these internal plasma parameters by the control of a few selected external plasma process parameters. These

parameters were plasma power, duty cycle and the monomer pressure during plasma polymerization.

It is well known that during the plasma deposition of monomers containing amino groups, fragmentation reactions occur. They result in elimination of amines as well as transformation of amino groups into imines and nitriles [92]. These transformations can result from the breaking of molecular bonds shown in the Fig. 4.37.

In this project, in order to minimize the transformation of the primary amino groups, the unsaturated monomer, namely allylamine ($\text{CH}_2=\text{CH}-\text{CH}_2-\text{NH}_2$), was used. The double bond was expected to be involved in the polymerization process thereby reducing the fragmentation of the monomer.

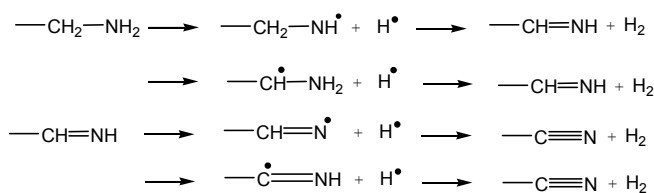


Figure 4.37. Reactions leading to the imine and nitrile formation [93].

Plasma polymerized allylamine surfaces were explored previously by Sufal et al. concerning the effects of plasma parameters on total nitrogen yield [94]. By using CD-XPS along with NEXAFS, it is aimed to observe the amino group retention when plasma parameters are changed. Quantification of surface amino groups of plasma polymerized allylamine films is also studied.

4.3.2. Characterization of plasma polymerized allylamine films

Plasma depositions of allylamine films were performed at various duty cycle, power and pressure values in order to study the effect of plasma parameters on amino group retention. Two sets of samples were prepared for XPS and NEXAFS studies. TFBA and PFB were chosen as derivatization reagents since they react solely with primary amino groups and are easily detectable by XPS and NEXAFS due to the high fluorine content. XPS and NEXAFS measurements were done before and after derivatization. Again, a set of derivatization reactions containing 1, 5, 20, 45, 90 and 180 min. were performed in order to determine the reaction time required for saturation. XP F1s spectra of PFB derivatized samples showed a second peak, besides the expected C-F binding energy, indicating side

reactions. Thus, only TFBA derivatized samples will be explored. This limitation of PFB as a derivatization reagent in plasma polymerized samples will be considered later in this chapter.

In order to define the time of reaction completion, plasma polymerized allylamine samples of 20W, 0.5 duty cycle, 15 Pa and 40 nm were exposed to TFBA vapor for different reaction times. Both F/C and N/C ratios are corrected as explained in 4.2.1.3. Both $F/C^{\text{corrected}}$ and $N/C^{\text{corrected}}$ vs time graphs (4.38) show a clear 90 min. saturation.

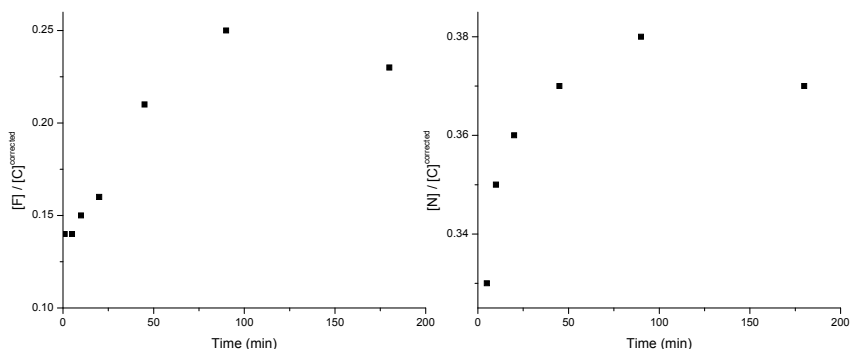


Figure 4.38. Plasma polymerized allylamine surfaces were derivatized with TFBA for 1, 5, 10, 45, 90 and 180 minutes to determine the time required for reaction completion. $F/C^{\text{corrected}}$ and $N/C^{\text{corrected}}$ vs time graphs indicate a 90 min. reaction time.

As a test sample, a plasma polymerized allylamine film was prepared at 20W, 0.5 duty cycle and 15 Pa in order to study the spectral differences between underivatized and TFBA derivatized sample. Because of the fragmentation which occurs during plasma deposition and due to the air exposure, a complex surface carrying different functional groups is expected. Fig. 4.39 shows a scheme of the selective derivatization of surface amino groups.

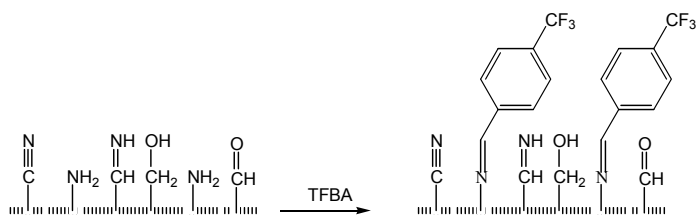


Figure 4.39. A scheme of the selective derivatization reaction between surface amino groups and the marker reagent, TFBA.

The stoichiometrical data of the derivatization is calculated from the coupling reaction between poly(allylamine) and TFBA (Fig.4.40). The data obtained by XPS is expected to show deviations from the ideal case due to the different functional groups, formed by fragmentation in plasma deposition. Table 4.23 summarizes calculated stoichiometries and atomic percentages [at%] obtained from XP survey spectra.

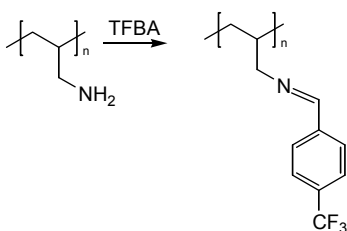


Figure 4.40. TFBA derivatization of poly(allylamine).

Table 4.23. Calculated stoichiometry and atomic percent [at%] from XP survey spectra of plasma deposited underivatized allylamine and 90 min TFBA-derivatized allylamine films.

	calculated stoichiometry [at%]						obtained from XPS results [at%]					
	[C]	[N]	[O]	[F]	[C]/[N]	[F]/[N]	[C]	[N]	[O]	[F]	[C]/[N]	[F]/[N]
underivatized	3	1	-	-	3	-	75	24	1	-	3	-
derivatized	11	1	-	3	11	3	64	14	4	18	4.6	1.3

4. Derivatization of primary amines

The XP survey scan, the C1s and N1s spectrum of the underderivatized sample as well as the 90 min. TFBA derivatized sample are shown in Fig. 4.41. The XP survey scan of the underderivatized sample consists of carbon and nitrogen along with traces of oxygen. The source of oxygen is the air exposure due to the time, (approximately 5 min.), between plasma deposition and XPS measurement. As expected, in situ XPS measurements showed no oxygen on the surface. The C1s spectrum of the sample is fitted by fixing the binding energies according to the data found in the literature [62].

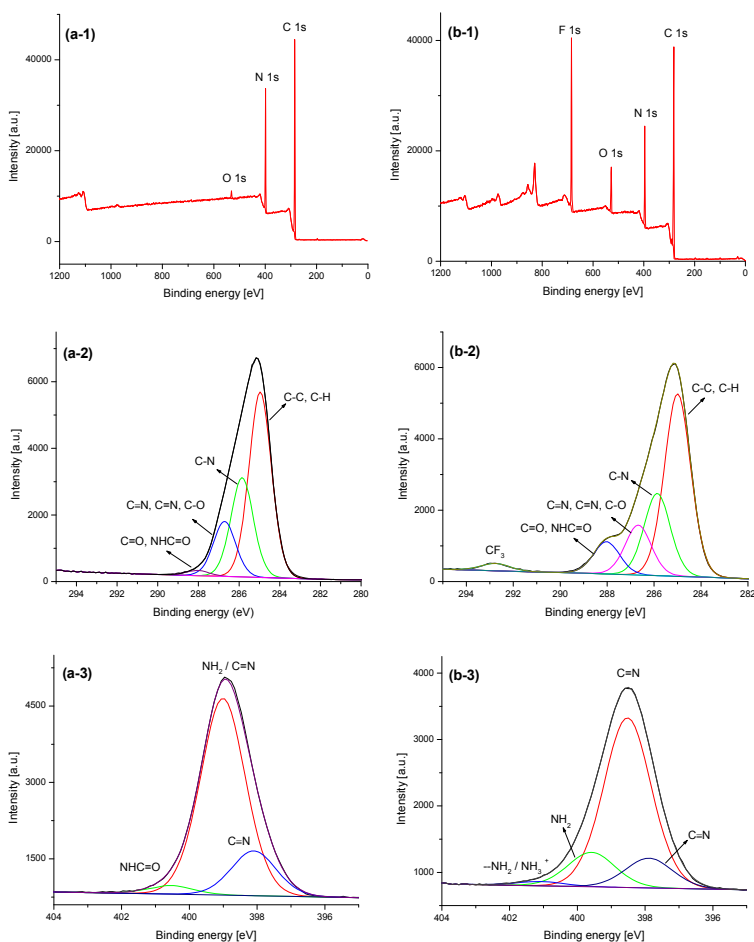


Figure 4.41. XP survey scan (a-1), C1s (a-2) and N1s (a-3) spectrum of the underderivatized poly(allylamine) film that was deposited at 20W, 0.5 duty cycle and 15 Pa are shown on the left row. The right row displays XP survey scan (b-1), C1s (b-2) and N1s (b-3) of the 90 min TFBA derivatized poly(allylamine) film deposited at 20W, 0.5 duty cycle and 15 Pa.

The XPS measurement was repeated after the same film was derivatized with TFBA. Unlike the underivatized sample, the XP survey scan of the derivatized film shows an additional fluorine peak due to the trifluoromethyl groups attached to the derivatization reagent. The reaction between the surface primary amino groups and TFBA can be proved by the CF_3 peak appears at 292.8 eV in the XP C1s spectrum. Due to the fact that the surface nitrogen content of the derivatized sample consists of different nitrogen species, the $[\text{F}]/[\text{N}]$ ratio is less than the theoretical value calculated from the polyallylamine structure.

Table 4.24. Binding energies [BE(eV)] and area percentages [area%] of carbon and nitrogen functionalities of plasma deposited underivatized polyallylamine and TFBA derivatized polyallylamine films. Plasma deposition was carried out at 20W, 0.5 duty cycle and 15 Pa, derivatization time 90 min. Binding energies and area percentages are obtained from high resolution XP C1s and N1s spectra.

	high resolution XP C1s spectra					high resolution XP N1s spectra					
	C-C C-H	C-N	C=N C-O C≡N	C=O NHC=O	CF_3	N=C	NH_2	N=C	NHC=O	-- NH_2 NH_3^+	
underivatized sample	285.0	285.9	286.7	288.0	-	398.0	399.0		400.5	-	BE(eV)
	54	28	16	2	-	18	79		3	-	[area%]
derivatized sample	285.0	285.9	286.7	288.0	292.8	398.0	399.5	398.5	-	401.8	BE(eV)
	51	23	14	9	3	13	14	71	-	2	[area%]

High resolution XP N1s of the underivatized sample shows a nitrogen peak of 79% at 399.0 eV (Table 4.24). The binding energy of amino groups are expected between 399.0 and 399.6 eV whereas imino groups appear between 397.8 and 399.0 eV. As a result, the peak at 399.0 eV is assigned as a combination of free amino groups and the imine species on the surface where imine functionalities are also expected due to the plasma deposition of allylamine.

The binding energy difference between the components C-N and C-OR as well as C=N is small. Thus, it is not convenient to rely on the C-N component area of C1s spectrum to estimate the surface concentration of primary amines on the surface. The yield of the reaction can be calculated from the area percentages of the high resolution XP N1s spectrum of the derivatized sample. From the analysis of the N1s high resolution spectrum we obtain 71 area% of the C=N component versus 14 area% for unreacted amino species and 2 area% for protonated amines. This result can be interpreted as a yield of 81% for the coupling reaction (71 area% / (71+14+2) area%). The peak at 398.0 eV can be attributed to C≡N formed during

plasma polymerization, which is also observed in the high resolution N1s spectrum of the underivatized sample. Yields of derivatization reactions carried out in liquid phase (between 78% - 88%) are explained in 4.1 and expected to be the upper limit of gas-phase surface derivatization reactions. 81% yield of the TFBA derivatization reaction of the plasma deposited allylamine film is in this range.

Before starting with variations of plasma parameters, the potential radiation damage on TFBA is studied. In order to confirm an X-ray damage originating from the use of X-rays, it is applied a ten-hour survey scan measurement. An allylamine sample was deposited at 20W, 0.5 duty cycle and 15 Pa and was derivatized with TFBA for 90 min. 127 survey scans were run between 250-720 eV in 10 h. The resulting spectrum is shown in Fig. 4.42.

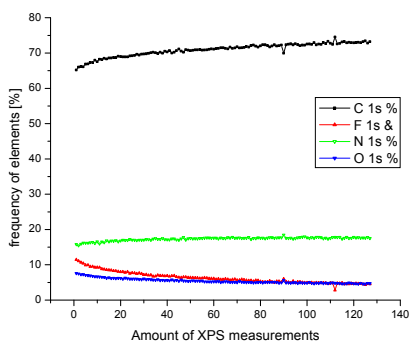


Figure 4.42. The effect of prolonged X-ray beam on plasma polymerized allylamine film deposited at 20W, 0.5 duty cycle and 15 Pa. The surface was then derivatized with TFBA for 90 min.

In 10 h, the fluorine amount on the surface decreases from 11.5% to 4.4%. However, the beam damage cannot be attributed as the only reason for the C-F cleavage since, during a regular XPS measurement, for a survey scan of 0-1200 eV, samples are exposed to an X-ray beam for 23 min. A total measurement with survey scan, high resolution XP C1s, N1s, O1s and F1s takes around 2 h. Consequently, influence of radiation damage effects at our experimental conditions are supposed to be negligible.

4.3.3. Effects of external plasma parameters on amino group retention

Three different sets of plasma polymerized allylamine samples were prepared and all samples were derivatized with TFBA for 90 min. Then the samples were measured by XPS and NEXAFS. The spectra of the TFBA derivatized and underivatized samples were then compared in order to observe the effect of plasma parameters on primary amino group retention in the films. Table 4.25 shows the experimental details of underivatized and TFBA derivatized samples of plasma deposited allylamine films.

Table 4.25. Experimental details of plasma deposited allylamine films and external plasma parameters employed for their deposition during XPS and NEXAFS studies.

Samples	underivatized			TFBA-derivatized		
	duty cycle	sample names	fixed parameters	duty cycle	sample names	fixed parameters
Duty cycle variation	0.05	UZ_30	20W, 5Pa 40 nm	0.05	UZ_29	20W, 5Pa 40 nm
	0.1	UZ_32		0.1	UZ_31	
	0.5	UZ_34		0.5	UZ_33	
	1.0	UZ_36		1.0	UZ_35	
Power variation	power (W)	sample names	fixed parameters	power (W)	sample names	fixed parameters
	20	UZ_36	1.0, 5Pa, 40nm	20	UZ_35	1.0, 5Pa, 40nm
	30	UZ_38		30	UZ_37	
	50	UZ_40		50	UZ_39	
pressure (Pa)	sample names	fixed parameters		pressure (Pa)	sample names	
Pressure variation	2	UZ_42	0.1, 20W, 40 nm	2	UZ_41	0.1, 20W, 40 nm
	5	UZ_32		5	UZ_31	
	15	UZ_46		15	UZ_43	

The correlation between surface amino group concentration and external plasma parameters are studied by using the $[CF_3]$ component area obtained from high resolution XP C1s spectra. Since TFBA selectively reacts with primary amino groups on the surface, $[CF_3]$ area percentage is directly related to the quantity of surface amino groups. Fig. 4.43 shows the dependence of $[CF_3]$ area percentage on duty cycle (a) and power (b).

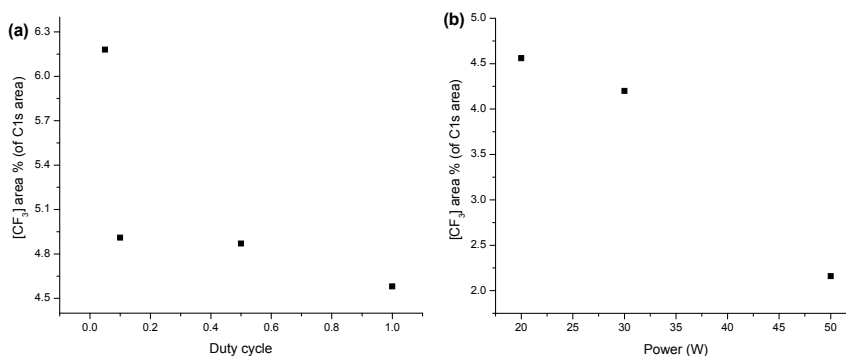
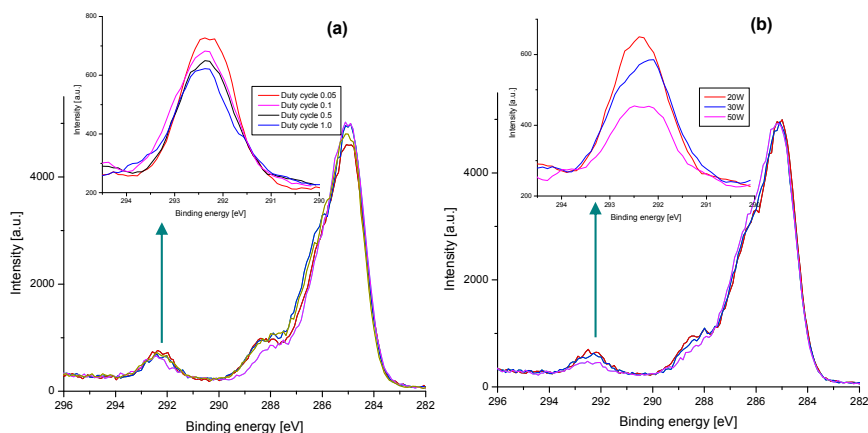


Figure 4.43. Dependence of [CF₃] % area on (a) duty cycle (b) power. Duty cycle values of 0.05, 0.1, 0.5 and 1.0 were applied during plasma depositions of allylamine at 20W and 5 Pa. Film thicknesses were kept at 40 nm. Plasma polymerized allylamine samples were then derivatized with TFBA in gas-phase for 90 min. 20, 30 and 50W were applied for power variation where a duty cycle of 1.0 and a pressure of 5 Pa was used. Film thicknesses were 40 nm. Plasma polymerized allylamine samples were then derivatized with TFBA in gas-phase



for 90 min.

Figure 4.44. Overlay of high resolution XP C1s spectra of TFBA derivatized poly(allylamine) samples showing a duty cycle variation (a) and power variation (b). Binding energy range of 290-294 eV is enlarged in order to observe the effect of varied plasma parameter on [CF₃] area. The region is smoothened for a better vision. Duty cycle values of 0.05, 0.1, 0.5 and 1.0 were applied at 20 W and 5 Pa (a). 20, 30 and 50W were the applied power values at 1.0 duty cycle and 5 Pa (b). Film thicknesses were kept at 40 nm. Plasma polymerized allylamine samples of both sets were then derivatized with TFBA in gas-phase for 90 min.

Figure 4.44 displays an overlay of high resolution XP C1s spectra of TFBA derivatized poly(allylamine) samples which vary in their duty cycles (a) and powers (b). In both figures, an enlarged region of 290-294 eV is shown to observe the CF₃ area differences of the samples. Variations in both duty cycle and power, show a clear effect on the [CF₃] area, also revealed by Fig. 4.43.

Either an increase of the duty cycle or in the plasma power increases the electron energy [99]. This leads to an increase in electron density. The mean free path of plasma particles decreases as the electron density increases. Consequently, the collision rate of the particles increases. This results in higher fragmentation and rearrangements of monomer molecules. It is clearly observed from Fig. 4.43 and 4.44, as duty cycle and power increases, the [CF₃] area percentage decreases resulting in a descending trend of primary amino group retention on the plasma polymerized surface.

Fig. 4.45 shows the dependence of [CF₃] area % on pressure. As in the case of duty cycle and power dependence graphs, [CF₃] component areas were obtained from high resolution XP C1s spectra.

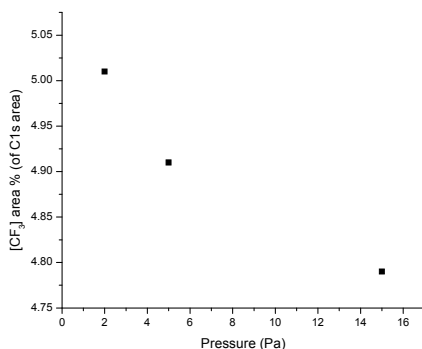


Figure 4.45. Dependence of [CF₃] area % (of C 1s area) on pressure. Pressure values of 2, 5 and 15 Pa were applied during plasma deposition of allylamine at 20 W and 0.5 duty cycle. Film thicknesses were kept at 40 nm. Plasma polymerized allylamine samples were then derivatized with TFBA in gas-phase for 90 min.

Pressure is a more complex plasma parameter than power or duty cycle due to competing mechanisms. An increase in pressure results in an increase in particle density that leads to a decrease in the mean free path of the plasma particles. Thus, the collision rate increases which results in higher fragmentation rate. However, a decrease in mean free path of electrons leads to a decrease in the electron energy. This subsequently decreases the

fragmentation and rearrangement rate of the monomer molecules. However, some amount of control can still be exercised on the chemistry of the plasma polymers using the monomer pressure as a parameter.

Fig. 4.46 displays the overlay of high resolution XP C1s spectra of TFBA derivatized poly(allylamine) samples which vary in their pressure. The binding energy region of 290-294 eV is enlarged in order to observe the CF_3 area differences of the samples. Variations in pressure show a clear effect on the $[\text{CF}_3]$ area, also revealed by Fig. 4.45.

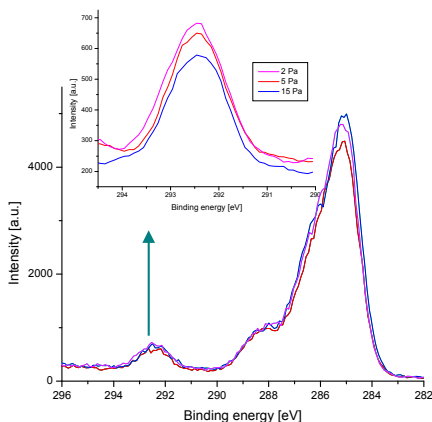


Figure 4.46. Overlay of high resolution XP C1s spectra of TFBA derivatized poly(allylamine) samples showing a pressure variation. Binding energy range of 290-294 eV is enlarged in order to observe the effect of varied pressure on $[\text{CF}_3]$ area. The region is smoothed for a better vision. Pressure values of 2, 5 and 15 Pa were applied at 20 W and 0.5 duty cycle. Film thicknesses were kept at 40 nm. Plasma polymerized allylamine samples were then derivatized with TFBA in gas-phase for 90 min.

$[\text{CF}_3]$ area % of plasma deposited allylamine surfaces increases as pressure increases. Consequently, they display an ascending trend of surface amino group retention. Here, an increase in pressure leads to a decrease in mean free path of electrons resulting in a decrease in the electron energy. This subsequently decreases the fragmentation and rearrangement rate of the monomer molecules.

4.3.4. NEXAFS characterization of plasma polymerized allylamine films

NEXAFS was used in combination with XPS in order to study the effect of plasma process parameters on the amount of amino functionalities at the surface of plasma polymerized allylamine films. The films were characterized with NEXAFS before and after TFBA derivatization. Samples were exposed to air during the time passed between NEXAFS measurements and derivatizations.

Fig. 4.47 presents C K-edge spectra of selected plasma polymerized allylamine films deposited at 20W, 5Pa and 0.05 duty cycle. Fig. 4.47(a) shows the spectrum of the underderivatized film whereas Fig. 4.47(b) displays the C K-edge spectrum of the same sample after 90 min gas-phase derivatization with TFBA. Fig. 4.47(c) shows the difference spectrum of the previous two spectra.

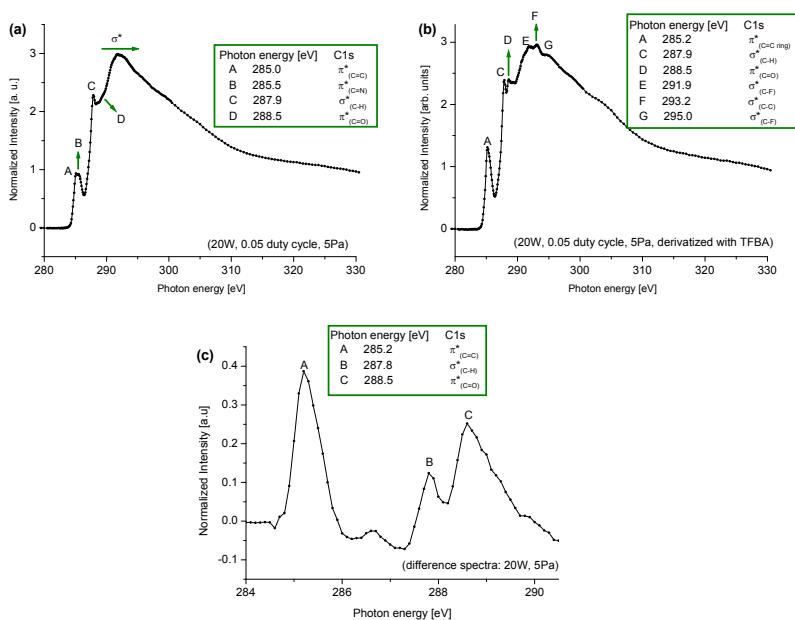


Figure 4.47. (a) NEXAFS C K-edge of plasma polymerized allylamine film (20W, 0.05 duty cycle, 5Pa). (b) NEXAFS C K-edge of (a) after 90 min derivatization of TFBA. (c) The difference spectrum of the previous two spectra.

Fig. 4.47(a) displays four main peaks. The peak A appears at 285.0 eV ($C1s \rightarrow \pi^*_{(C=C)}$), the peak B at 285.5 eV ($C1s \rightarrow \pi^*_{(C=N)}$), C at 287.9 eV ($C1s \rightarrow \sigma^*_{(C-H)}$) resonance, D at 288.5 eV ($C1s \rightarrow \pi^*_{(C=O)}$). There are various σ^* resonances above 292 eV [35,95].

The C K-edge NEXAFS spectrum of the derivatized film, displayed in Fig. 4.47(b), differs from the C K-edge NEXAFS spectrum of the underderivatized allylamine film especially in the σ^* region (above 292 eV). Absorption features at 291.9 (E) and 295 eV (G) are tentatively assigned to transitions of C core electrons to σ^* C-F orbitals, feature F at 293.2 eV to a σ^* (C-C) transition [96].

Fig. 4.47(c) shows the difference spectrum which displays a sharp peak at 285.2 eV (A) due to the new contribution of signal originating from the aromatic rings of TFBA. The peak at 288.5 eV (C) indicates an increase of oxygen species, most probably amides, due to the aging of the sample.

Fig. 4.48 shows the trend of duty cycle variation in terms of C K-edge changes, for a set of derivatized samples prepared at fixed process parameters of 20 W and 5 Pa.

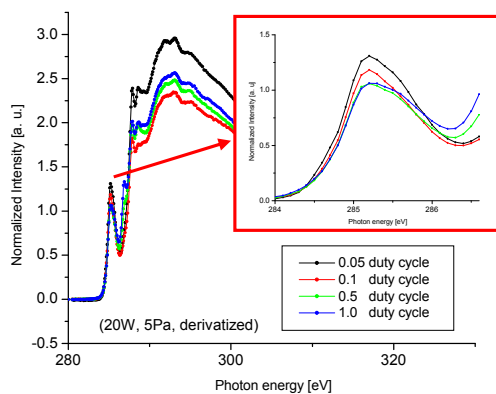


Figure 4.48. Expanded NEXAFS C K-edge spectra of TFBA derivatized plasma deposited allylamine films at different duty cycles used during plasma deposition. Plasma deposition of allylamine was carried out at 20 W and 5 Pa and at a film thickness of 40 nm. Samples were then derivatized with TFBA in gas-phase for 90 min.

The effect of duty cycle on the content of surface amino groups can be monitored by the resonance intensity at 285.2 eV. As we go from "hardest" (1.0 duty cycle) to "mildest" (0.05 duty cycle) plasma conditions, the intensity of the peak increases due to the increase in the number of marker entities derived from TFBA.

The interpretation is that milder plasma conditions promote the retention of amino groups originating from the allylamine monomer during plasma polymerization. This supports the XPS characterization results of derivatized samples shown in Fig. 4.48(a). There, an increase in the retention of primary amino groups is also observed when duty cycle values are decreased.

Fig 4.49 shows the trend of power variation in terms of C K-edge changes, for a set of derivatized samples prepared at fixed process parameters of 1.0 duty cycle and 5 Pa.

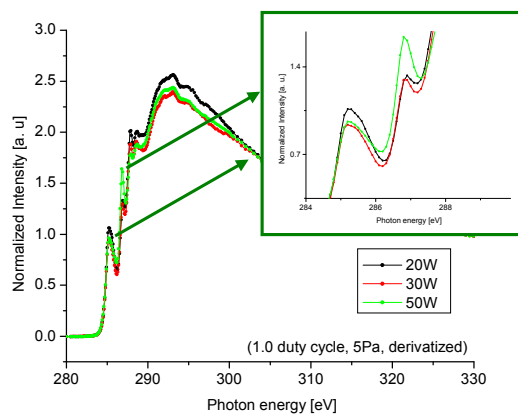


Figure 4.49. Expanded NEXAFS C K-edge spectra of TFBA derivatized plasma deposited allylamine films at different power values (20 W, 30 W and 50 W) used during plasma deposition. Plasma deposition of allylamine was carried out at 1.0 duty cycle, 5 Pa and at a film thickness of 40 nm. Samples were then derivatized with TFBA in gas-phase for 90 min.

The NEXAFS C K-edge spectra of different power values can be interpreted by the resonance intensity at 285.2 eV for $C1s \rightarrow \pi^*_{(C=C)}$. The feature observed at 287.7 eV is due to $C1s \rightarrow \pi^*_{(C=O)}$ since the derivatization reactions were carried out ex-situ.

Although, the $C1s \rightarrow \pi^*_{(C=C)}$ resonance at 285.2 eV does not show a big difference for 30 W and 50 W, the expected trend is observed due to the increased intensity at 20 W. This is due to the higher rate of derivatization in "milder" plasma conditions resulting from the amino group retention. Data obtained by XPS characterization of plasma deposited allylamine films of different power values show similar results (Fig. 4.43b, 4.44b).

As explained previously, pressure is a rather complex plasma parameter. An increase in pressure leads to a decrease in mean free path, which means higher fragmentation due to the increase in collision rate. However, when mean free path decreases, electron energy also

decreases resulting in a lower rearrangement rate. Fig. 4.50 displays the expanded NEXAFS C K-edge spectra of TFBA derivatized plasma deposited allyl amine films deposited at 2, 5 and 15 Pa. Unlike XPS results (Figs. 4.45, 4.46), the spectrum shows no real trend between 3 different pressure values. However, the film deposited at 5 Pa has the most derivatized surface due to the resonances at 285.2 eV for $C1s \rightarrow \pi^*$ ($C=C$).

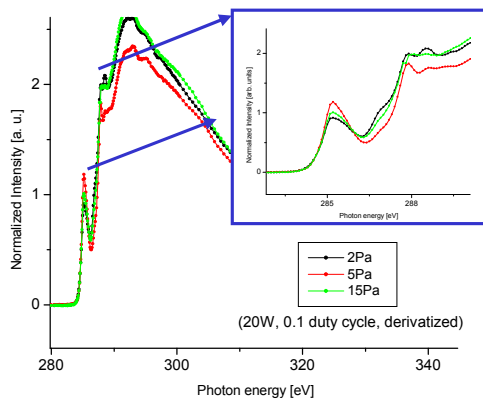


Figure 4.50. Expanded NEXAFS C K-edge spectra of TFBA derivatized plasma deposited allylamine films at different pressure values (2 Pa, 5 Pa and 15 Pa) used during plasma deposition. Plasma deposition of allylamine was carried out at 20 W, 0.1 duty cycle and at a film thickness of 40 nm. Samples were then derivatized with TFBA in gas-phase for 90 min.

4.4. Quantification of surface amino groups on plasma polymerized allylamine surfaces

The amino group concentration on plasma deposited allylamine surfaces can be calculated using two different data sets. The first set of calculations is called QEA (Quantitative Elemental Analysis) and was established by quantification of XPS survey scans covering C 1s and F 1s photo peaks. The second one, called PFA (Peak Fit Analysis), handles spectral interpretation of highly resolved C1s spectra. The two different methods will be discussed in detail in 5.1.

For the QEA based quantification, Equation 4.7 is used. [C] and [F] values are obtained from XP survey scans.

$$[NH_2]_s = \frac{[F]_{at\%}}{3[C]_{at\%} - 8[F]_{at\%}} \cdot 100 \quad (\text{Equation 4.7})$$

For PFA based quantification, Equation 4.8 is used. $[CF_3]$ and $[C_{rest}]$ values are obtained from C1s high resolution spectra.

$$[NH_2]_s = \frac{[CF_3]}{[C_{rest}]} \cdot 100 \quad \text{(Equation 4.8)}$$

$[C_{rest}]$ is the area % of the high resolution C1s spectrum when the $[CF_3]$ and the $[C-C]$ influence of the derivatization reagent (TFBA) is excluded. Equation 4.9 defines this value.

$$[C_{rest}] = 100 - [CF_3] - [C-C]_{TFBA} \quad \text{(Equation 4.9)}$$

In order to define the $[C-C]$ area of TFBA, the derivatization reagent is measured by XPS. The high resolution XP C1s of TFBA is shown in Fig. 4.51.

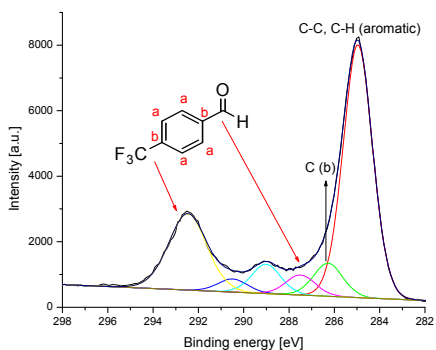


Fig. 4.51. High resolution XP C1s of TFBA. Carbons labeled as "a" appear at 285.0 eV however the ones labeled as "b" shifts to 286.0 eV due to neighboring effects of fluorine and carbonyl group.

The characteristic CF_3 component in the C1s spectrum was found at 292.5 eV. The XP spectrum of trifluoromethyl benzene given in [97] revealed the effect of trifluoromethyl groups on the chemical shift of the BE of aromatic carbon atoms [98]. Carbon atoms labeled as "a" appear at 285.0 eV. Carbon atoms directly attached to the trifluoromethyl and carbonyl groups will however appear at 286.0 eV due to the neighboring effect of CF_3 and $C=O$ groups.

Using the PFA approach, hydrocarbon impurities that are found at 285.0 eV and thus not separable from specific aliphatic / aromatic C-C species, are excluded. They are a source of uncertainty for the quantification data. Consequently, the contribution of the derivatization

needs to be subtracted in order to obtain a result for the fraction of C atoms bound to NH_2 in the underivatized molecule. Thus, $[\text{C-C}]_{\text{TFBA}}$ should include all carbon atoms of the ring and can be obtained simply by adding the area percentages of the aromatic carbons labeled by "a" and "b" ($[\text{C-C}] + [\text{C}_b]$).

For the PFA calculations $[\text{C-C}]_{\text{TFBA}}$ is calculated as 60 since $[\text{C-C}]$ peak area at 285.0 eV is 54 % whereas $[\text{C}_b]$ peak area at 286.0 eV is 6 %.

Table 4.26 displays $[\text{C}]$, $[\text{F}]$ values obtained from XP survey scans, $[\text{CF}_3]$ values obtained from high resolution C1s spectra and $[\text{NH}_2]_s$ values calculated by QEA and PFB methods for plasma polymerized allylamine samples.

Table 4.26. $[\text{C}]$ at%, $[\text{F}]$ at% (from XP survey scans), $[\text{CF}_3]$ (from high resolution C1s spectra) and $[\text{NH}_2]_s$ values calculated by QEA and PFA methods are presented. Plasma deposited allylamine samples of different plasma parameters are used as samples shown in Table 4.25. Samples are then derivatized with TFBA in gas-phase for 90 min.

	Duty cycle				Power (W)			Pressure (Pa)		
	0.05	0.1	0.5	1.0	20	30	50	2	5	15
$[\text{C}]$ at%	59	65	64	65	65	66	70	63	65	64
$[\text{F}]$ at%	13	13	12	12	12	11	8	13	13	12
$[\text{CF}_3]$	6.2	4.9	4.8	4.5	4.5	4.2	2.1	5.1	4.9	4.7
$[\text{NH}_2]_s$ (QEA)	18	14	13	12	12	10	5	15	14	13
$[\text{NH}_2]_s$ (PFA)	18	14	13	12	12	11	5	15	14	13

Figure 4.52 displays the Youden plot of the QEA and PFA methods when applied for duty cycle variations. Both methods give the same surface amino group concentration on plasma polymerized allylamine samples of different duty cycles. From the graph, it is also observed that as the plasma conditions change from mild to hard, fragmentation increases resulting in a successive decrease in surface amino group concentration.

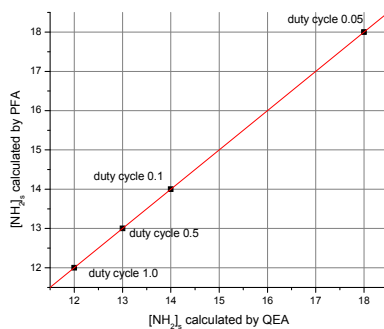


Figure 4.52. Youden plot of $[\text{NH}_2]_s$ on plasma polymerized allylamine samples of different duty cycles. Samples are derivatized with TFBA after deposition. Coupling reactions were carried out in gas-phase at room temperature and for 90 min. $[\text{NH}_2]_s$ values are obtained by using QEA and PFA methods. Quantitative Elemental Analysis was established by quantification of XPS survey scans covering C 1s and F 1s photo peaks, whereas Peak Fit Analysis handled spectral interpretation of highly resolved C1s spectra.

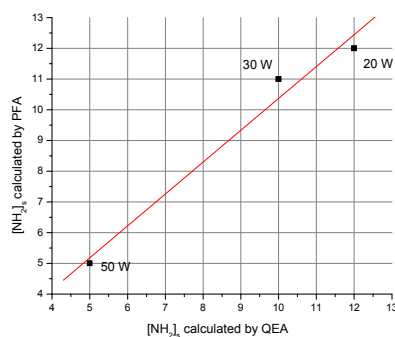


Figure 4.53. Youden plot of $[\text{NH}_2]_s$ on plasma polymerized allylamine samples of different power applications. Samples are derivatized with TFBA after deposition. Coupling reactions were carried out in gas-phase at room temperature and for 90 min. $[\text{NH}_2]_s$ values are obtained by using QEA and PFA methods. Quantitative Elemental Analysis was established by quantification of XPS survey scans covering C 1s and F 1s photo peaks, whereas Peak Fit Analysis handled spectral interpretation of highly resolved C1s spectra.

A Youden plot is also applied for the samples of different power values. (Fig. 4.53) deposited allylamine surfaces. This is due to the increased fragmentation rate by an increase in power. QEA and PFA methods give similar results. Reasons of possible deviations are explained in chapter 5 where an inter-laboratory comparison is studied. From the Youden plot, it is observed that an increase in power results in a decrease in the primary amino group retention of plasma

Figure 4.54 displays the Youden plot of the amino group quantification of plasma polymerized allylamine samples at different pressure values. Surface amino groups are calculated by QEA and PFA methods. Both methods give the same surface amino group concentration. It was already explained that pressure is a rather complex plasma parameter due to possible competing processes. Here, we observe, as the pressure increases amino group concentration on plasma deposited allylamine surfaces decreases. Consequently, the dominating process of pressure variation is the decrease in mean free path and the successive increase in the fragmentation rate.

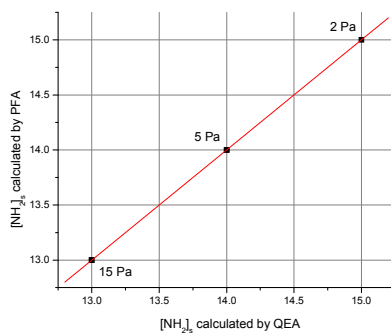


Figure 4.54. Youden plot of $[\text{NH}_2]_s$ on plasma polymerized allylamine samples of different power applications. Samples are derivatized with TFBA after deposition. Coupling reactions were carried out in gas-phase at room temperature and for 90 min. $[\text{NH}_2]_s$ values are obtained by using QEA and PFA methods. Quantitative Elemental Analysis was established by quantification of XPS survey scans covering C 1s and F 1s photo peaks, whereas Peak Fit Analysis handled the spectral interpretation of highly resolved C1s spectra.

4.5. C-F bond cleavage during derivatization reactions of plasma polymerized allylamine surfaces

During data evaluation, it is observed that XP F1s spectra of both TFBA and PFB derivatized polyallylamine samples show in some cases an unexpected fluorine species at a binding energy corresponding to F^- . This may be due to a beam damage or a side reaction. C-F bond cleavage in case of prolonged exposure to X-ray beam has been reported for poly(thiocarbonyl fluoride), poly(vinylidene fluoride) [99] and for polytetrafluoroethylene [27]. However, as explained in chapter 4.2.2.6 and 4.3.2, the studied beam damage experiments in our laboratory show negligible effects of beam damage.

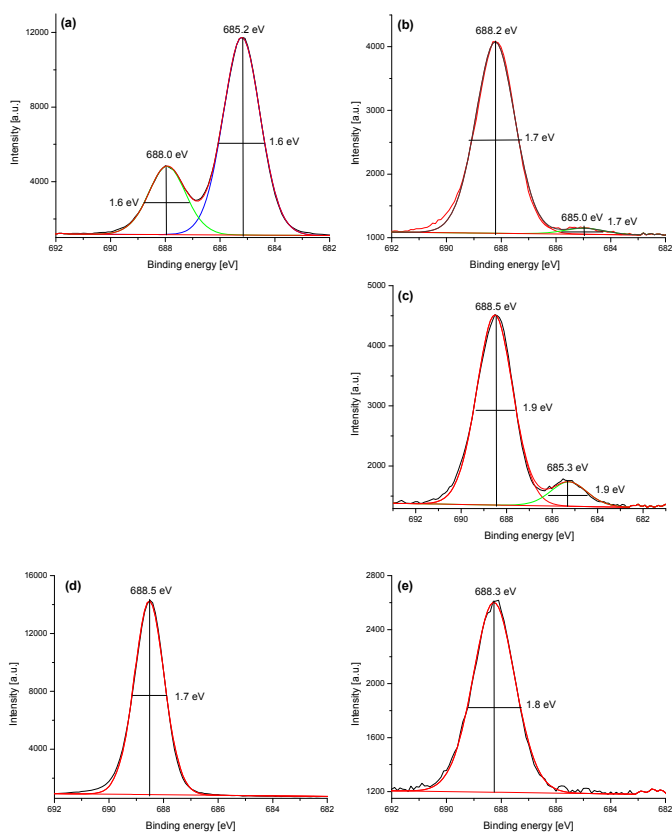


Figure 4.55. XP F1s spectra obtained with plasma polymerized allylamine films (20W, 15 Pa, 0.5 duty cycle, 40 nm) 10 min derivatized by (a) PFB and (b) TFBA, (c) with a 90 min TFBA derivatized aminated plasma oxidized PE film (cf. ref. [9]) and with spin coated 4,4'-methylenebis(2,6-diethylaniline) films 10 min derivatized by (d) PFB and (e) TFBA.

Fig. 4.55 displays examples of XP F1s spectra of gas phase derivatized plasma polymerized allylamine films. Both surfaces were derivatized for 10 min. Fig.4.55(a) shows the F1s spectrum of a PFB derivatized sample revealing two peaks, one at around 688.0 eV (25 % relative area) and another at 685.2 eV (75 % relative area). Fig.8.15(b) shows the F1s spectrum of a TFBA derivatized plasma polymerized allylamine film that also reveals two peaks, one at 688.2 eV (95 % relative area) and the other at 685.0 eV (5 % relative area). Recently, it is also observed two fluorine species in the course of derivatization of another kind of plasma processed amination of surfaces as described elsewhere [100]. Using that approach a clean polyethylene (PE) foil was subjected to low pressure O₂ r.f. plasma (10 W, 10 sccm, 10 s) as the first step. In a second step it was rinsed by an ethylenediamine in diethylether solution at r.t. for 90 min to form reactive amino groups on the surface. Finally the foil was rinsed with H₂O and ethanol and derivatized with TFBA at 50°C for 90 min. In the respective F1s XP spectrum, the CF₃ peak was observed at 688.5 eV whereas a second minor (11 % relative area) peak appeared at 685.3 eV (cf. Fig. 2c).

In difference to the expected situation, derivatization of plasma aminated surfaces by using either PFB or TFBA reagents obviously lead to two peaks in the XP F1s spectrum. This phenomenon must be understood for the formation of two different fluorine-containing moieties in the course of a gas-phase surface reaction at a chemically complex surface. The character of one of them is obvious because a peak at a binding energy (BE) of approximately 688.0 to 688.5 eV can be assigned to either aromatic CF or CF₃ bonds. A first discussion of possible origins of the unexpected second F species will be given later on.

In parallel experiments with a chemically well defined aminated surface, 4,4'-methylenebis(2,6-diethylaniline) films are spin coated onto Si wafers and XP F1s spectra were acquired after derivatization [101]. Selected XPS results are displayed as Figs. 4.55d and e. Fig. 4.55(d) shows the F1s spectrum after 10 min of reaction between 4,4'-methylenebis(2,6-diethylaniline) and PFB and Fig. 4.55(e) the one obtained for the TFBA derivatization case. In these experiments single CF and CF₃ F1s peaks appeared at 688.5 eV and 688.3 eV, respectively. No other F1s peaks have been observed. Single F1s peaks were obtained in other experiments with self assembled monolayers prepared from NH₂-terminated alkane thiols after derivatization with TFBA and PFB as well. XPS studies of TFBA and PFB samples deposited on Si wafers also revealed only single component F1s photopeaks.

As mentioned above, two F1s peaks are found exclusively for derivatized aminated surfaces which have been prepared by plasma technology. This also shows that beam damage is not the reason for the C-F cleavage. For the derivatized allylamine plasma polymers, the

relative peak areas of the additional peak at around 685 eV increase with the time of derivatization. The effect is stronger when PFB is used as the derivatization reagent.

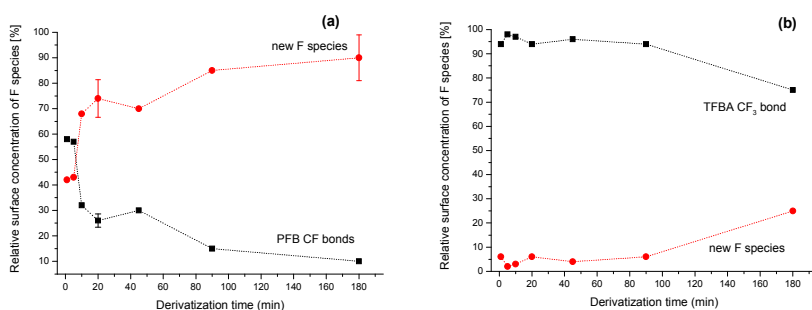


Figure 4.56. Relative peak F1s areas for CF and CF₃ species related to the derivatization agents and the F species due to CF-bond cleavage observed after derivatization of allylamine plasma polymers vs. time of derivatization when using (a) PFB or (b) TFBA. Error bars for expanded statistical uncertainties ($k = 2$) of measurement are evaluated for selected cases following the approach described in the text.

Fig. 4.56 displays the development of the relative peak areas of F 1s peaks vs. time of derivatization, Fig. 4.56(a) shows the derivatization with PFB, Fig. 4.56(b) with TFBA. The uncertainty of measurement related to data points, displayed in Fig. 4.56, originates mainly from the limited reproducibility of the combination of deposition and derivatization. A batch of five plasma polymerized allylamine samples was analysed for reproducibility at fixed derivatization and analysis conditions. The total F surface concentration was taken to investigate the variance of the results. A relative standard deviation of 5 % was obtained for statistical errors in this experiment. The statistical uncertainty related to the evaluation of the F1s spectra in terms of peak areas resulting from peak fit analysis was rather small for two typical cases (20 and 180 min PFB derivatization). It was analysed by seven independent peak fittings for each case and the relative standard deviation was 0.9 % in the worst case (C-F peak at 180 min). However it will be much higher in cases represented by Fig. 4.55(b).

A tentative discussion of possible origins of the unexpected F species which was observed after derivatization of plasma processed samples starts with an information taken from the NIST XPS Data Base: The F1s BE at approximately 685 eV is characteristic for F in fluorides, i.e. F⁻ [102].

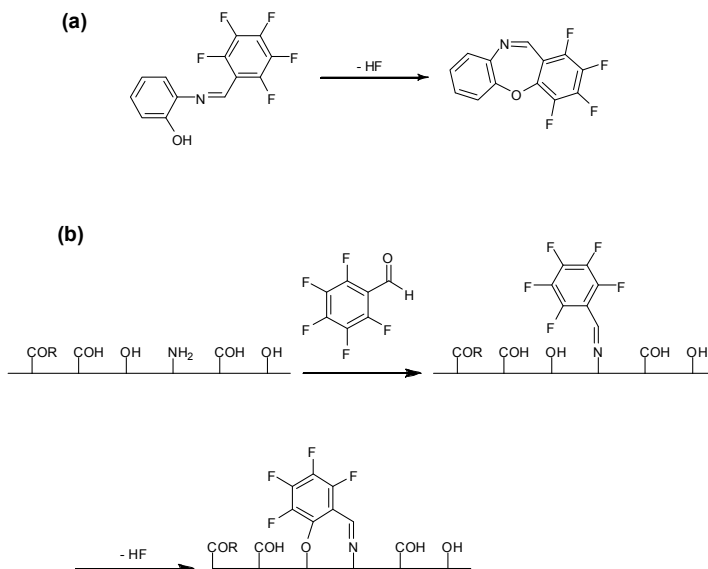


Figure 4.57. (a) Intramolecular S_NAr reaction of 2-[(pentafluorophenyl)methylene]amino]phenol $C_6H_4(OH)-2-N=CH(C_6F_5)$ yielding 1,2,3,4-tetrafluorodibenz-[b,f][1,4]-oxazepine and releasing HF [16]. This reaction resembles an anticipated attack of a surface OH group at the fluorine in the *ortho*-position to the surface bound $N=CH(C_6F_5)$ group at a plasma polymerized allylamine film under release of HF, as displayed in (b).

The known literature on fluoro-organic chemistry has been searched extensively but only limited information was obtained for the PFB case and almost no for TFBA. For the PFB derivatized surface the first step to open up a reaction pathway, which leads to HF or F^- , is a C-F bond cleavage at the fluorinated aromatic moieties. Because fluorinated aromatic molecules are highly susceptible to nucleophilic aromatic substitution, such an initial step seems to be likely [103]. Therefore, a reaction with a surface OH group might lead to the formation of HF, which can then be trapped by surface OH or imine entities *via* hydrogen bonding. Moreover, it has been reported in the literature that 2-[(pentafluorophenyl)methyleneamino]phenol $C_6H_4(OH)-2-N=CH(C_6F_5)$ may react by an intramolecular S_NAr reaction to yield a dibenz-[b,f][1,4]-oxazepine (Fig. 4.57(a)) [104]. This anticipated reaction scheme resembles an attack of a surface OH group at the fluorine in the *ortho*-position to the also surface bound $N=CH(C_6F_5)$ group to give HF shown in Fig. 4.57(b).

The probability for fluoride to serve as a leaving group - when the CF_3 of TFBA derivatized surface is considered - is low. This is in accordance with the XPS spectra which indicate a lower fluoride content (*vide supra*). A simple nucleophilic substitution pathway is

in this case unlikely. However, negative hyper conjugation can be invoked to explain a higher reactivity of perfluoroalkyl groups and a population of antibonding $\sigma^*_{\text{C-F}}$ orbitals in α,α,α -trifluorotoluene have been proposed [105]. Irradiation of $t\text{BuNH}_2$ with α,α,α -trifluorotoluene leads to the generation of $\text{PhCF=N}t\text{Bu}$ [106].

In principle, alkyl fluoride abstraction is also conceivable *via* radical reaction pathways, although such a reaction would presumably mainly lead to the formation of C-F bonds and is thought to be very slow [104, 107, 108]. However, the occurrence of radical species at plasma deposited aminated surfaces has been proved [103,107].

As a result, the additional reactions causing in additional peaks in XP F1s spectra, must be C-F bond cleavages followed by HF release. HF could be trapped at the surface by hydrogen bonding but also be released from the surface. As a consequence of these additional reaction(s), a quantification procedure for amines relying on the F surface concentration or the C1s CF or CF₃ component peak areas will indeterminately underestimate the amine content.

5. Derivatization of OH groups on plasma surfaces

5.1. An inter-laboratory comparison

Many reagents and surface analytical methods are comprehensively investigated through the years in order to find an optimum procedure to determine surface hydroxyl groups. The main ideas were discussed in the previous chapter. Chemical derivatization of hydroxyl groups using TFAA and a successive measurement of XPS is the most applied method. However, the new indications of some recent literature [108,109] show that some of the derivatization reactions proved to be successful in the CD-XPS approach of "classical" polymers do not work for the more complex plasma samples. The reason is that the plasma-modified surfaces have a more complex surface chemistry than "classical" polymers. Thus, an inter-laboratory comparison using international standards is of great importance for the "plasma community". The aim of the present inter-laboratory comparison was to investigate the reliance of CD-XPS using TFAA for the determination of the relative concentration of hydroxyl groups, X_{OH} , at the surface of a plasma oxidized poly(propylene) sample. In order to reduce the variability of technical approaches across the participating laboratories, a number of reasonable constraints was applied and distributed as a part of the protocol of the comparison such as:

1. Derivatization had to be done in every participating lab immediately before analysis of XPS.
2. A gas phase TFAA derivatization had to be applied.
3. The repeatability of the XPS measurement for a lab had to be determined by repeating survey scan and highly resolved C 1s spectra seven times, each of them at a different position at the sample dispatched when possible.

In this chapter the results obtained from the measurement in different laboratories will be displayed, illustrating the degree of equivalence which can be achieved today. Standard deviations, calculated following ISO 5725-2:1994 [110], which may characterize the state-of-the-art for the so-called simple and rather often practised case of TFAA CD-XPS of C-OH species on a plasma oxidized polyolefin surface, will be presented.

5.2. Plasma modification procedure of poly(propylene) and chemicals used

The sample for the inter-laboratory comparison has been prepared by BAM Division VI.5. An A4 formatted poly(propylene) foil (Hoechst, Germany) was treated by a radio frequency (13,56 MHz) low pressure ($p = 7,6$ Pa) oxygen plasma at 100 W for 90 s. More details are given in Ref. [44]. Subsequently, the sample was stirred in 12 ml dry tetrahydrofuran (THF) and 3 ml of 1 M diborane (Aldrich, Germany) solution under N_2 atmosphere at room temperature for 18 hours. Then, the foil was removed from the bath and immersed in an alkaline H_2O_2 solution of water and THF for 2 hours. After that, the foil was washed once in THF, three times in water and once in methanol. Finally, it was dried and stored for more than five months to reach a status, sufficiently stable for the use as a test sample in the comparison. The wet chemical treatment was applied to reduce a considerable number of oxidized carbons (e.g. C=O and COOR species), formed by the oxygen plasma treatment of the polypropylene foil.

It is well known that plasma oxidized polymer surfaces suffer from ageing phenomena. However, experimental data carefully elaborated at BAM-VI.5, revealed that the surface of the polypropylene foil treated and stored as described above, is sufficiently stable in terms of surface chemistry. Furthermore, low molecular weight debris as produced during plasma modification is removed in course of washing steps. The poly(propylene) foil sample was shared and dispatched to the participants.

The homogeneity of the shared test sample in terms of x_{OH} was carefully investigated by XPS. Results were evaluated by appropriate statistical methods. A relative inhomogeneity of $< 2.6\%$ had been determined across the full A4 foil surface.

5.3. Derivatization protocol

The derivatization chamber was already shown in the Fig. 3.11. After the sample was introduced, the chamber was pumped down to approximately 10 mbar or lower. Then the valve between the TFAA reservoir and the reaction chamber was opened in order to let the reagent vapor to penetrate into the chamber. The reaction shown in Fig. 5.1 was carried out at room temperature.

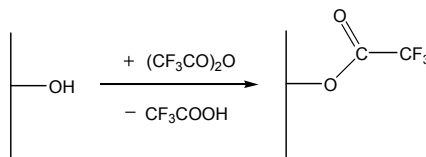


Figure 5.1. Reaction of TFAA with OH functionalized C atoms.

The sample was exposed to the reagent vapor for 15, 30 and 60 min. in order to find the time necessary for the derivatization reaction to be completed. Fig. 5.2 shows that more than 15 min. are necessary for the saturation. After the TFAA line was disconnected, the pumping line to the chamber was opened again for 30 min. in order to remove non-reacted TFAA and the side products from the sample surface.

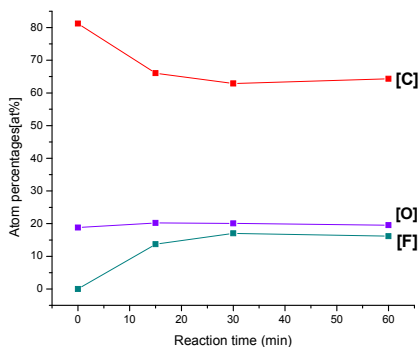


Figure 5.2. [At%] vs. time(min) graph showing that the time necessary for a complete reaction.

The transfer of the sample from the derivatization chamber to the vacuum system of the spectrometer took approximately 15 min.

5.4. XPS analysis and data evaluation

Using XPS, two kinds of data sets were measured by the participating labs. The first set, called QEA (Quantitative Elemental Analysis), was established by quantification of XPS survey scans covering C 1s and F 1s photo peaks, where the second one, PFA (Peak Fit Analysis), handled spectral interpretation of highly resolved C1s spectra. The QEA data set was corrected for additional atoms introduced by the derivatization reaction of TFAA. All participating labs shared the information on used quantification software, sensitivity factors,

peak fit strategies and instrumental parameters (e.g. excitation source, charge compensation, transmission function and times of exposure to X-rays). A sample was subjected to seven independent measurements in order to define the mean values and the standard deviations for QEA and PFA.

At BAM VI.43, X-ray photoelectron spectroscopy (XPS) with a Kratos Axis Ultra DLD with charge neutralization involving monochromatized Al K α X-rays at an emission angle of 0° and a source-to-analyzer angle 54° at pass energies of 80 eV for survey spectra and 20 eV for core level spectra were used. The spectra had been taken by setting the instrument to the hybrid lens mode and the slot mode, providing approximately an analysis area of 300 x 700 μm^2 .

Fig. 5.3 displays the survey scan, C1s and F1s spectra of the TFAA derivatized poly(propylene) sample.

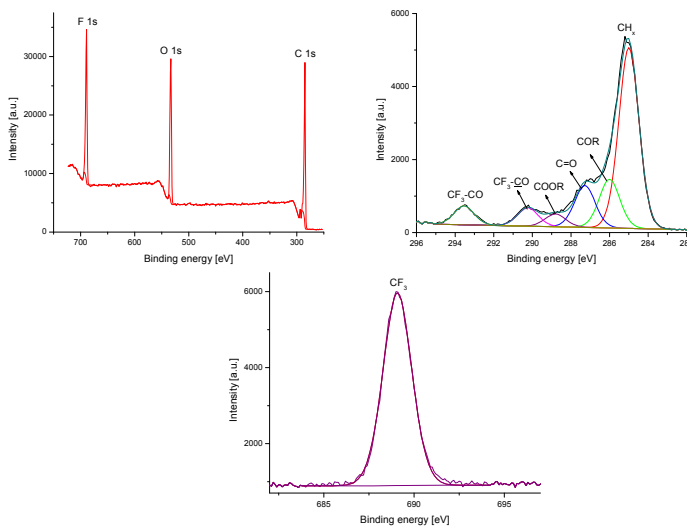


Figure 5.3. A typical shortened survey scan, high resolution C1s and F1s spectra of a TFAA derivatized poly(propylene) film.

The relative concentration of hydroxyl groups, expressed as a percentage, is described by the Equation 5.1:

$$X_{\text{OH}} = 100 \cdot n_{\text{COH}} / (n_{\text{COH}} + n_{\text{CR}}) \quad (\text{Equation 5.1})$$

In the C 1s spectrum of the derivatized sample, the CH_x BE was constrained to 285.0 eV, the BEs of the components C-OR, C=O and COOR were constrained to 286.0-286.5 eV, 287.0-287.8 eV, and 288.8-289.2 eV windows, respectively. The areas of the two fluorine containing components CF₃-CO and CF₃-CO were constrained to be equal and their BEs were left free to run. Finally, the highly resolved F1s spectrum showed one component at around 689.0 eV due to the F atoms of -CF₃ group.

When using the QEA procedure, we determined the OH concentration (X_{OH}) by the following equation where n_F is the relative fluorine concentration and n_C is the carbon concentration determined from the shortened survey scan (Fig. 5.2):

$$X_{OH} = 100 \cdot n_F / (3n_C - 2n_F) \quad \text{(Equation 5.2)}$$

Applying the PFA procedure, X_{OH} was determined by the equation 5.3 where I_i are the intensities of CH_x, C-OR, C=O, COOR and CF₃-CO components determined by peak fitting the highly resolved C 1s spectrum, displayed in Fig. 5.3.:

$$X_{OH} = 100 \cdot I_{\underline{C}F_3-CO} / (I_{CH_x} + I_{C-OR} + I_{C=O} + I_{COOR}) \quad \text{(Equation 5.3)}$$

The other participating labs applied the defined derivatization procedures and measured the samples with their own X-ray photoelectron spectrometers. Quantification by peak fittings was also applied by their own methods. The details of the measurement modes or reaction procedures are explained in Gross et al [111].

5.5. Results and discussion

The results of the statistical evaluation of the QEA and PFA data are displayed in Fig. 5.3 and 5.4. They reveal a dominant scatter of data between the participating labs for both data sets, QEA and PFA. There are systematic deviations between the labs. This is not unexpected and inevitable for the implementation of such procedures in different laboratories. No consolidation level is observed which is usually to be expected near to the consensus value.

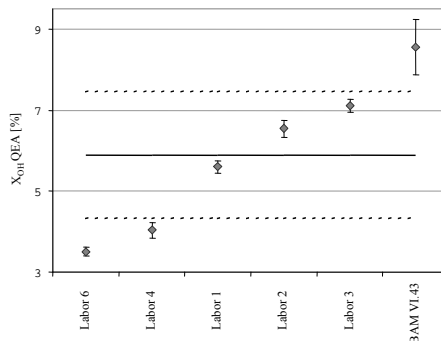


Figure 5.4. Laboratory means for x_{OH} with expanded ($k=2$) standard deviations (diamonds with bars) and mean of the laboratory means (bold solid line) with its expanded ($k=2$) standard deviation (dashed line), obtained after statistical evaluation of Quantitative Elemental Analysis (QEA) data derived from XPS survey scans covering C 1s and F 1s photo peaks. The ordinate expresses the x_{OH} of the inter-laboratory comparison as a percentage.

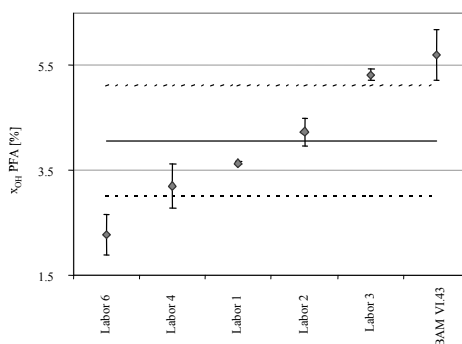


Figure 5.5. Laboratory means for x_{OH} with expanded ($k=2$) standard deviations (diamonds with bars) and mean of the laboratory means (bold solid line) with its expanded ($k=2$) standard deviation (dashed line) obtained after statistical evaluation of Peak Fit Analyses (PFA) data for highly resolved C 1s spectra. The ordinate expresses the x_{OH} of the inter-laboratory comparison as a percentage.

These results show a systematic deviation between QEA and PFA procedures due to the results obtained. In order to eliminate the differences, occurred by QEA and PFA applications of different labs, a bi-functional variance test has been applied, resulting in a clear significance of both factors [112]. This shows that there is no compatibility between QEA and PFA procedures even when they are applied in different lab environments. Moreover, the Youden plot displayed in Fig. 5.6 reveals similar and significant differences for results, obtained by both procedures QEA and PFA across all participating labs.

Results of compatible analytical procedures must occur in a Youden plot distributed closely around the diagonal $y = x$. However, this does not apply for the given comparison. The PFA procedure consistently results in lower (by $\sim 33\%$) X_{OH} data as QEA.

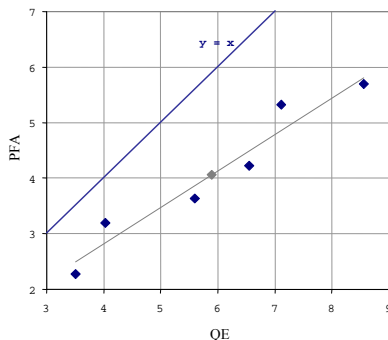


Figure 5.6. Youden-Plot for X_{OH} data obtained by either QEA (Quantitative Elemental Analysis by XPS) or PFA (Peak Fit Analyses of highly resolved XP C1s XP-spectra) in different labs. Dark diamonds are the experimental data points, grey line is the regression graph, grey diamond is the centre of gravity of data. *

Hollaender et al. recently published a report about TFAA derivatization for $-OH$ and $-NH_2$ groups on different polymers, where they calculated the functional group concentrations with both QEA and PFA methods [67]. They obtained similar results in terms of higher functional group concentrations, when calculated with QEA method. The reason is explained by the slower TFAA diffusion rate into the sample surface than the reaction with $-OH$ and $-NH_2$ groups. As a result, the reaction runs under the surface in a front like profile. When the reactions do not proceed long enough, the front might be situated within the XPS analysis depth causing an inhomogeneous analysis region. Thus, the ratio of converted and shielded groups can be different for different elements. This results in different values, depending on the element data used for calculations. They showed that values obtained by both methods intersect when the reaction reaches complete conversion.

The reproducibility standard deviation s_R has been found to be as high as 33% for both procedures (QEA and PFA), used to determine X_{OH} by chemical derivatization XPS using TFAA. Consequently, the associated degree of equivalence reached by the participating laboratories in this comparison is low.

This inconvenience may arise due to the following reasons:

1. There may be some inconvenience due to the derivatization method. A validated derivatization procedure, that can be easily controlled in each lab, has not been established yet. To reach consistent results across different labs, the derivatization protocol should be standardized including the hardware used more in detail.
2. The derivatized sample may undergo beam damage in terms of losses of F and CF_3 -species during the XPS analysis. We determined the beam damage of relative concentration of hydroxyl groups expressed as a percentage (X_{OH}) during QEA measurements. X_{OH} was 9.7% after 5 min X-ray exposure and 7.9% after 25 min.

Consequently, for a validated CD-XPS protocol, control and correction of X-ray degradation is necessary. The quality of spectra defined by acquisition times must be compromised to minimize X-ray degradation.

6. Conclusions

Different amino group carrying surfaces, prepared by spin coating, self-assembly and plasma polymerization, were successfully investigated by XPS and NEXAFS. Amino groups were derivatized with the widely used primary amino group tags, PFB and TFBA, prior to analysis. Primary amino group quantification was then carried out according to the spectroscopic data.

The gas-phase derivatization reactions of PFB and TFBA were also studied in order to understand their reaction behaviour, the spectral differences they cause and the time required for reaction completion. For the determination of maximum reaction yields of gas-phase surface derivatizations, a set of liquid-phase derivatization reactions was carried out. The selected amino compounds with a different degree of steric hindrance were reacted with PFB and TFBA. The yields (78-89%) were accepted as the upper limit of the gas-phase surface derivatizations.

Thin films were prepared by spin coating of 4,4'-methylenebis(2,6-diethylaniline) on Si wafers and were reacted with the markers at 50°C. The saturation time was found to be 15 min. for both reactions. XPS measurements showed the formation of a CF_3 or C-F peak and a BE shift of the corresponding C=N group indicating a successful reaction. The NEXAFS results supported the XPS data by showing a sharp $\pi^*_{(\text{C}=\text{N})}$ resonance. The CF_3 and C-F resonances were observed in the σ^* region. The yields of the reactions were calculated from the component areas of the high resolution XP N1s spectra and from the [F]/[N] ratios. The surface amino groups were calculated from the stoichiometry and from the XP survey scans. The results were consistent with each other and showed a yield of 80-90% for PFB and 60-70% for TFBA.

Self-assembled monolayers (SAMs) of different terminal groups were prepared and investigated with XPS and NEXAFS. The spectral properties of aliphatic and aromatic SAMs were compared to the reference surfaces of poly(allylamine) and 4,4'-methylenebis(2,6-diethylaniline) spin coated on Si wafers. NEXAFS was used to determine the orientation of SAMs. An angle resolved NEXAFS was applied at the C K-edge in order to prove a successful SAM deposition on Au. The intense peaks in the difference spectra are due to the polarization dependence in the orbital responsible for the NEXAFS resonance showing a successful bond/functional group orientation.

The gas-phase surface derivatization of two amino terminated SAMs, 4-aminophenylbutane-1-thiolate and 11-amino-1-undecanethiol, were studied. 4-aminophenylbutane-1-thiolate was derivatized with TFBA whereas 11-amino-1-undecanethiol with PFB at room temperature for 90 min. The stoichiometrical data were compared to the atomic percentages obtained from the XPS spectra and the results were consistent with each other. The yields of the reactions (60-80%) were obtained from the high resolution N1s spectra.

Since a certain number of spectra had to be acquired to reach reasonable S/N ratios, a considerable danger of beam damage in the NEXAFS measurements occurs. The potential radiation damage effects on the C and N K-edge of 11-amino-1-undecanethiol film on Au was studied. The spectral differences before and after 1 h radiation exposure were investigated. The intensities of resonances related to unsaturated species such as C=C and C=N were increased for the C K-edge spectra. The NEXAFS N K-edge spectra of 11-amino-1-undecanethiol film showed no significant irradiation effect.

Plasma deposited allylamine samples were successfully investigated by XPS and NEXAFS. Primary amino group quantification on plasma deposited allylamine surfaces was carried out by derivatization after plasma deposition.

TFBA and PFB showed side reactions when plasma polymerization was used. Due to the radical mechanisms, C-F bond cleavages followed by HF releases occurred resulting in a second peak formation in XP F1s spectra. PFB derivatized surfaces suffer more from the C-F bond cleavage since fluorinated aromatic molecules are highly susceptible to nucleophilic aromatic substitution. Potential X-ray beam damage of TFBA was studied by a 10 h XPS measurement and showed a fluorine degradation. Due to the short measurement times, X-ray beam damage can be neglected.

Since HF release on the TFBA surfaces are lower in percentage, it was used as the marker reagent for the coupling reactions. A series of samples deposited at 20W, 0.5 duty cycle and 15 Pa were derivatized to determine the time required for saturation (90 min.).

Plasma polymerized allylamine samples with different duty cycle, power and pressure values were prepared in order to study the effects of external plasma parameters on the primary amino group retention. The $[CF_3]$ area percentages, obtained from the high resolution XP C1s spectra, vs. plasma parameter variations were compared. Duty cycle, power and pressure variation experiments showed the same trend on amino group retention. The more the plasma conditions move from mild to hard, the more rearrangements occur on the surface.

Milder plasma conditions promote the retention of amino groups originating from the allylamine monomer.

QEA (Quantitative Elemental Analysis) and PFA (Peak Fit Analysis) methods were used for the quantification of surface amino groups, depending on the XPS data. The results of two data evaluation methods were compared by using a Youden plot showing no deviation.

NEXAFS was used along with XPS in order to study plasma parameter effects on amino groups. As being sensitive against unsaturated moieties, NEXAFS was successfully applied to plasma deposited allylamine surfaces. An increase in fragmentation rate due to a variation in plasma parameters was followed by intensity changes in NEXAFS C K-edge spectra.

An inter-laboratory comparison of hydroxyl group determination on plasma surfaces was carried out. Hydroxyl groups on polypropylene foil, treated with oxygen plasma at 100 W for 90 s, were coupled with TFAA. The surfaces were investigated with XPS and the [OH] amount on the surfaces was calculated by QEA and PFA methods showing a 33% deviation between the two methods.

CD-XPS is applied successfully in order to determine different functional groups on the thin film surfaces. However, a validated derivatization procedure, which can be easily applied in each lab, should be established. The used hardware and the peak fitting procedures of XPS should be defined in detail for the validation. The sample inhomogeneity and the effects of beam damage play a role on the deviations of the results. The surface thickness should be optimized for consistency.

By the derivatization reactions, the surface amino groups are successfully quantified. As the next step, the studied surfaces can be used for potential biological applications, such as coupling the available amino groups with DNA or stem cells.

Zusammenfassung

Ziel dieser Arbeit war die Charakterisierung und Quantifizierung von Aminofunktionalitäten auf Oberflächen mittels der Analyseverfahren Röntgen-Photoelektronenspektrometrie (XPS) und Röntgen-Absorptionsspektrometrie (Analyse der Feinstruktur an der Absorptionskante, NEXAFS). Die Oberflächen wurden durch Spin coating, Selbstassemblierung oder Plasmapolymersation hergestellt und die primären Aminogruppen mit den dafür oft genutzten Markern PFB und TFBA derivatisiert.

Die Gasphasenderivatisierungen mittels PFB und TFBA wurden auch genutzt, um Reaktionsverhalten, Reaktionszeit und die resultierenden spektroskopischen Unterschiede genauer zu ermitteln. In nasschemischen Untersuchungen reagierten abgeschirmte Amine mit PFB und TFBA unterschiedlich stark mit Ausbeuten von 78-89%, was als maximale Ausbeute der Oberflächenderivatisierung in der Gasphase angesehen wird.

Die Dünnschichtfilme wurden mittels Spin coating von 4,4'-Methylen-bis(2,6-diethylanilin) auf Si-Wafern hergestellt und reagierten bei 50 °C mit den Markern. Die Sättigungszeit betrug in beiden Fällen 15 min.

Die XPS Messungen zeigten die erfolgreiche Umsetzungen durch das Auftreten eines neuen CF_3 - bzw. C-F-Signals und einer BE-Verschiebung der entsprechenden C=N-Gruppe. In Übereinstimmung mit den XPS-Daten, zeigen die NEXAFS-Spektren eine scharfe $\pi^*_{(\text{C}=\text{N})}$ Resonanz und die CF_3 bzw. C-F Resonanz in der σ^* -Region. Die Ausbeuten der Reaktionen wurden aus den Komponenten-Flächen der hochaufgelösten XP N1s Spektren und aus den $[\text{F}]/[\text{N}]$ -Verhältnissen berechnet. Stöchiometrie und XP-Übersichtsspektren dienen zur Bestimmung der Aminofunktionalitäten an den Oberflächen. Die Resultate waren konsistent und zeigten eine Ausbeute von 80-90% für PFB und 60-70% für TFBA.

Für die Untersuchung von selbstorganisierenden Monoschichten (SAMs) mit unterschiedlichen Funktionalitäten wurden spektroskopische Daten von aliphatischen und aromatischen SAMs mit denen von Si-Wafern, welche mit Polyallylamin und 4,4'-Methylenbis(2,6-diethylanilin) beschichtet wurden, verglichen.

Die Orientierung der Monoschichten wurde mittels der winkelaufgelösten NEXAFS an der C K-Kante bestimmt. Die scharfen Signale im Differenzspektrum zeigen eine erfolgreiche Orientierung der Bindungen bzw. funktionellen Gruppen und resultieren aus der Polarisationsabhängigkeit der NEXAFS-Resonanzen an relevanten Molekülorbitalen.

Die Gasphasen-Oberflächenderivatisierungen von zwei SAMs mit Aminofunktionalitäten (4-Aminophenylbutan-1-thiolat und 11-Amino-1-undecanthiol) wurden untersucht. Für eine Zeit von 90 min. wurde 4-Aminophenylbutan-1-thiolat mit TFBA bzw. 11-Amino-1-undecanthiol mit PFB bei RT umgesetzt. Die stöchiometrischen Daten der Umsetzungen waren in Übereinstimmung mit den Elementkonzentrationen, welche sich aus den XPS-Daten ableiten ließen. Die Ausbeuten wurden mit Hilfe der N1s-Spektren berechnet und betragen 60-80%.

Da für eine aussagekräftige NEXAFS-Messung eine gewisse Anzahl von Spektren aufgenommen werden muss, steigt die Gefahr der Schädigung der Probe durch Strahlung. Aus diesem Grund wurde ein 11-Amino-1-undecanthiol-Film auf Au für 1 h mit weichem Röntgenlicht bestrahlt und die spektroskopischen Unterschiede an der C und N K-Kante untersucht. Es zeigte sich kein signifikanter Unterschied für die N K-Kante, allerdings erhöhten sich die Intensitäten der C=C und C=N-Spezies im C K-Kanten-Spektrum, was für einen Strahlenschaden spricht.

Mittels Allylamin als Plasmagas und Si-Wafern wurden plasma-chemisch abgeschiedene Allylaminfilm Oberflächen hergestellt und untersucht. Der Einfluss der externen Plasmaparameter (Duty Cycle, Plasmaleistung und Druck des gasförmigen Monomers im Reaktor) auf den chemischen Charakter des abgeschiedenen Films wurde im Detail analysiert.

Die anschließenden Gasphasen-Oberflächenderivatisierungen mit TFBA und PFB zeigten Nebenreaktionen. C-F-Bindungsbruch und HF-Abspaltung führten zu einem zusätzlichem Signal im XP F1s Spektrum. Oberflächen, welche mit PFB derivatisiert wurden, zeigten einen höheren Anteil von C-F-Bindungsbrüchen, da an fluorierten aromatischen Molekülen leicht nukleophile aromatische Substitutionen stattfinden. Potentielle Schäden durch Röntgenstrahlung wurden mittels TFBA derivatisierter Proben, welche für 10 h der Strahlung ausgesetzt wurden, studiert. Es zeigte sich eine Abnahme der Fluorgehalte an der Oberfläche, allerdings hat dieser Effekt aufgrund der kurzen Messzeiten praktische keine Auswirkung bei der Datenerfassung.

Da die HF-Abspaltung auf TFBA-Oberflächen prozentual geringer ist, wurde es als Marker für alle weiteren Kupplungsreaktionen genutzt. Eine Serie von Proben, welche bei einer Plasmaleistung von 20W, 0,5 Duty Cycle und einem Druck von 15 Pa derivatisiert wurden, zeigten eine Sättigungszeit von 90 min.

Bei variierenden Plasmabedingungen wurden die unterschiedlichen $[\text{CF}_3]$ -Flächenprozent in den hochaufgelösten XP C1s Spektren miteinander verglichen. Duty Cycle, Plasmaleistung und Druck zeigten identische Trends in der Retention der Aminogruppen.

Grundsätzlich führt die Anwendung von harten Plasmabedingungen, d.h bei hoher effektiver Plasmaleistung, zu Filmen mit einer vergleichsweise geringen Retention der Aminofunktionalitäten. Darüber hinaus sind diese Filme stark vernetzt bzw. verzweigt. Eine hohe Anzahl ungesättigter Kohlenstoffspezies ist ebenfalls typisch.

In Abhängigkeit von den XPS-Daten wurden für die Quantifizierung der Aminogruppen an der Oberfläche die Methoden QEA (Quantitative Elementar-Analyse) und PFA (Peak Fit Analyse) genutzt. Die Berechnungen wurden mittels Youden-Plot verglichen und zeigten keine Abweichung voneinander.

NEXAFS wurde zusätzlich genutzt, um den Einfluss der Plasmaparameter auf die Aminogruppen zu studieren, da die Methode empfindlich gegenüber ungesättigten Spezies ist. Eine Zunahme der Fragmentationsraten bei Veränderungen in den Plasmaparametern konnten aus Intensitätsveränderungen in den NEXAFS C K-Kanten Spektren abgeleitet werden.

Ein Ringversuch für die Bestimmung von Hydroxylgruppen auf mit Plasma behandelten Oberflächen wurde ebenfalls durchgeführt. Dafür wurde eine Polypropylenfolie, welche Sauerstoffplasma bei 100 W für 90 s ausgesetzt wurde, mit TFAA derivatisiert. Die Oberfläche wurde mittels XPS untersucht und der $[\text{OH}]$ -Gehalt mittels QEA und PFA bestimmt. Die Methoden zeigten eine Abweichung von 33% voneinander.

CD-XPS wurde erfolgreich zur Bestimmung unterschiedlicher Funktionalitäten auf Dünnschichtfilmen eingesetzt. Allerdings bedarf es für den Erhalt von in sich konsistenten Datensätzen einer validierten Derivatisationsprozedur, die in jedem Labor angewendet werden muss. Die verwendete Hardware und die Peak-Fitting-Prozeduren bei XPS-Untersuchungen müssen ebenfalls im Detail beschrieben werden. Die Inhomogenitäten und eventuelle Strahlungsschäden führen zu Abweichungen in den erhaltenen Resultaten. Die gemessene Schichtdicke muss auch für konsistente Ergebnisse optimiert werden. Dünnere Schichten führen zu weniger Hintergrundrauschen.

Die erfolgreich durchgeführten Derivatisierungsreaktionen zeigten die Verfügbarkeit der Aminogruppen an der Oberfläche. In einem nächsten Schritt können an diese Funktionalitäten z.B. Stammzellen oder DNA gekoppelt werden, was hochinteressant in Hinblick auf potentielle biologische Anwendungen ist.

7. References

1. J. F. Watts, J. Wolstenholme, "An introduction to surface analysis by XPS and AES", **2003**, John Wiley & Sons Ltd, England.
2. A. Choukourov, H. Biederman, I. Kholodkov, D. Slavinska, M. Trchova, A. Hollaender, *Journal of Applied Polymer Science*, **92**, **2004**, 979-990.
3. R.M. France, R.D. Short, R.A. Dawson, S. MacNeil, *J. Mater. Chem.*, **8**, **1998**, 37-42.
4. J.G. Steele, G. Johnson, K.M. McClean, G. Meumer, H.J. Griesner, *J. Biomed. Mater. Res.*, **50**, **2000**, 475-82.
5. L. Tang, Y. Wu, R.B. Timmons, G.W. Gross, *J. Biomed. Mater. Res.*, **42**, **1998**, 156-63.
6. H. Biederman, I.H. Boyaci, P. Bilkova, D. Slavinska, S. Mutlu, J. Zemek, M. Trchova, J. Klimovie, M. Mutlu, *J. Appl. Polym. Sci.*, **81**, **2001**, 1341-52.
7. Q. Chen, L. Dai, M. Gao, S. Huang, A. Mau, *J. Phys. Chem B*, **105**, **2001**, 618-622.
8. Z.F. Li, and A.N. Netravali, *J. Appl. Polym. Sci.*, **44**, **1992**, 333-346.
9. I.H. Loh, *Polymer preprint from the American Chemical Society Meeting, Denver, CO, Vol. 34*, **1993**, 661-662.
10. W.R. Gombotz, A.S. Hoffman, *Journal of Applied Polymer Science*, **42**, **1988**, 285.
11. K. Hoffmann, R. Mix, U. Resch-Genger, J. F. Friedrich, *Langmuir*, **23**, **2007**, 8411-8416.
12. U. Oran, S. Swaraj, A. Lippitz, W.E.S Unger, *Plasma Process. Polym.*, **3**, **2006**, 288-298.
13. R.J. Anderegg, *Mass. Spectrom. Rev.*, **7**, **1988**, 395-424.
14. F. Truica-Marasescu, P.-L. Girard-Lauriault, A. Lippitz, W. E. S. Unger, and M. R. Wertheimer, *Thin Solid Films*, **21**, **2008**, 7406-7417.
15. P.-L. Girard-Lauriault, P. Desjardins, W.E.S. Unger, A. Lippitz and M. R. Wertheimer, *Plasma Process. Polym.*, **5**, **2008**, 631-644.
16. A. Hollaender, *Surf. Interface Anal.*, **36**, **2004**, 1023-1026.
17. J. Kim, D. Jung, Y. Park, Y. Kim, D.W. Moon, T.G. Lee, *Applied Surf. Sci.*, **253**, **2007**, 4112 – 4118.

18. a) R. Förch, Z. Zhang, W. Knoll, *Plasma Process. Polym.*, **2**, **2005**, 351. b) P.-L. Girard- Lauriault, F. Mwale, M. Iordanova, C. Demers, P. Desjardins, M. R. Wertheimer, *Plasma Process. Polym.*, **2**, **2005**, 263.
19. N. M. Bashara and C. T. Day, *J. Appl. Phys.*, **35**, **1964**, 3498.
20. N. Inagaki, M. Matsunnaga, *Polymer Bulletin* **13**, **1985**, 349.
21. C. Malitesta, I. Losito, L. Sabbatini, P.G. Zambonin, *Journal of Electron Spectroscopy and Related Phenomena*, **97**, **1998**, 199-208
22. A. Hollaender, F. Pippig, M. Dubreuil, D. Vangeneugden, *Plasma Process. Polym.*, **5**, **2008**, 345-349.
23. A. Chikolti, B.D. Ratner, D. Briggs, *Chem. Mater.*, **3**, **1991**, 51-62.
24. A. Chilkoti and B. D. Ratner in *Surface Characterization of Advanced Polymers*, Ed by L. Sabbatini and P. G. Zambonin, VCH, Weinheim, **1993**, pp. 221-256.
25. F. Truica-Marasescu, M.R. Wertheimer, *Plasma Processes and Polymers*, **5**, **2008**, 44.
26. S. Rangan, F. Bournel, J.J. Gallet, S. Kubsky, K. Le Guen, G. Dufour, F. Rochet, F. Sirotti, G. Piaszenski, R. Funke, M. Knepe, U. Köhler, *Journal of Physical Chemistry B*, **109**, **2005**, 12899.
27. F. Pippig, A. Holländer, *Applied Surface Science*, **253**, **2007**, 6817.
28. D. Briggs, D.M. Brewis, R.H. Dahm, I.W. Fletcher, *Surface and Interface Analysis*, **35**, **2003**, 156.
29. A.G. Shard, J.D. Whittle, A.J. Beck, P.N. Brookes, N.A. Bullett, R.A. Talib, A. Mistry, D. Barton, S.L. McArthur, *Journal of Physical Chemistry B*, **108**, **2004**, 12472.
30. R.A. Andoa, G.M. do Nascimento, R. Landers, P.S. Santos, *Spectrochim. Acta Part A*, **69**, **2008**, 319.
31. A.J. Beck, J.D. Whittle, N.A. Bullett, P. Eves, S. Mac Neil, S.L. McArthur, A.G. Shard, *Plasma Processes and Polymers*, **2**, **2005**, 641.
32. Rangan, *PhD thesis*, Université Paris 6, Paris, France **2004**.
33. J. Stöhr, *NEXAFS Spectroscopy*, Springer, Heidelberg, Germany, **1992**.
34. J.E. Baio, T. Weidner, J. Brison, D.J. Graham, L.J. Gamble, D.G. Castner, *Journal of Electron Spectroscopy and Related Phenomena*, **172**, **2009**, 2.
35. I. Retzko, J.F. Friedrich, A. Lippitz, W.E.S. Unger, *Journal of Electron Spectroscopy and Related Phenomena*, **121**, **2001**, 111.

36. O. Dhez, H. Ade, S.G. Urquhart, *Journal of Electron Spectroscopy and Related Phenomena* 128 (2003) 85.
37. Rasmussen, J. R., Bergbreiter, D. E. and Whitesides, G. M., *J. Am. Chem. Soc.*, 99, 1977, 4746-4756.
38. T.A. Dang, R. Gnanasekaran, *Surface and Interface Analysis*, 15, 1990, 113-118.
39. A. Choukourov et al., *Vacuum*, 75, 2004, 195-205.
40. C. N. RAILLEY, D.S. Everhart, *Applied Electron Spectroscopy for Chemical Analysis*, Wiley- Interscience, New York, 1982.
41. Y. Nakayama, T. Takahagi, F. Soeda, K. Hatada, S. Nagaoka, J. Suziki, A. Ishitani, *J. Polym. Sci.: Part A: Polym. Chem.*, 26, 1988, 559-572.
42. I. Losito, E. D. Giglio, N. Cioffi, C. Malitesta, *J. Mater. Chem.*, 11, 2001, 182.
43. M. Okamoto, R. Yakawa, M. Wakasa, T. Wakisaka, *Bunseki Kagaku*, 47, 1998, 261.
44. G. Kühn, S. Weider, R. Decker, A. Ghode, J. Friedrich, *Surf. Coat. Technol.*, 116-119, 1996, 796.
45. Y. Nakayama, K. Takahashi, T. Sasamoto, *Surf. Interface Anal.*, 24, 1996, 711
46. D.S. Everhart, C.N. Reilley, *Anal. Chem.*, 53/4, 1981, 665.
47. A. Chilkoti, B.D. Ratner, *Surface and Interface Analysis*, 17, 1991, 567-574.
48. V.B. Ivanov, J. Behnisch, A. Hollaender, F. Mehdorn, H. Zimmermann, *Surface and Interface Analysis*, 24, 1996, 257-262.
49. B.L. Frey, R.M. Corn, *Anal. Chem.*, 68, 1996, 3187.
50. E.E. Johnston, B.D. Ratner, *J. Electron Spectrosc.*, 81, 1996, 303.
51. N. Hasirci, *J. Appl. Polym. Sci.*, 34, 1987, 135.
52. B.L. Frey, R.M. Corn, *Anal. Chem.*, 68, 1996, 3187.
53. D.G. Hanken, R.M. Corn, *Anal. Chem.*, 67, 1995, 3767.
54. C. Xu, L. Sun, L.J. Kepley, R.M. Crooks, *Anal. Chem.*, 65, 1993, 2107.
55. R.S.S. Murthy, D.E. Leyden, *Anal. Chem.*, 58, 1986, 1228.
56. J.C. Love, D.B. Wolfe, R. Haasch, M.L. Chabinye, K.E. Paul, G.M. Whitesides, R.G. Nuzzo, *J. Am. Chem. Soc.*, 125, 2003, 2597.
57. S.R. Holmes-Farley, G.M. Whitesides, *Langmuir*, 2, 1986, 266-281.
58. C. Henneuse-Boxus, A. De Ro, P. Bertrand, J. Marchand-Brynaert, *J. Polymer*, 41, 2000, 2339-2348.
59. K. Siegbahn, "ESCA: Atomic, molecular and solid state structure studied by means of electron spectroscopy", Almquist & Wiksells Boktryckeri AB, Uppsala 1967.

60. ISO 15472:2001, Surface chemical analysis - X-ray photoelectron spectrometers Calibration of energy scales.
61. ISO 19318:2004, Surface chemical analysis - X-ray photoelectron spectroscopy - Reporting of methods used for charge control and charge correction.
62. G. Beamson, D. Briggs, *High Resolution XPS of Organic Polymers*, Wiley, Chichester, **1992**.
63. P.E. Batson, *Physical Review B*, **48**, **1993**, 2608.
64. G. Solomons, C. Fryhle, *Organic Chemistry*, **2000**, John Wiley & Sons Inc, New York.
65. N. Graf, E. Yegen, T. Gross, A. Lippitz, W. Weigel, S. Krakert, A. Terfort, W.E.S. Unger, *Surface Science*, **603**, **2009**, 2849-2860.
66. H. Wang, S.F. Chen, L.Y. Li, S.Y. Jiang, *Langmuir*, **21**, **2005**, 2633.
67. F. Pippig, S. Sarghini, A. Hollaender, S. Paulussen, H. Terryn, *Surf. Interface Anal.*, **41**, **2009**, 421-429.
68. E. Yegen, U. Zimmermann, A. Lippitz, W.E.S. Unger, in *BESSY Annual Report*, **2007**, Berlin, 149-151.
69. S. Pan, G.C. Castner, B.D. Ratner, *Langmuir*, **14**, **1998**, 3545-3550.
70. A. Ulman, *An Introduction to Ultrathin Organic Films From Langmuir-Blodgett to Self-Assembly*, Academic Press, London, **1991**.
71. <http://www.ifm.liu.se/applphys/ftir/sams.html>
72. R. Valiokas, S. Svedhem, S.C.T. Svensson, B. Liedberg, *Langmuir*, **15**, **1999**, 3390.
73. A.V. Shevade, J. Zhou, M.T. Zin, S.Y. Jiyang, *Langmuir*, **17**, **2001**, 7566.
74. L. Bertilsson, B. Liedberg, *Langmuir*, **9**, **1993**, 141.
75. D.A. Hutt, G.J. Leggett, *Langmuir*, **13**, **1998**, 2740.
76. H.J. Himmel, K. Weiss, B. Jaeger, O. Dannenberger, M. Grunze, C. Wöll, *Langmuir*, **13**, **1997**, 4943.
77. T.M. Willey, A.L. Vance, T. van Buuren, C. Bostedt, L.J. Terminello, C.S. Fadley, *Surface Science*, **576**, **2005**, 188.
78. T.J. Horr, P.S. Arora, *Colloids and Surfaces A – Physicochemical and Engineering Aspects*, **126**, **1997**, 113.
79. Y. Zubavichus, A. Shaporenko, M. Grunze, M. Zharnikov, *Journal of Physical Chemistry A*, **109**, **2005**, 6998.

80. N. Graf, E. Yegen, A. Lippitz, W.E.S. Unger, in *BESSY Annual Report*, **2007**, Berlin, 107-109.
81. J.R.I. Lee, T.M. Willey, J. Nilsson, L.J. Terminello, J.J. De Yoreo, T. van Buuren, *Langmuir*, **22**, **2006**, 11134.
82. M. Kinzler, A. Schertel, G. Hahner, C. Woll, M. Grunze, H. Albrecht, G. Holzhter, T. Gerber, *Journal of Chemical Physics*, **100**, **1994**, 7722.
83. A. Patnaik, K.K. Okudaira, S. Kera, H. Setoyama, K. Mase, N. Ueno, *Journal of Chemical Physics*, **122**, **2005**.
84. S. Frey, V. Stadler, K. Heister, W. Eck, M. Zharnikov, M. Grunze, B. Zeysing, A. Terfort, *Langmuir*, **17**, **2001**, 2408.
85. E.M.E. Kristensen, F. Nederberg, H. Rensmo, T. Bowden, J. Hilborn, H. Siegbahn, *Langmuir*, **22**, **2006**, 9651.
86. M. Zharnikov, M. Grunze, *Journal of Vacuum Science & Technology B* **20** (2002) 1793.
87. L. O' Toole, R. D. Short, *J. Chem. Soc., Faraday Trans.*, **93**(6), **1997**, 1141.
88. C. L. Rinsch, X. Chen, V. Panchalingam, R. C. Eberhart, J. H. Wang, R. B. Timmons, *Langmuir*, **12**, **1996**, 2995.
89. A. J. Ward, R. D. Short, *Polymer*, **34**, **1993**, 4179.
90. A. J. Ward, R. D. Short, *Surface and interface analysis*, **22**, **1994**, 477.
91. A. J. Beck, S. Candan, R. M. France, F. R. Jones, R. D. Short, *Plasma and Polymers*, **3**, **1998**, 97.
92. C.G. Gölander, M.W. Rutland, D.L. Cho, A. Johansson, H. Ringblom, S. Jönsson, H.K. Yasuda, *J. Appl. Polym. Sci.*, **49**, **1993**, 39-51.
93. F. Fally, C. Doneux, J. Riga, J.J. Verbist, *J. Appl. Polym. Sci.*, **56**, **1995**, 597- 614.
94. S. Swaraj, *PhD thesis*, FU Berlin, Germany, **2005**.
95. S. Swaraj, U. Oran, A. Lippitz, W. Unger; in *BESSY Annual Report*, **2005**, Berlin, 320.
96. D.G. Castner, K.B. Lewis, D.A. Fischer, B.D. Ratner, J.L. Gland, *Langmuir*, **9**, **1993**, 537-542.
97. D.T. Klark, D. Kilcast, W.K. Musgrave, *J. Chem. Soc. D Chem. Commun.*, **1971**, 516.
98. S. Devouge, C. Salvagnini, J. Marchand-Brynaert, *Bioorg. Med. Chem. Lett*, **15**, **2005**, 3252.
99. D.R. Wheeler, S.V. Pepper, *J. Vac. Sci. Technol.*, **20**, **1982**, 226.

100. E. Yegen, A. Lippitz, D. Treu, W.E.S.Unger, *Surf. Interface Anal.*, **2008**, *40*, 176-179.
101. NIST X-ray Photoelectron Spectroscopy Database, NIST Standard Reference Database 20, Version 3.5.
102. a) P. Kirsch, *Modern Fluoroorganic Chemistry*, Wiley-VCH, Weinheim **2004**. b) T. Hiyama, *Organofluorine Compounds*, Springer, Heidelberg **2000**. c) T. Braun, A. Steffen, V. Schorlemer, B. Neumann, H.-G. Stammler, *Dalton Trans.*, **2005**, 3331-3336. d) T. Braun, V. Schorlemer, B. Neumann, H.-G. Stammler, *J. Fluorine Chem.*, *127*, **2006**, 367-372.
103. J. Shen, V. Grill, R.G. Cooks, *J. Am. Chem. Soc.*, *120*, **1998**, 4254-4255.
104. a) N. I. Petrenko, M.M. Kozlova, T. N. Gerasimova, *J. Fluorine Chem.*, *36*, **1987**, 93-98. b) C. L. Allaway, M. Daly, M. Nieuwenhuyzen, G. C. Saunders, *J. Fluorine Chem.*, *115*, **2002**, 91-99.
105. a) D. O'Hagan, *Chem. Soc. Rev.*, *37*, **2008**, 308-319. b) B. M. Kraft, W. D. Jones, *J. Am. Chem. Soc.*, *124*, **2002**, 8681-8689.
106. A. Gilbert, S. Krestonosich, D. L. Westover, *J. Chem. Soc. Perkin Trans. I*, **1981**, 295-302.
107. a) R. N. Perutz, T. Braun in *Comprehensive Organometallic Chemistry III*, Vol. 1, R. H. Crabtree, M. P. Mingos (Edts.), Elsevier, Oxford **2007**, 725-758. b) W. D. Jones, *Dalton Trans.*, **2003**, 3991-3995; c) T. Braun, R. N. Perutz, *Chem. Commun.* **2002**, 2749-2575; d) J. Burdeniuc, B. Jedlicka, R. H. Crabtree, *Chem. Ber./Recl.*, *1997*, *130*, 145-154.
108. R.A. Morgan, J.D. Whittle, D. Barton, R.D. Short, *J. Matter. Chem.*, *14*, **2004**, 408-412.
109. E. Yegen, U. Zimmermann, W.E.S. Unger, T. Braun, *Plasma Processes and Polymers*, *6*, **2009**, 11-16.
110. ISO 5725-2:1994, Accuracy (trueness and precision) of measurement methods and results – Part 2: Basic method for the determination of repeatability and reproducibility of a standard measurement method. ISO, Geneva.
111. T. Gross, G. Kühn, W.E.S. Unger, *Surf. Interface Anal.*, *41*, **2009**, 445-448.
112. The bi-functional variance test and the Youden plot were derived by Dr. W. Bremser from BAM I.1.